Separation & Purification Reviews
Publication details, including instructions for authors and subscription information:
http://www.informaworld.com/smpp/title~content=t713597294

MICROPOROUS INORGANIC MEMBRANES

Y. S. Lin[a]; I. Kumakiri[bc]; B. N. Nair[d]; H. Alsyouri[a]
[a] Department of Chemical Engineering, University of Cincinnati, Cincinnati, OH, U.S.A. [b] CNRS-Institut de Recherches sur la Catalyse, Villeurbanne, France [c] SINTEF Materials Technology, Oslo, Norway [d] Research and Development Center, Noritake Company Ltd., Aichi, Japan

Online publication date: 26 November 2002

To cite this Article Lin, Y. S. , Kumakiri, I. , Nair, B. N. and Alsyouri, H.(2002) 'MICROPOROUS INORGANIC MEMBRANES', Separation & Purification Reviews, 31: 2, 229 — 379
To link to this Article: DOI: 10.1081/SPM-120017009
URL: http://dx.doi.org/10.1081/SPM-120017009

MARCEL DEKKER, INC. • 270 MADISON AVENUE • NEW YORK, NY 10016

SEPARATION AND PURIFICATION METHODS
Vol. 31, No. 2, p. 229–379, 2002

MICROPOROUS INORGANIC MEMBRANES

Y. S. Lin,[1,*] I. Kumakiri,[2,†] B. N. Nair,[3] and H. Alsyouri[1]

[1]Department of Chemical Engineering, University of Cincinnati, Cincinnati, OH 45221, USA
[2]CNRS–Institut de Recherches sur la Catalyse, 2, av. A. Einstein, 69626 Villeurbanne, France
[3]Research and Development Center, Noritake Company Ltd., Miyoshi, Aichi 470-0293, Japan

CONTENTS

*Corresponding author. E-mail: jlin@alpha.che.uc.edu
†Current address: SINTEF Materials Technology, Forskningsveien 1, BP124 Blinden, N-0314 Oslo, Norway.

DOI: 10.1081/SPM-120017009 0360-2540 (Print); 1525-6022 (Online)

ABSTRACT

Recent development in microporous inorganic membranes represents a significant advance in materials for separation and chemical reaction applications. This paper provides an in-depth review of synthesis and properties of two groups (amorphous and crystalline) of microporous inorganic membranes. Amorphous microporous silica membranes can be prepared by the sol-gel and phase separation methods. Flat sheet, tubular and hollow fiber amorphous carbon membranes have been fabricated by various pyrolysis methods from polymer precursors. A large number of synthesis methods have been developed to prepare good quality polycrystalline zeolite membranes. Several techniques, including vapor and liquid approaches, are reviewed for pore structure modification to prepare microporous inorganic membranes from mesoporous inorganic membranes. Chemical, microstructural

MARCEL DEKKER, INC. • 270 MADISON AVENUE • NEW YORK, NY 10016

and permeation properties of these microporous membranes are summarized and compared among the several microporous membranes discussed in this paper. Theory for gas permeation through microporous membranes is also reviewed, with emphasis on comparison with the experimental data. These inorganic microporous membranes offer excellent separation properties by the mechanisms of preferential adsorption, selective configurational diffusion or molecular sieving.

1. INTRODUCTION

Membrane is a physical barrier allowing selective transport of mass species. Membranes consist of three large groups: biological, organic (polymeric) and inorganic membranes. Inorganic membranes can be further classified into ceramic and metallic membranes. According to the membrane pore size (or the size of the particles that can move through the membranes), both organic and inorganic membranes can be divided into microfiltration (MF), ultrafiltration (UF), nanofiltration (NF) (reverse osmosis) and gas separation membranes. According to the definition of IUPAC in terms of the material pore size,[1] the MF, UF and NF membranes correspond respectively to macroporous (pore diameter $d_p > 50$ nm), mesoporous (2 nm $< d_p <$ 50 nm) and microporous ($0 < d_p < 2$ nm) membranes. Therefore, the microporous membranes reviewed in this article are limited to those porous inorganic membranes with a pore diameter smaller than 2 nm (20 Å).

The major advantages of inorganic membranes as compared to polymeric membranes are their thermal, chemical and mechanical stability. Recent work also shows that some microporous inorganic membranes possess unique perm-separation properties for gases and vapors unavailable to polymeric gas separation membranes. Therefore, microporous inorganic membranes offer potential applications in membrane separators for gas/vapor/liquid separation and membrane reactors for chemical reactions to improve reaction conversion or product selectivity.[2,3] Typical examples of applications of the microporous inorganic membranes are enrichment of hydrogen from hydrocarbons/hydrogen stream by microporous carbon membranes[4] and isobutane dehydrogenation reaction in a zeolite silicalite membrane reactor.[5]

Structurally, microporous inorganic membranes include crystalline (mainly zeolites) and amorphous (mainly SiO_2 and carbon) materials. The membranes are usually prepared as thin films on porous inorganic supports that provide the mechanical strength. The thickness of the microporous film varies from a few ten-nanometers to a few microns. Figure 1 shows cumu-

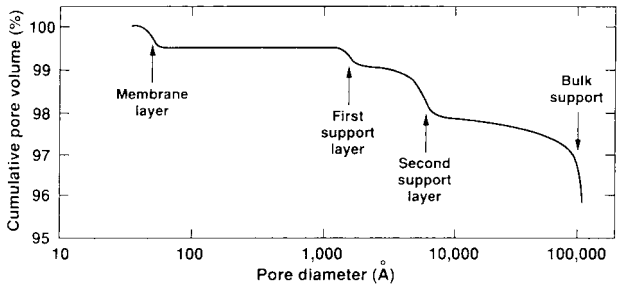

Figure 1. Pore size distribution of a four-layered alumina membrane (After Ref. [6]).

lative pore volume versus pore diameter of a four-layer ceramic support with a UF mesoporous membrane top-layer.[6] In most cases, the microporous membrane film is coated on the surface of the UF (or mesoporous) inorganic membrane layer. Disk and single-tube are the most common geometries of the microporous inorganic membranes although some researchers reported synthesis of microporous membranes in the hollow fiber and flat-sheet geometries.

Characterization of the pore size of the supported microporous membranes still remains a major technical challenge in the membrane community. Methods (such as nitrogen adsorption porosimetry) for characterizing microporous materials (not membranes) are available, and can be used to measure the pore size and pore size distribution of microporous membranes in the unsupported form.[7] However, such information is related to but not necessarily the same as that for the microporous membranes when coated on porous inorganic supports. Some flow-through methods useful for characterization of MF and UF membranes, such as the permporosimetry method[7,8] have been used to measure microporous silica–zirconia membranes.[9] Strictly speaking, however, these methods are not applicable for supported microporous membranes because the physical models used in these methods do not apply to the microporous membranes. Therefore, most researchers have used results obtained by indirect methods to indicate the pore size range of a microporous membrane.

The transport properties for microporous inorganic membranes are commonly reported in permeance, permeability and separation factor. The permeance, with a unit of mass/area/time/pressure, is defined as the permeation flow rate divided by membrane area and transmembrane pressure. Permeability is the permeance times the thickness of the microporous membrane layer (mass/length/time/pressure). Since the actual thickness of a microporous mem-

brane layer is often not known, permeability is less commonly used to indicate the permeation properties of microporous inorganic membranes. Ideal separation factor is the ratio of the pure gas permeance for one species to that for another. Multi-component separation factor is defined by the ratio of the molar fractions of two species in the influent of the permeate side to that in the retentate side. Multi-component separation factor depends not only on the thermodynamic and transport properties of the membrane/fluid-mixture system but also on the configuration of the permeation cell and the flow conditions of the permeation measurement.

This review is focused on synthesis and properties of microporous inorganic membranes. Applications of microporous membranes for separation of gas/liquid mixtures, and improvement of yield and selectivity of chemical reactions are not included in this review. Research on the sol-gel synthesis of microporous silica and other oxide membranes represents the major and earlier effort on inorganic microporous membranes. These topics are covered in the first section. Microporous zeolite membranes have been a topic of extensive study for the past ten years and are covered in the second section. Other microporous inorganic membranes, such as carbon, glass, and those membranes achieved by narrowing the pores of mesoporous membranes, are dealt in the third section. The transport (permeation) properties of various microporous membranes will be discussed in each section dealing with the specific membranes. The last section will be devoted to review and discussion of the theory of gas permeation through microporous inorganic membranes, and generalized observations of gas permeation and separation properties of various microporous inorganic membranes.

2. SOL-GEL DERIVED MICROPOROUS MEMBRANES

Sol-gel methods are known to be the most successful methods for processing microporous silica membranes. The first paper on sol-gel derived ceramic membranes that received extensive attention and helped accelerate inorganic membrane research was published by Burggraaf and co-workers in 1984.[10] Later, the groups of Asaeda at University of Hiroshima and Burggraaf at University of Twente were among the first to extend the sol-gel method to prepare microporous silica membranes.[11–13] Since then a large number of microporous inorganic membranes have been prepared by the sol-gel methods. In almost all cases a good quality microporous inorganic membrane is coated as a thin film on a sol-gel derived mesoporous ceramic support. Because of the technical importance of these mesoporous supports in microporous ceramic membranes, they are first reviewed next.

2.1 Mesoporous Ceramic Membrane Supports and Slip-Casting Coating Process

The sol-gel derived mesoporous ceramic membrane provides two major advantages as the support surface for thin microporous ceramic layers. The pore openings of the mesoporous membranes are around 3 to 5 nm. This will avoid infiltration of the microporous ceramic into the support pores, minimizing the effective thickness of the microporous membrane layer. The mesoporous membrane layer usually has very smooth surface with minimum defects if it is prepared carefully. This ensures formation of a thin uniform microporous ceramic layer without defects on this support surface.

Common crystalline mesoporous ceramic membranes include γ-alumina, zirconia and titania. These porous ceramic membranes consist of small crystallites of alumina, zirconia or titania of which the intercrystalline space gives rise to the mesopores of the membranes. These membranes are generally prepared by the sol-gel methods. It starts with the alumina (boehmite), zirconia or titania sols either directly prepared by dispersing the fine solid particles of these oxides in aqueous solution, or from the inorganic or metal-organic precursors of these oxides. The latter approach is preferred as it gives the sol containing solid particles with a more uniform size distribution from which mesoporous membranes with fairly uniform pore size can be prepared.

Yoldas[14] pioneered synthesis of inorganic sol (in particular boehmite) from metal alkoxide precursors. Alumina (boehmite), titania and zirconia sols can be prepared by the following typical procedures.[15] A stable 1 M alumina (boehmite) sol can be synthesized by dissolving 260 ml of aluminum tri-sec-butoxide in 1 liter of water at 70–90°C. The boehmite precipitate formed from the hydrolysis and condensation is then peptized by adding 70 ml 1 M HNO_3 solution at 90–100°C under refluxing condition. A stable 0.25 M titania sol

Table 1. Characteristics of Phase Transformation of Sol-Gel Derived Mesoporous Alumina, Zirconia and Titania Membranes

Material	Initial Phase and Lattice Parameter (Å)	Final Phase and Lattice Parameter (Å)
Alumina	γ-alumina (cubic) a = 7.8	α-alumina (hexagonal) a = 4.8, b = 13.0
Zirconia	Tetragonal a = b = 5.1, c = 5.3	Monoclinic a = 5.14, b = 5.2, c = 5.3, β = 99.2°
Titania	Anatase (tetragonal) a = b = 3.8, c = 9.5	Rutile (tetragonal) a = b = 4.9, c = 3.0

(From Ref. [15].)

can be prepared by dissolving 74 ml titanium tetra-isopropoxide (with 500 ml isopropanol) in 450 ml water in a nitrogen box. The titania precipitate should be washed with water to remove alcohol and diluted with 1 liter of water. The product is finally peptized by adding 72 ml of 1 M HNO_3 at 75°C under refluxing condition. A stable 0.25 M zirconia sol can be prepared by hydrolysis and condensation of 0.25 mole zirconium n-propoxide in a water (900 ml)/ isopropanol (500 ml) solution. The white zirconia precipitates are filtered with vacuum suction and washed in water several times to remove the isopropanol. In this process, a small amount of water is added to the zirconia precipitates to help filtering, and the washed water is filtered again to prevent the loss of zirconia precipitates. The filtered zirconia cake is then diluted in 1 liter of water and peptized with 125 ml of 1 M HNO_3 solution at 90–100°C overnight.

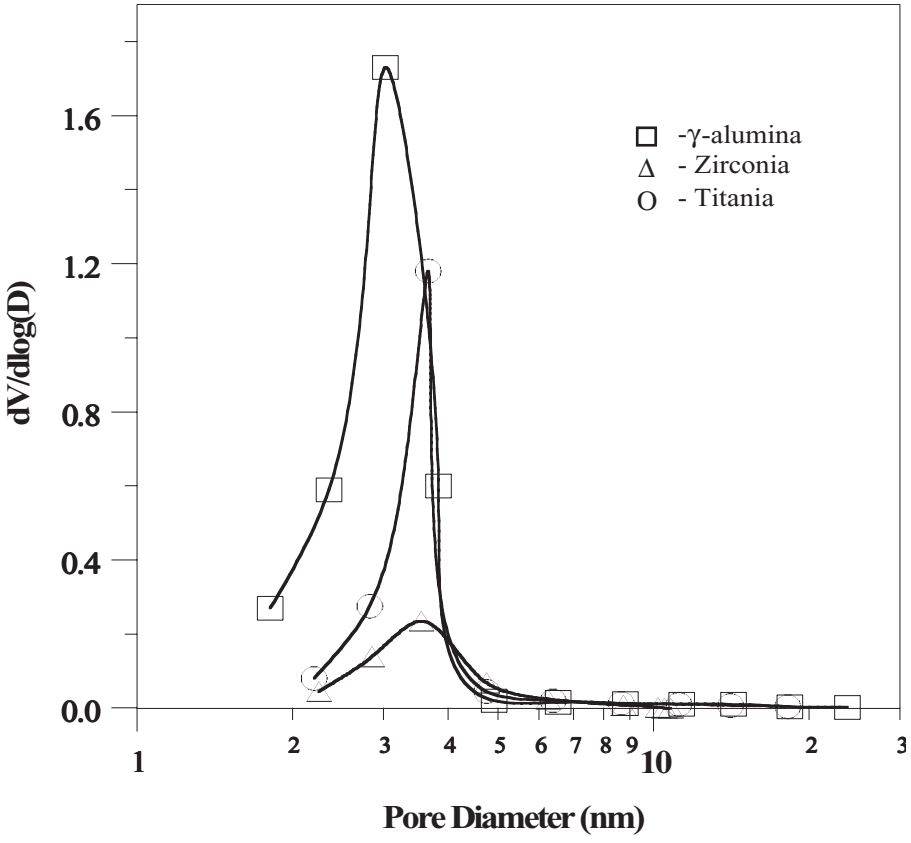

Figure 2. Pore size distribution of unsupported mesoporous gamma-alumina, zirconia and titania membranes prepared by the sol-gel method.

Unsupported alumina, titania or zirconia membranes of 20–200 μm in thickness can be prepared by pouring respective sols in a given quantity in petri dishes, followed by drying and calcination under controlled conditions. XRD data revealed that alumina particles in the sol are of boehmite crystalline structure and the particles in zirconia and titania sols are amorphous.[15] The alumina, titania and zirconia samples obtained from the sols after gelation and calcination in air at 450°C are respectively in the phases of γ-alumina, tetragonal zirconia and anatase. These are thermodynamically meta-stable phases, and may transform to the thermodynamically stable phases, which are α-alumina, monoclinic zirconia and rutile. The crystallite structure and lattice parameters of these phases are listed in Table 1.

Figure 2 shows the pore size distributions of unsupported γ-alumina, titania (anatase) and tetragonal zirconia (after calcination at 450°C for 3 hours) (obtained by nitrogen adsorption porosimetry). The pore structure data of these three membranes are compared in Table 2. As shown in Figure 2, the pore size distributions of these materials are rather narrow, with an average pore diameter of about 3 nm. The flow-through permporosimetry method gives pore size distributions of supported γ-alumina membranes prepared by the sol-gel method similar to those for the unsupported membranes.[7] Such nanosized pores and narrow pore size distribution are determined mainly by the basic properties of the primary crystallite particles. The particles of the sol-gel derived alumina, titania and zirconia, due to the Ostwald ripening mechanism, are usually in nanoscale size, with a uniform particle size distribution.[16] γ-alumina crystallites are of plate-shape[10] with a size in the range from about 5 to 20 nm. The sol-gel derived γ-alumina consists of such plate-shaped crystallite particles, which give rise to a relatively large surface area. Crystallites of tetragonal zirconia and rutile appear to be of more spherical shape, with a crystallite size in the range of about 15 nm and 11 nm, respectively.[15]

Alumina, titania and zirconia in their metastable phases can transform to their stable phases. Such phase transformation usually occurs via a nucleation and crystal growth process. Kinetically, however, the phase transformation can

Table 2. Pore Structure of γ-Al_2O_3, Titania and Zirconia Membranes (Calcined at 450°C for 3 h)

Materials	Average Pore Size (nm)	Pore Volume (ml/g)	Surface Area (m^2/g)
γ-Al_2O_3	2.8	0.33	373
TiO_2	3.4	0.21	147
ZrO_2	3.8	0.11	57.2

(Revised from Ref. [15].)

not be observed at low temperatures. Lin and co-workers[15,17] studied the phase transformation of alumina, titania and zirconia membranes by heat-treating these ceramics in metastable phase at different temperatures for 30 hours. They found that γ-Al_2O_3 transformed to α-Al_2O_3 (via δ- and θ-alumina) at temperatures above 900°C. Similarly, they found that metastable tetragonal zirconia and amatase titania transformed to the stable monoclinic zirconia and rutile at temperatures above 700°C and 450°C respectively. For all three mesoporous ceramic membranes, the phase transformation is accompanied with a sharp decrease in the surface area and increase in the pore size. The activation energy for phase transformation is respectively about 600, 570 and 213 kJ/mol for the sol-gel derived alumina, zirconia and titania.[15] These data were obtained when these materials were exposed to air. Presence of steam in the atmosphere appears to reduce the activation energy for phase transformation, thus enhancing the rate of the pore structure change of the membrane materials at a given temperature.

The surface area and pore size of γ-Al_2O_3, tetragonal zirconia and anatase respectively decrease and increase with time due to sintering or coarsening at temperatures lower than the lowest phase transformation temperatures indicated above. However, the rate of the structural change due to sintering and coarsening is much smaller than that due to phase transformation.[15] The structure stability of these mesoporous ceramic membranes can be improved by coating lanthanum oxide on the grain surface.[17–22] It is also possible to kinetically stabilize the pore structure of these ceramic membranes by heat-treating the membranes at a temperature a few hundred degrees higher than the application temperature of the membranes.

For practical use these mesoporous γ-alumina, titania or zirconia membranes, of about 3–6 μm in thickness, are supported on coarse-pore ceramic supports most commonly of α-alumina. For industrial applications the supports are multi-layer with the top-most layer (on which the mesoporous layer is coated) typically having a pore diameter of about 0.2 μm and porosity of about 50% (see Figure 1). For laboratory study the supports could be symmetric with properties similar to the top-most layer of the supports used in commercial membranes. The coating of the mesoporous layers on the supports are generally accomplished by one or another form of slip casting process. Similar slip casting process is also used to form microporous silica layer on the surface of the mesoporous support.

In the slip-casting process, the support surface is brought in contact with sol for a few seconds. The capillary pressure drop between the support pores and the liquid dip sol drives the sol into the support. Since the pore size of the support top-layer is selected such that it is close to the size of the aggregates in the sol (about 0.1–0.2 μm for boehmite, titania or zirconia sol), the solid particles in the sol being sucked into the support are blocked by the support

surface. Therefore, immediately after contacting the dip sol, the support pore mouths get partially plugged with particles from the dip sol. This process is called the initial layer formation.[3] When liquid flows through this initial layer particles get deposited and the layer thickness gradually increases.

The thickness of the mesoporous membrane layer, L, can be correlated to the diping time in the slip-casting step by:[23,24]

$$L = K.\frac{2\gamma_{lv}\cos\beta\Delta P_g}{\eta}\sqrt{t} + L_a \tag{1}$$

where L_a is the initial layer thickness formed by adhesion between the support and the dip sol, γ_{lv} is the surface tension, β is the contact angle and η is the

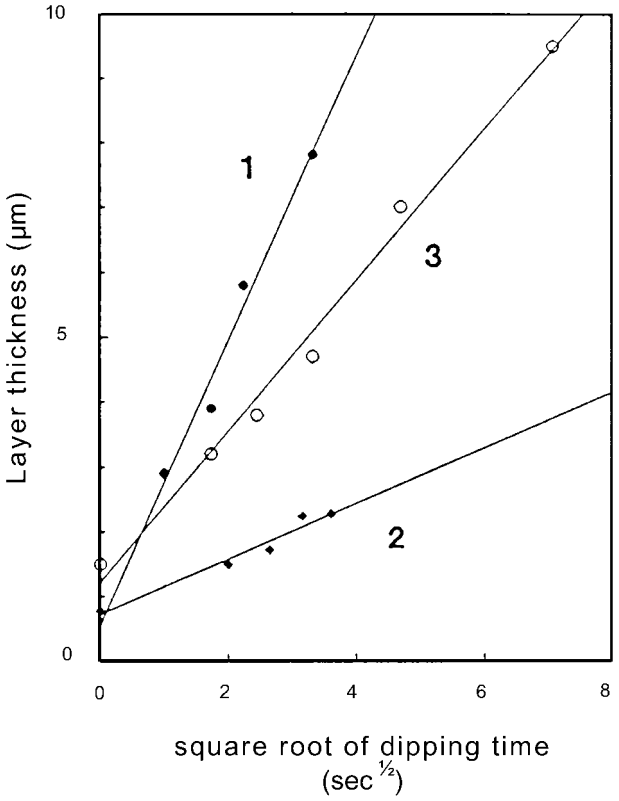

Figure 3. Layer thickness of dipped-coated alumina films versus square root of the dipping time for dipping sols with and without polyvinyl alcohol (PVA); 1 = without PVA, 2 = with PVA and 3 = second dipping, without PVA (After Ref. [46]).

solution viscosity. The pressure across the gel layer ΔP_g is calculated from the total pressure drop ΔP_c generated by the support pores as follows

$$\Delta P_g = \Delta P_c - \Delta P_s \tag{2}$$

where ΔP_s is the pressure drop across the support. Total pressure drop ΔP_c is given by

$$\Delta P_C = \frac{2\gamma_{lv}\cos\beta}{r} \tag{3}$$

where r is the radius of the support pores.

The kinetics of film formation could be, hence, controlled by a variety of parameters including the viscosity of the dip sol. Addition of organic binders into the dip sol is a good way to tailor the viscosity of the solution. The resulting increase in viscosity of the sol should decrease the membrane formation rate. Figure 3 shows the relationship between film thickness and dipping time for layer formation on an α-alumina support from boehmite sol as reported by Uhlhorn.[25] Layer thickness formed with and without application of polymer binder [such as poly(vinyl alcohol), PVA] is shown. In addition, the figure also shows the layer formation rate of membranes made on an already coated support. The growth rate is smaller in the second step and should be contributed by the increased resistance offered by the initially dipped layer. This two-step coating technique is generally useful to heal the defects remaining after the initial dipping coating.

The wet-gel layer formed by the slip-casting process is subsequently dried to remove the solvent. Cracks develop easily during the drying process and the most-effective way to avoid cracks is to add the polymer binder, such as PVA mentioned above, in the sol before slip-casting. The dried gel layer is then heat-treated at around 400°C for a few hours to strengthen the structure of the mesoporous layer and bond between the mesoporous layer and support surface.

2.2 Sol-Gel Derived Microporous Silica Membranes

Microporous silica membranes can be made by three different sol-gel methods as shown in Figure 4. The well known method of silica membrane processing starts from a sol with silica polymers (Figure 4(a)). These polymers are made by the hydrolysis and condensation of alkoxysilane precursor, such as tetraethyloxosilane (TEOS) under controlled conditions. Generally more or less linear polymers are the best for processing microporous membranes. This means that condensation reactions are seldom completed while in the liquid and may proceed during the subsequent processing stages. Because of such condensation reactions and the ability of the polymers to

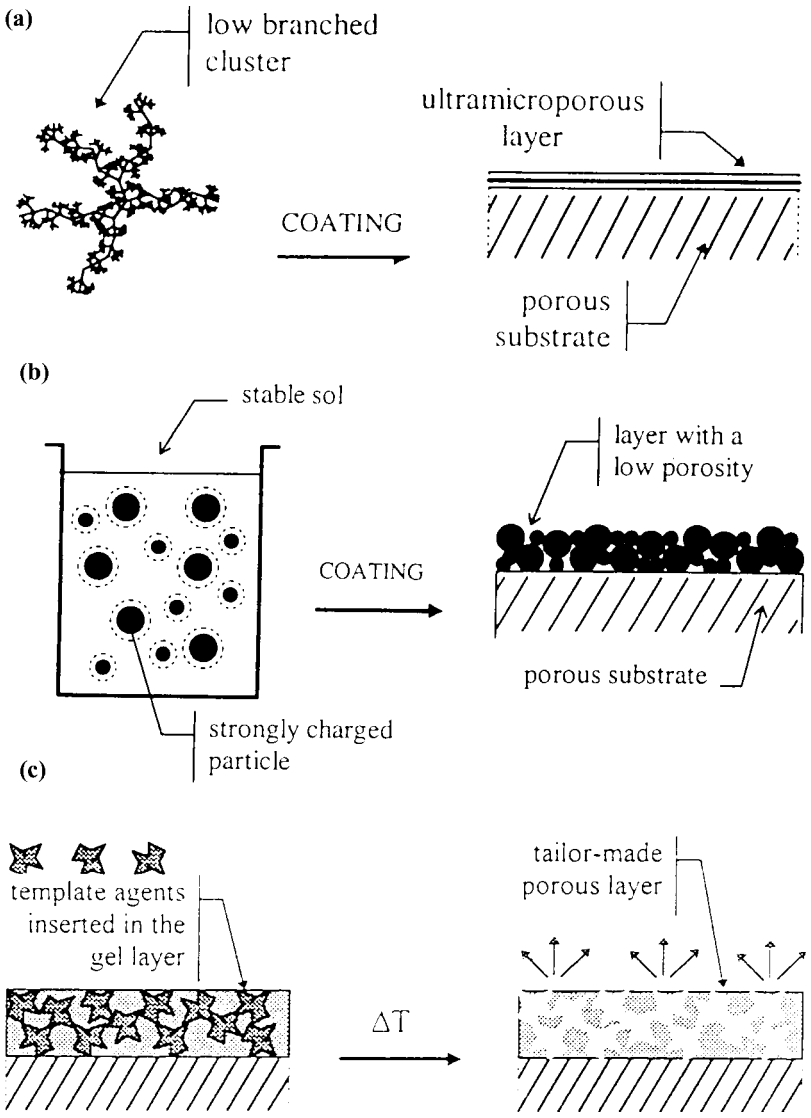

Figure 4. Schematic of the three important sol-gel routes used for preparation of microporous membranes (Redrawn from Ref. [3]).

pack and rearrange while gel shrinkage the drying stage is very important in deciding the final properties of the membrane. Yet, under otherwise similar conditions control of membrane structure is possible by manipulating the sol synthesis parameters.[26,27]

The second method (Figure 4(b)) is based on the packing of nanoparticles to make a highly porous structure as advocated by Asaeda and coworkers.[28–33] The technique is to make silica particles of different sizes and then pack them into the support substrate to process membranes with different pore sizes. The inability for particles to pack is the major hurdle in designing crack-free membranes by this method. Another point is the potential infiltration of particles in the support pores while coating because of the absence of mutual cohesion between the particles. The use of organic binders is the simplest method to solve the both problems mentioned above. Another way is the hierarchical packing of particles on support surface. In this method each layer acts as a potential healer of defects in the underlying layer as well as it modifies the active pore size distribution of the membrane.

The third method involves the use of organic templates, as shown Figure 4(c). The purpose of the organic part is to leave a residual porosity in the membrane matrix on their burnout under heat treatment. Surfactant molecules, which could arrange the matrix molecules around them by means of noncovalent interactions as well as organic ligands and polymers, which are bonded covalently to the siloxane, have been reported as templates.

In all cases the microporous silica membranes are coated on mesoporous support, in most cases, γ-alumina membranes. The permeability of the microporous membrane is low due to its small pore size. Therefore the coated microporous silica layer should be as thin as possible (down to a few ten nanometers) in order to obtain high permeance. This creates two challenges, one is the control of the thickness of the deposited film and the other is the avoidance of the mesoporous and macroporous defects and pinholes. Good quality microporous silica membranes could be obtained only when the microstructure of the gel can be controlled and good integrity of the coated film can be achieved. Next we will review the three different sol-gel routes that control the microstructure of the silica membrane and then discuss the coating process to successfully obtain a good quality of thin microporous silica layer on porous supports.

Synthesis via Polymeric Route

In general, polymeric silica sol for microporous membranes is prepared by acid catalyzed hydrolysis and condensation of TEOS in the presence of a mutual solvent, usually water and ethanol mixture.[34–41] The hydrolysis re-

action replaces alkoxide groups with hydroxyl groups.[16] Subsequent condensation between silanol groups produces siloxane bonds. In most cases, a catalyst, e.g., a mineral acid (HNO_3) or a base (NH_3) is employed. Since water and alkoxide do not mix sufficiently, alcohol is usually used as solvent. Typical sol composition (in molar ratio) was 3.8 for ethanol/TEOS, 6.5 for deionized water/TEOS and 0.09 for nitric acid/TEOS.[34,35,41] In experiment, solutions of TEOS/ethanol and nitric acid/water are prepared separately and then mixed in a flask equipped with a reflux condenser. The mixture is rapidly heated to and stayed at 90°C for 3 hours with vigorously stirring. Finally, the resulted sol is cooled naturally to room temperature.

In the case of acid catalyzed reaction, the hydrolysis proceeds through an electrophilic attack of the H^+-ion. This causes a decrease in reactivity as the number of OR groups on the Si decreases with the progress of hydrolysis. Complete hydrolysis of silicon to $Si(OH)_4$ is thus small and the condensation reaction will start before the hydrolysis has been completed. Acid-catalyzed condensation is believed to take place via protonated silanol species (Si–HOR^+), analogous to hydrolysis. Protonation of the silanol makes the silicon more electrophilic and thus more susceptible to attack by water. Since Si–O groups are strongly electron-withdrawing (even stronger than –OH), the most basic silanol species are silanol in monomers or weakly branched oligomers, which are therefore the most likely to be protonated.

The reaction rate constant for hydrolysis is about 30 times the water-producing condensation reaction rate constant and at least 200 times higher than the reaction rate constant for the alcohol producing condensation reaction. As a consequence, a large amount of hydrolyzed species is present at the moment condensation becomes significant. The condensation at the beginning will happen between monomers, the concentration of which will drop eventually to zero value. Further condensation can only proceed through condensation between the bigger counterparts. Hence aggregation in the acid catalyzed system is termed as cluster–cluster aggregation. This is different from the base catalyzed systems where the clusters react selectively with monomers.

The degree of hydrolysis of a monomer, the extent of branching, and the rates and mechanisms of these secondary reactions determine the structure of the solid particles (or clusters) in the sol. Depending on synthesis conditions, the structure of the particles in the sol can vary between nearly linear polymer and well branched polymer structure. As already explained a variety of parameters influence the structural formation kinetics. The most important parameters are the type of alkoxysilane and its functionality, type and amount of catalyst used, amount of water, temperature and reaction time as well as type and amount of mutual solvent.[16] The pore structure of a polymeric sol derived silica membrane depends on the structure of the inorganic polymer clusters in the sol and how these polymeric clusters are packed during the film

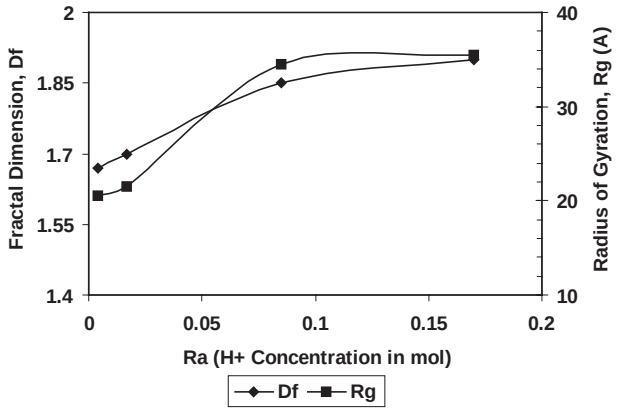

Figure 5. Correlation of fractal dimension (Df) and radius of gyration (Rg) of silica polymers to the reactivity of the synthesis solution (After Ref. [26]).

formation process. The membrane microstructure in turn will affect the gas permeation and separation properties.

Nair et al.[42] reported on the conditions under which silica polymers, suitable for microporous membranes, could be prepared by these sol-gel reactions of TEOS. By controlling the amount of reactants they shown that a variety of polymeric silica structures could be obtained.[43] Figures 5 and 6 show the effect of the amount of catalyst on the structure of the fractal ag-

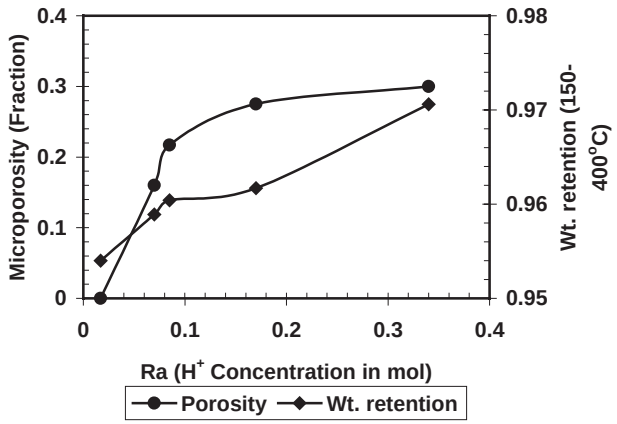

Figure 6. Correlation of reactivity of solution to weight retention during wet gel to xerogel transition and to the microporosity of the calcined gel (After Ref. [26]).

gregates of the silica sol and thus on the porous behavior of the gels made by drying and calicining these sols. In the figures R_a represents the amount of catalyst in the reactant mixture in comparison to the amount of silicon ions. The size and shape of aggregates after aging 40 days in room temperature is shown in Figure 5. The pattern of increase is also reflected in the microporosity values of the gel shown in Figure 6.

de Lange et al.[38–40,44] reported that drying atmosphere is very important in deciding the final pore structure of the silica gels and membranes. Partially hydrolyzed silica sol samples prepared with sub-stoichiometric amounts of water showed great dependence on drying atmosphere. For an R_w (molar ratio of water to TEOS in the synthesis mixture) value of 1, de Lange et al. reported a change in nitrogen sorption amount (at 78 K) from 120 cc/gm for gels dried under ambient conditions to 20 cc/gm for gels dried at 40°C and 60% relative humidity. Because of the effect of drying rate on the pore structure development absolute comparison of gel and membrane properties is difficult. However for membranes and gels made under controlled conditions the pore structure of the gel can give a good indication of the membrane structure as reported by Nair et al.[27]

Figure 7 compares the changes in microporosity values of the gel to the gas permeation behavior of the supported membranes made from similar silica sols. It is shown in Figure 7(a) that the increase in porosity of gel increases the permeation of helium gas molecules through the membrane. However, as shown in Figure 7(b), this increase in permeation may not necessarily reflect an increase in He/N_2 selectivity available through the membrane. The selectivity in fact decreases with increase in porosity. Same is the case with activation energy for helium permeation through the membrane. By properly controlling the reactant conditions Nair et al.[45] showed that molecular sieving membranes could be prepared and the membrane gave He/N_2 ideal selectivity values as high as 1230 at 408 K.

Nair et al.[27] reported the mechanism of pore formation in silica pores. The primary pore size is made by the porosity of the fractal polymers. This size probably remains the same irrespective of the growth of the polymers eventually contributing a great portion of the ultra micropores. The secondary (leakage) pore structure, on the other hand, depends on the growth of the polymers. The polymeric growth seems to amplify the presence of these nonselective pores in the membrane. Hence these bigger pores might be the interfractal voids produced by the opaqueness of the polymers.[16,36] The sizes of these secondary pores are difficult to be quantified.

Since the late 1980's, several research groups have reported synthesis of various microporous inorganic membranes by the polymeric route of the sol-gel method. Burggraaf and co-workers[3,13,25,34,35,46] pioneered in the processing of microporous membranes by the polymeric route. The membranes in

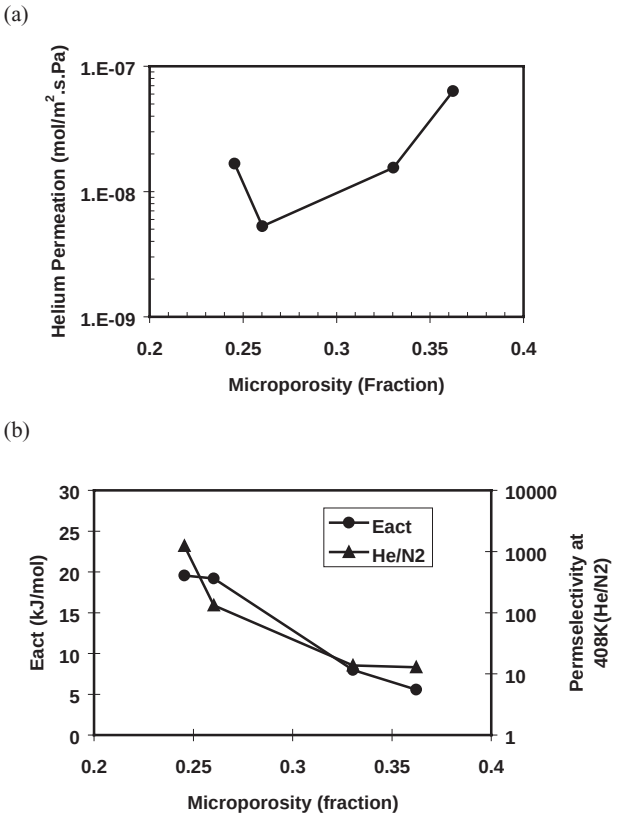

Figure 7. Correlation of microporosity of the gel to helium permeance (a) and activation energy for helium permeance (E_{act}) and He/N_2 selectivity at 408K (b) (After Ref. [26]).

this case were prepared on a mesoporous substrate by a sol dipping process. They have synthesized silica membranes showing activated diffusion for He and H_2. The thickness of the membrane was only 50 nm. A very high separation factor of 200 at 200°C was reported between H_2 and propylene. de Lange[38–40] has made ultra thin (60 nm) microporous membranes with pores of molecular dimensions of 0.5–0.7 nm. Gas transport was activated for hydrogen ($E_{act} = 21.7$ kJ/mol) and molecular sieve like separation factors are obtained for H_2/C_3H_6 mixtures (200 at 260°C).

Maier et al.[47] reported the sol-gel synthesis of a variety of microporous gels by the polymeric route. They succeeded in obtaining average pore sizes of 0.6 nm for zirconia, 0.7 nm for titania and 1 nm for silica and alumina on

unsupported membranes. Supported silica membranes made on alumina/silica supports with average pore radius of 1 μm showed activated diffusion. However the same on alumina ($d_{av} = 20$ nm) or Vycor glass ($d_{av} = 4$ nm) supports showed only Knudsen flow. de Vos et al.[48–50] reported on the formation of defect free silica membranes in a high purity environment. The membranes showed molecular sieving behavior and pore size reduction on calcination at higher temperatures. The polymeric sol approach has also been extended to prepare supported microporous titania membrane with pore diameter in the range of about 0.5 to 1 nm.[51]

The polymeric sol can be also prepared by hydrolysis and condensation in two steps.[16,52–54] The two-step sol-gel approach appears to provide a greater pore size tailorability allowing superior gas separation performance over single-step sol-gel method. Diniz da Costa et al.[55] compared microstructure and gas separation properties of microporous silica membranes prepared from silica sol of same composition (molar composition of 1.0 TEOS, 3.8 ETOH, 6.0 H_2O, 0.1 1 M HNO_3) respectively, but synthesized by one step and the two-step methods. In the two step method, hydrolysis and condensation of TEOS were conducted first with smaller amounts of water and acid (molar composition of 1.0 TEOS, 3.8 ETOH, 1.0 H_2O, 7.0×10^{-4} 1 M HNO_3) at 60°C for 3 hrs. Additional water and acid were added to the system at room temperature. The two-step method gives a weakly branched silica sol, resulting in silica membrane with smaller pore size than that prepared by the one step method. Thus, compared to the silica membrane prepared by the one-step method, the two-step sol-gel derived silica membrane shows better gas separation properties, with a lower gas permeance and higher activation energy for diffusion of the large gas molecules.

Synthesis by Particulate-Sol and Template Methods

Microporous amorphous inorganic membranes can also be prepared from particulate sol containing small silica or mixed-oxide particles. This method was based on compacting nanoscale ceramic particles prepared by the sol-gel method. Asaeda and co-workers[28–33] reported processing of the silica colloidal sol by hydrolysis and condensation of TEOS in the presence of a catalyst, followed by boiling of the sol to grow the particles. A hot coating method was suggested to be the best method to process crack free membranes. In a typical experiment, Asaeda et al.[29] used three kinds of sols prepared with different reactant composition as listed in Table 3. The sols have silica particle sizes of 31.4 nm, 11.9 nm and 4.8 nm, which decreases with increasing water to TEOS ratio in the sol. The pore size of the unsupported silica membranes derived from these sols increases with the particle size. Sols with particles

Table 3. Characteristics of the Sols Prepared Under Different Conditions and the Pore Size of the Gels Derived from These Sols

	TEOS (gm)	H_2O (gm)	HNO_3 (gm)	Sol Particle Diameter (nm)	Membrane Pore Diameter (nm)
Sol-A	20	10	0.5	31.4	10
Sol-B	10	20	0.5	11.9	4
Sol-C	5	25	0.5	4.8	1

(From Ref. [29].)

smaller than 5 nm can give microporous silica membranes with pore diameter of about 1 nm.

To prepare the supported membranes, these sols were coated on a hot α-alumina support (at support temperature of about 200°C) 3 times each for processing the membranes. Silica membranes formed by the progressive coating of the sols containing smaller silica particles were prepared. The pore sizes of each layers, determined by the particle sizes in the sol used in coating the layer, are respectively 10 nm, 4 nm and 1 nm. Such a composite membrane showed excellent gas permeation and separation properties. Propylene/propane perm-selectivity values as high as 75 were measured on the membrane at 35°C.[30] Chu and Anderson[56] also reported the formation of microporous silica gels by the particulate route. They have shown that highly porous gels with pore sizes of 1–2 nm could be prepared by the colloidal route. Munoz-Agudo and Gregorkiewitz[57] made colloidal silica based membranes using sol-gel procedures starting from sodium silicate solutions. The pore size was measured as 1.6 nm and porosity as 35%. These membranes were thermally stable up to 873 K. Gas transport characteristics showed intermediate behavior between Knudsen and surface diffusion. The reproducibility of membrane synthesis was very high.

Asaeda and co-workers recently reported synthesis of microporous silica–zirconia membranes exclusively from colloidal particles.[58,59] They also reported that silica membranes with pore sizes smaller than 0.5 nm could be prepared by this colloidal processing method.[33,58] These microporous silica membranes exhibit excellent gas separation properties. For example, for such a sol-gel derived silica membrane of 1 μm in thickness, Asaeda and Yamasaki[33] reported very high hydrogen permeance of (1.3×10^{-6} mol/m^2/s/Pa) with ideal hydrogen to propane selectivity of 6300 at 300°C. Tsuru et al.[58] also reported H_2/N_2 ideal selectivity as high as 210 at 500°C for a similar sol-gel derived silica membrane.

The exact structure of these silica particles has not been reported. However, under the conditions of synthesis (with acid as catalyst) it is unlikely

that dense particles of silica could be formed. It appears that the pore size of the membrane is directly related to the particle size, rather than the particle microstructure. Therefore, the advantage of this method is that pore size control of the membrane could be easily achieved by processing silica particles of controlled sizes. On the negative side, the supported membranes is prepared by a tedious progressive coating method.

The third method of microporous silica membrane processing involves the use of templates. Mainly two types of templates have been used for tailoring porous structures. In the first case surfactant molecules, which could arrange matrix molecules around them by means of non-covalent interactions, are incorporated in the matrix. The burn-out of the template leaves a residual porosity in the membrane, as shown in Figure 4(c). The control of pore size and shape could be easily achieved by this method. Julbe et al.[60] reported the processing of microporous silica gels with pore sizes in the range of 3–7 Å by employing non-ionic surfactants. These surfactants formed a shell around the silica aggregates preventing them from aggregation and leaving a residual porosity on their burnout. The range of pore sizes that could be achieved by this method is limited by the chain length of the surfactant molecule. Raman et al.[61] suggested a possible range of pore sizes from 15 Å to 45 Å.

The second case involves the use of organic ligands and polymers, which are bonded covalently to the siloxane matrix. Raman and Brinker[62] made sols via the co-polymerization of methyltriethoxysilane (MTES) and TEOS. On pyrolysis of the methyl ligands membranes with microporous structure have been retained. A similar method using 3-methacryloxypropyl trimethoxysilane (MPS) and TEOS was reported by Cao et al.[63] Membranes made from sols containing 20 mol% MPS were microporous, with CO_2/N_2 ideal selectivity values as high as 44.

The use of covalently bonded ligands also helps to control the hydrophobicity of the silica gels and membrane. Hydrophobic silica gels could be made by incorporating alkoxy radicals together with alkyl radicals. Schwertferger et al.[64] and Liu and Komarneni[65] reported on the surface area, density and hydrophobicity of a variety of silica gels made by this method. de Vos et al.[50,66] reported the formation of silica membranes with hydrophobic properties using a combination of MTES and TEOS as in the case of Raman et al.[61] These membranes are reportedly more stable against water vapor than their hydrophilic counter parts.

Coating Methods for Microporous Membrane Formation

Dip coating (slip-casting) is the most common method used to coat microporous layer on a porous support. In this method the support substrate is

either tangentially or vertically dipped into the sol and withdrawn without creating surface tears or non-uniform deposits.[38–40,46] Dipping periods from a few seconds to few minutes have been reported based on the sol and substrate properties. The thickness of the layer formed could be controlled by manipulating the dipping time as shown in Figure 3. Dip sol of particles are generally made with a binder, and those of polymers without the presence of a binder. The dipped supports are usually dried under controlled conditions first to evaporate the solvent remaining in the pores of the layer formed and in the support pores, and then calcined at the required temperature.

The slip-casting method can be also applied to coat the microporous silica membranes on the tubular support.[57] In this case the tubes are firstly filled with the dip solution and then emptied by lifting the tube from the surface. Unlike the dip coating process detailed in the last paragraph the dip solution here is moved relative to a static support surface. The method showed reliable performance. Another method for preparing the supported microporous membranes uses a hot substrate in order to avoid penetration of particles into the support pores.[28] The substrate here is heated to a temperature of about 200°C before coating it with a particulate sol. It was found that heated substrate ensures a lesser infiltration of the particles compared to dip coating process with a heated substrate. This is probably because the immediate evaporation of the liquid component on the heated substrate pore destructs the vapor/liquid interface, lowering the capillary force. As a result, the driving force for the slip-casting is reduced.

It should be pointed out that due to much small pore size the microporous ceramic membrane offers much higher resistance than the mesoporous ceramic membranes. Typical thickness of mesoporous ceramic membranes is about 5 μm. For a microporous silica membrane to have permeance similar to a 5 μm thick mesoporous γ-alumina membrane, the thickness of the microporous membranes should be around 50 nm. Therefore, very thin (less than 100 nm) microporous silica membrane layers should be coated on porous ceramic supports. Since defects or pinholes are more likely formed on the thin films, the coating conditions and substrate quality become very important in preparation of supported microporous ceramic membranes.

The theoretical factors that affect formation of mesoporous ceramic membranes, as discussed in Section 2.1, also affect film formation of microporous membranes on the support surface. A control of contacting time and viscosity of the suspension should allow the formation of crack-free membrane layers of desired thickness. To coat thin silica films, polymeric silica sol with very dilute solid concentration is used. The thermal expansion mismatch between the substrate and the thin layer may become a problem under certain conditions. The size of the polycrystalline grains from which the substrate surface is made of is another important factor. In practice the thickness of the

Table 4. Summary of Microporous Ceramic Membranes Prepared by the Sol-Gel Method and Permeation/Separation Data Measured

Membrane Material	Method	Permeation/Separation Data Available (Gas Phase)	1st Author, Year	Ref.
Silica	Polymeric	He, H_2, CO_2, CH_4, C_3H_6	Uhlhorn, 1990	[46]
Silica	Col./Poly.	He, H_2, N_2	Kitao, 1990	[276]
Silica	Colloidal	Ethanol/(Toluene, Benzene, cyclo-Hexane)	Asaeda, 1992	[29]
Silica	Colloidal	Ethanol/(Toluene, Benzene, cyclo-Hexane)	Asaeda, 1992	[29]
Silica	Polymeric	He, N_2, O_2, CO_2	Brinker, 1993	[37]
Silica	Polymeric	H_2, N_2, i-C_4H_{10}	Maier, 1993	[277]
Silica	Col./Poly.	He, Ar, N_2, CH_4, C_2H_4, C_2H_6, C_3H_6, C_3H_8	Asaeda, 1994	[30]
Titania	Polymeric	He, O_2, N_2, C_3H_6	Peterson, 1994	[278]
Silica	Polymeric	Water/(Methanol, Ethanol. 2-Propanol), Methanol/MTBE	van Gemert, 1995	[279]
Silica	Polymeric	He, H_2, CO_2, N_2, CH_4, C_3H_6, i-C_4H_{10}	de Lange, 1995	[39]
Silica	Polymeric	He	Brinker, 1995	[53]
Silica	Poly./Template	He, CO_2, N_2, CH_4, SF_6	Raman, 1995	[62]
Silica/Alumina	Col./Poly.	He, C_3H_6, C_3H_8	Nair, 1996	[42]

MARCEL DEKKER, INC. • 270 MADISON AVENUE • NEW YORK, NY 10016

Silica	Poly./Template	He, N_2, C_3H_6, SF_6	Cao, 1996	[63]
Silica	Poly./Template	He, CO_2, N_2, CH_4, C_3H_6, SF_6	Raman, 1996	[61]
Silica	Polymeric	He, Ar, O_2, N_2, C_3H_6, C_3H_8, n-C_4H_{10}, i-C_4H_{10}	Nair, 1996	[42]
Silica–Zirconia	Colloidal	He, H_2, CO_2, N_2, O_2, Vapor/Liquid Phase	Tsuru, 1998	[58]
Silica	Polymeric	Methanol/MTBE	Nair, 2000	[70]
Silica–Zirconia	Col./Poly.	Water/IPA	Asaeda, 1996	[31]
Silica–Zirconia	Colloidal	Ethanol/(Benzene, cyclo-Hexane), Methanol/ (Benzene, MTBE)	Tsuru, 1998	[58]
Silica	Polymeric	H_2, CO_2, O_2, N_2, CH_4	de Vos, 1998	[50]
Silica	Poly/Template	H_2, N_2, CH_4, CO, CO_2	Tsai, 2000	[67]
Silica	Poly/Template	H_2, CO_2, N_2, CH_4, C_2H_6, C_3H_6, SF_6	Kim, 1992	[280]
Silica	Colloidal	H_2, CO_2, N_2, CH_4, C_2H_6, C_3H_8	Asaeda, 2001	[33]
Silica	Polymeric	H_2, C_3H_8	Schafer, 2001	[54]
Silica	Polymeric	He, H_2, CO_2, O_2, CH_4, N_2	Diniz da Costa, 2002	[55]

MARCEL DEKKER, INC. • 270 MADISON AVENUE • NEW YORK, NY 10016

superimposed layer in limited by the grain size. Subsequently, an intermediate layer with finer particles is generally necessary while making sol-gel derived microporous layer on bigger grain sized substrates. Since the film is very thin, the support surface characteristics play a significant role in deciding the layer properties in practice. In most studies, the microporous silica films are coated on the surface of the sol-gel derived mesoporous γ-alumina membranes.

The presence of particular matters in the air during coating of microporous silica membranes can introduce significant pinholes or defects in the film formed. de Vos and Verweij[48,49] reported coating of microporous silica membranes of about 30–50 nm in thickness on γ-alumina support under the clean-room conditions. Clean-room coating avoids formation of pin-holes in the thin silica film. The regular sol-gel derived γ-alumina membrane surface often does not provide sufficient smoothness to obtain high quality microporous silica membranes. This 4 nm pore sol-gel derived γ-alumina surface was further modified with a 200 nm thick γ-alumina[48,49] or template derived silica layer[67] with finer pore size to improve the surface smoothness. The ultrathin silica membranes formed on these improved substrate, or prepared under clean-room conditions exhibit much higher selectivity as compared to the microporous silica membranes reported earlier.

It should be noted that coating conditions may also affect the pore size of the supported silica membranes. It is known that the pore size control of silica gels could be obtained by controlling the extent of gel shrinkage and collapse of the gel network. The easiest way to achieve this is to control the composition of the pore fluid.[68] Change in hydrogen bond formation inside the gel pores can cause changes in capillary pressure while removing solvent. This also changes the stress distribution inside the pore, causing differences in shrinkage rates of the gel. As a result, it also affects the pore size of the final dry membrane.

2.3 Characteristics of Sol-Gel Derived Silica Membranes

Permeation and Separation Properties

Table 4 summarizes microporous silica membranes and gas separation data reported by several research groups. Some microporous silica membranes have shown very good liquid/vapor and gas separation properties. Tables 5 and 6 list respectively some results of pervaporation and permeation separation of liquid and vapor/gas mixture by the microporous silica membranes. As shown in Table 5, ethanol/toluene separation factors of about 300 were measured at 323 K. Ethanol/benzene separation factor of 200 and ethanol/cyclo-hexane separation factor of 500 were also reported by the same authors.

Table 5. Summary of Reported Results on Pervaporation Sepration by Microporous Sol-Gel Derived Silica Membranes

Feed (A)	Feed (B)	Feed, B%	Temperature	Selectivity, A/B	Flux, Kg/m^2.hr	1st Author, Year	Ref.
Water	MeOH	90% (mol)	–	60	0.2	Asaeda, 1996	[31]
Water	EtOH	90% (mol)	–	110	–	Asaeda, 1996	[31]
Water	IPA	90% (mol)	–	90	0.2	Asaeda, 1996	[31]
Ethanol	Toluene	90% (mol)	323 K	280	5	Asaeda, 2001	[33]
Ethanol	Benzene	90% (mol)	323 K	~500	5	Asaeda, 2001	[33]
Ethanol	c-Hexane	90% (mol)	323 K	200	5	Asaeda, 2001	[33]
Water	MeOH	98 (wt%)	333 K	400	0.05	van Gemert, 1995	[279]
Water	EtOH	98 (wt%)	343 K	200	0.15	van Gemert, 1995	[279]
Water	PrOH	98 (wt%)	343 K	600	0.16	van Gemert, 1995	[279]
MeOH	MTBE	91 (wt%)	308 K	18.7	0.04	van Gemert, 1995	[279]
MeOH	MTBE	80% (mol)	323 K	1500	3.2	Otani, 1997	[69]
Water	IPA	60% (mol)	355 K	1150	2	Asaeda, 1996	[31]
MeOH	MTBE	90 (wt%)	323 K	260	0.26	Nair, 1998	[27]
EtOH	c-Hexane	90% (mol)	323 K	2000	2	Tsuru, 2000	[58]
MeOH	Benzene	80% (mol)	~350 K	1000	2	Tsuru, 1998	[58]

MARCEL DEKKER, INC. • 270 MADISON AVENUE • NEW YORK, NY 10016

Table 6. Summary of Reported Gas Separation Results of Microporous Sol-Gel Derived Silica Membranes

Gas (A)	E_{act} of A (kJ/mol)	Gas (B)	Temp. (K)	Pressure (atm)	Selectivity A/B	Permeance (10^{-7}mol/ m^2.s.Pa)	Mechanism	1st Author, Year	Ref.
H_2	11	C_3H_6	473	3	156	26	Molecular-Sieving	Uhlhorn, 1990	[46]
CO_2	10	CH_4	373	–	65	10	Molecular-Sieving	Uhlhorn, 1990	[46]
H_2	8.3	N_2	543	3	185	0.5	Molecular-Sieving	Kitao, 1990	[276]
He	4	N_2	543	3	326	1	Molecular-Sieving	Kitao, 1990	[276]
He	0	C_3H_8	308	1	~200	15	Molecular-Sieving	Asaeda, 1994	[30]
C_3H_6	–	C_3H_8	308	5	75	1	Sorption	Asaeda, 1994	[30]
C_2H_4	–	C_3H_8	423	1	91	14	Molecular-Sieving	Asaeda, 1994	[30]
H_2	~14	CH_4	473	3	30	20	Molecular-Sieving	de Lange, 1995	[38–40]
H_2	~14	i-C_4H_{10}	473	3	200	20	Molecular-Sieving	de Lange, 1995	[38–40]
CO_2	–	CH_4	298	–	72	0.7	Molecular-Sieving	Raman, 1995	[62]

He	–	SF_6	298	–	328	0.5	Molecular-Sieving	Raman, 1995	[62]
He	0	SF_6	323	2.76	>2400	10	Molecular-Sieving	Cao, 1996	[63]
C_3H_6	–	SF_6	323	2.76	678	3	Molecular-Sieving	Cao, 1996	[63]
CO_2	–	N_2	323	2.76	44	100	Molecular-Sieving	Raman, 1996	[61]
He	~20	N_2	408	1.35	1230	0.9	Molecular-Sieving	Nair, 1997	[70]
He	~20	C_3H_8	303	1.35	200	0.17	Molecular-Sieving	Nair, 1997	[70]
H_2	8	N_2	423	1	76	10	Molecular-Sieving	de Vos, 1998	[50]
CO_2	–	CH_4	298	1	326	0.1	Molecular-Sieving	de Vos, 1998	[50]
H_2	8	CH_4	298	1	844	10	Molecular-Sieving	de Vos, 1998	[50]
H_2	15.7	CO_2	773	1	210	5.8	Molecular-Sieving	Tsuru, 1998	[58]
He	–	H_2	773	1	5.2	10	Molecular-Sieving	Tsuru, 1998	[58]

The separation mechanism was reported as a combination of molecular sieving and adsorption mechanism. Water/iso-propanol separation factors as high as 1150 were measured on silica composite membranes by the same authors. The membrane used was a silica–zirconia membrane, with a top layer made from a polymeric composite sol. The pore size of the top layer was around 5 Å. The mechanism of separation was competitive sorption of water on the silica membrane pores and surface.

It should be noted that almost all the reported separation factors for the sol-gel derived silica membranes were measured between small and large molecules. The same trend could be visualized in the gas separation results shown in Table 6. Almost all the results were obtained between gas molecules of obvious size difference. The major exception is the separation of C_3H_6 from C_3H_8 reported by Asaeda et al.[30] Based on the gas permeance versus kinetic diameter of the permeating molecule, many authors have suggested pore sizes ranging from 3–6 Å for silica membrane pores.

It can be assumed that molecular-sieving plays an important role in the separation process. But Otani et al.[69] clearly showed that adsorption also plays an important role too. They used silica–zirconia membranes of 3 different pore sizes of 1, 1.5 and 2 nm for pervaporation separation of methanol/methyl ter-butyl ether (MTBE) at 323 K. They found that the methanol permeation flux and methanol/MTBE separation factor increase with increasing membrane pore size. Nair et al.[27] also studied pervaporation separation of

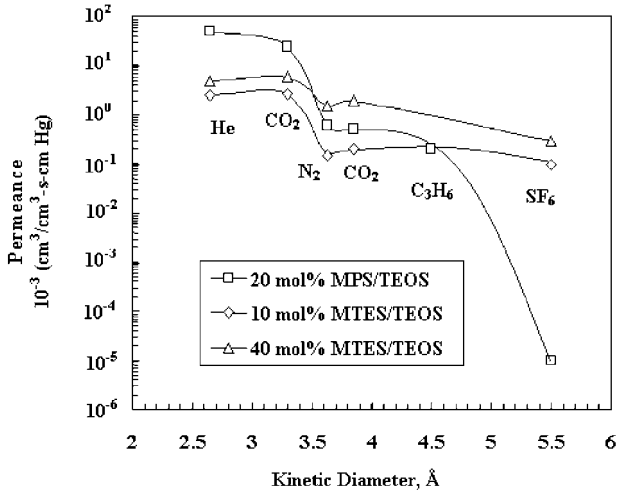

Figure 8. Permeance of hybrid silica membranes versus kinetic diameter of gas probe molecules (Redrawn from Ref. [61]).

methanol/MTBE by silica membranes made by the polymeric route. They reported that the ratio of diffusivity values calculated from sorption kinetic data is comparable to that measured by the pervaporation experiments. The ratio of the single component and mixture sorption studied, however, did not provide evidence showing any appreciable differences in the amounts adsorbed between the molecules. Based on the pervaporation and sorption data they have concluded that diffusion is the selectivity determining mechanism.

Figures 8, 9 and 10 show the single gas permeance versus the kinetic diameter of the gas for the sol-gel derived microporous silica membranes as reported by several research groups. Nair et al.[70] showed that the permeance of the gas molecules through the membranes decreases significantly as the molecular size increases from He to N_2. Based on the insignificant permeation values of N_2 compared to that of He the authors estimated a practical pore size of the silica membranes between the sizes of He (2.6 Å) and N_2 (3.64 Å). According to them the bigger molecules like N_2 may be permeating through the secondary inter-aggregate pores and the high perm-selectivity values between He and N_2 show that only a negligible portion of the cumulative pore volume belong to the secondary pores. The curves in Figure 8 follows the same trend as that of Figure 9 and hence indicate similarity in pore sizes.

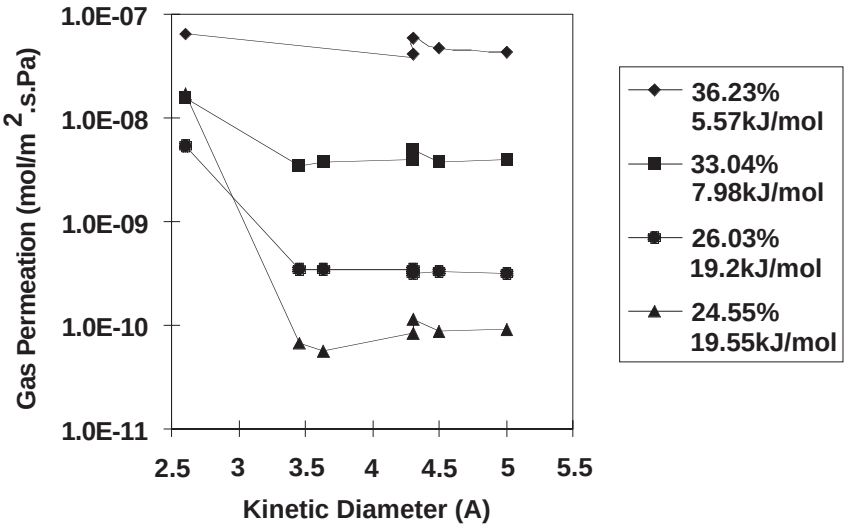

Figure 9. Dependence of gas permeation to kinetic diameter of the permeating molecules and to the synthesis history of the membranes. Legend shows the microporosity of the membrane material and activation energy for helium permeation (After Ref. [26]).

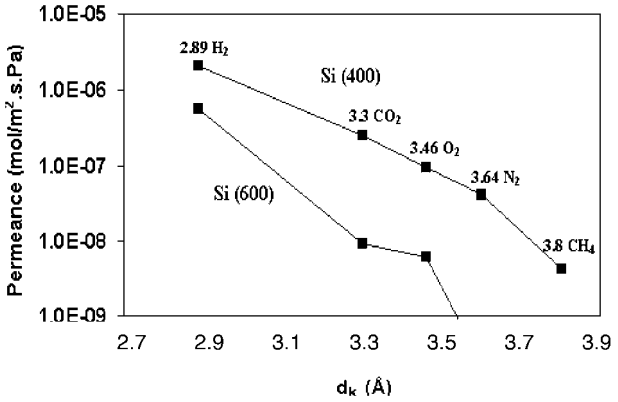

Figure 10. Permeance of various gases at 200°C for two sol-gel derived silica membranes calcined at 400 and 600°C (Redrawn from Ref. [48]).

However, the SF_6 flux of one of the membranes shown in Figure 8 is significantly lower than the values of hydrocarbon gas molecules. SF_6 molecules may be even less permeable through the secondary pores.

de Vos and Verweij[48–50] on the other hand reported permeation results at higher temperatures for silica membranes calcined at 400 and 600°C as shown in Figure 10. The permeance of all the molecules with a permeance above 1.0×10^{-9} mol/m^2.s.Pa (probably the limit of detection of the equipment used) follows a linear dependence on their sizes. Based on the permeation data they estimated a pore size value between the sizes of N_2 (3.64 Å) and CH_4 (3.8 Å) for their membranes calcined at 600°C and a pore size value between 3.8 and 5.5 Å for the membranes calcined at 400°C.

Table 7 shows the calculated diffusion coefficients of H_2 and CO_2 molecules through three different silica membranes, with different values of apparent activation energy for hydrogen permeation (7.4, 21.7 and 11.0 kJ/mol respectively for membranes samples 1, 2 and 3 listed in Table 7). The membranes showed an appreciable difference in diffusivity values between H_2 and CO_2 molecules. It has been reported by the author[44] that the calculated activation energy for diffusion of H_2 and CO_2 molecules through the silica membranes is higher than the values reported in the case of 4 Å zeolites.[71] This indicates pore sizes of these silica membranes smaller than 4 Å.

As discussed above, the sol-gel derived silica membranes prepared by different groups have different pore sizes. Such differences are certainly caused by the different preparation and calcination procedures for these silica membranes. However, the method of classification of micropore size itself should be reconsidered based on these evidences. Though the quantification or

Table 7. Permeation and Diffusion Data of H_2, CO_2 and CH_4 at 298 K for the Sol-Gel Derived Silica Membranes

Membrane	Gas	Permeance ($mol.m^{-2}.s^{-1}$) 298 K	Henry Constant ($mol.kg^{-1}.Pa^{-1}$) 298 K	Diffusion Coeff. ($m^2.s^{-1}$) 298 K
Sample 1	H_2	6.8×10^{-2}	1.44×10^{-7}	1.43×10^{-10}
	CO_2	3.6×10^{-2}	1.42×10^{-5}	7.68×10^{-13}
	CH_4	0.27×10^{-2}	1.57×10^{-6}	5.2×10^{-13}
Sample 2	H_2	2.28×10^{-2}	1.44×10^{-7}	4.8×10^{-11}
	CO_2	3.0×10^{-2}	1.42×10^{-5}	6.4×10^{-13}
Sample 3	H_2	12×10^{-2}	1.44×10^{-7}	2.5×10^{-10}
	CO_2	4.2×10^{-2}	1.42×10^{-5}	9.0×10^{-13}
	CH_4	0.78×10^{-2}	1.57×10^{-6}	1.5×10^{-12}
	i-C_4H_{10}	0.8×10^{-2}	7.30×10^{-5}	3.3×10^{-14}

(From Ref. [44].)

pore sizes based on cut-off values is a successful method in determining the pore sizes of UF or MF membranes, the application of the same principles for microporous membranes should be treated more carefully. The conditions of testing such as temperature and pressure can significantly alter the measured parameters such as permeance or selectivity. Based on pervaporation studies Nair et al.[42] suggested that the pore size values measured by these methods have only a practical value. As far as membrane separation is concerned, molecular sieving means only that the permeance measured is insignificant or immeasurably low. It is futile to classify pore sizes of membranes in absolute terms based on only such permeation studies.

Thermal Stability and Its Improvement

Sol-gel derived microporous silica films and membranes suffer from thermal and hydrothermal stability problems.[33,41,72–74] As with silica gels prepared by other methods, the sol-gel derived microporous silica membrane is not thermally stable at high temperatures, especially under humid atmosphere. Figure 11 compares the pore size distributions of an unsupported silica membrane before and after heat-treatment in humid air at 600°C for 30 hours. For pure silica membrane, the heat treatment results in 89% reduction in the surface area and a loss of 87% micropore volume. These results agree with the previous studies which indicated similar effects of steam and heat on the stability of silica.[44,74] de Lange et al.[74] also reported that the supported

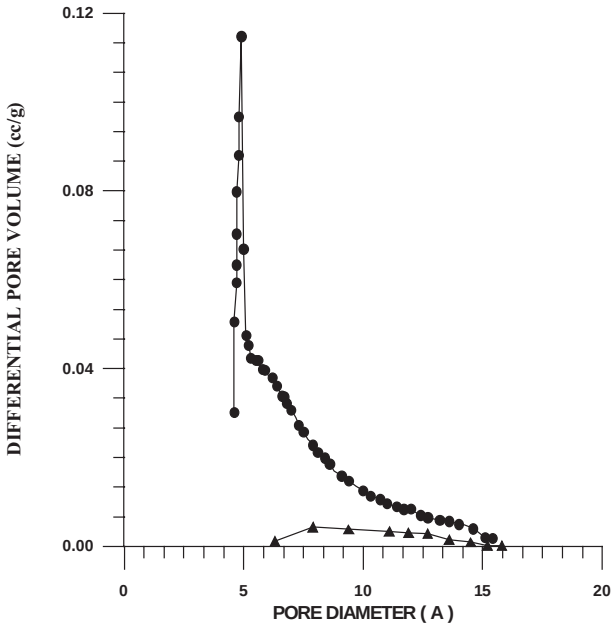

Figure 11. Comparison of the pore size distribution of a sol-gel derived silica membrane before (●) and after (▲) heat-treatment at 600°C for 30 hours.

membranes exhibited a decrease in permeation rate of gas molecules with aging. Crack growth during densification occurred and hence the activation energy values for permeation were lowered for the aged membranes. de Vos et al.,[66] however, reported an increase of the gas permeance and deterioration of selectivity of the microporous silica membranes during hydrothermal treatment. The membranes were exposed to 25 kPa water vapor at 350°C. After 914 hours of aging under the humid atmosphere the permanence of H_2, He, CO_2 and N_2 increased by 30%, 21%, 42.5% and 778%, respectively.

Table 8. Pore Structure of Pure Microporous Silica and Alumina Doped Silica Membranes

Materials	BET Surface Area (m^2/g)	Average Pore Diameter (Å)	Pore Volume (cm^3/g)
Pure SiO_2	588	6.4	0.24
1.5%Al_2O_3–SiO_2	660	6.5	0.26

(From Ref. [41].)

Obviously, the change in the microstructure of the silica membrane during heat-treatment and aging is due to continuous condensation ($\equiv Si-OH + \equiv Si-OH \Rightarrow \equiv Si-O-Si \equiv$) and sintering which can be enhanced with the presence of water vapor in the atmosphere. When the silica film is supported, these changes in the microstructure may cause growth, or shrink of the pores of the silica film, or may even damage the integrity of the film, deteriorating the separation properties of the microporous silica membrane. Several methods could be potentially used to improve the stability of the sol-gel derived silica membranes. One approach is to dope a small amount of aluminum in amorphous silica.[41] Table 8 compares the pore structure of the pure silica membrane and aluminum doped silica membrane. Both membranes have a similar pore structure. Figure 12 shows the pore size distributions of 3% Al-doped silica membrane prepared by the sol-gel method before and after exposure to dry air at 600°C for 30 hours. Compared with Figure 11, the Al-doped silica membrane exhibits a significantly improved thermal stability.

The binary zirconia–silica microporous membranes may also offer significantly improved stability compared to pure silica membranes.[9,75] However, the pore sizes of silica–zirconia microporous membranes appear larger

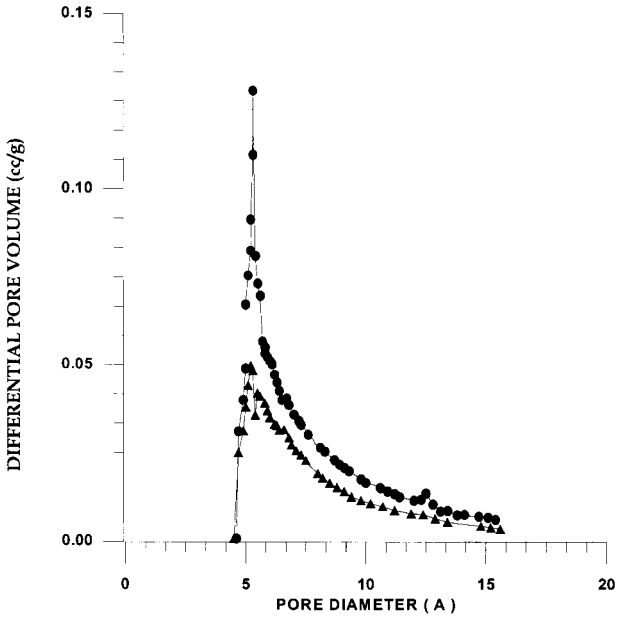

Figure 12. Comparison of the pore size distribution of a 1.5% alumina doped silica membrane before (●) and after (▲) heat-treatment at 600°C for 30 hours.

than the pure silica membranes. It is difficult to prepare the microporous binary inorganic membranes with lower silica content or microporous non-silica membranes. Another interesting approach reported recently was to replace $-OH$ groups on the pore surface by $-CH_3$ group.[66] This makes the microporous silica layer hydrophobic and in principle can also improve its thermal stability by reducing the condensation reaction at high temperatures (in oxygen free-atmosphere). However, the $-CH_3$ groups can be converted to $-OH$ groups in oxygen containing atmosphere at high temperatures. This will limit the applications of the hydrophobic microporous silica membranes to the non-oxidative environments.

3. ZEOLITE MEMBRANES

Zeolites are crystalline aluminosilicates materials having micropores (zeolitic pore) in their structures. Zeolites are built up by various connections of TO_4 (T = Si or Al) tetrahedral which result in the various zeolitic pore sizes and structures. Figure 13 shows several zeolite crystal structures with the sizes of the guest molecules that can pass through the zeolitic pores. General information about zeolites can be found in several reference books (e.g., Refs. [76–78]) and is now available from International Zeolite Association's website on zeolite structure at: www.iza structure.org/databases/. Zeolites are usually obtained as powder of micrometer size by hydrothermal synthesis. The micropore structure of zeolites provides molecular sieving ability in addition to

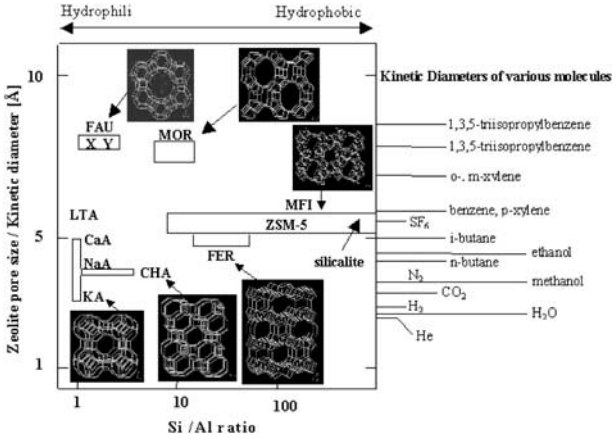

Figure 13. Pore sizes and Si/Al ratios of zeolites (Adopted from International Zeolite Association Database at the website: http://www.iza-sc.ethz.ch/IZA-SC/Atlas).

various unique adsorption properties. High silica zeolites also offer good thermal and chemical resistance. As shown in Figure 13, zeolites can have different pore structure and pore size. The surface properties (hydrophobicity, hydrophilicity, acidity etc.) can be controlled by varying the framework Si/Al ratio and type and concentration of non-framework cations present in the zeolite crystals for charge balance. Because of these properties, zeolites have been used widely as adsorbents and catalysts in various separation and chemical reaction processes.

First attempt to use zeolite in the form of membrane was reported as zeolite embedded polymer membrane.[79,80] These polymer-zeolite composite membranes suffer from poor thermal and chemical stability. Preparation of zeolite embedded inorganic materials was also reported,[81] though pure zeolite membranes are more desirable for practical applications. Pure polycrystalline zeolite membranes were prepared without any substrates.[82,83] These unsupported zeolite membranes have less mechanical strength, so most of the recent zeolite membranes reported are prepared on or within porous substrates. The first work on practically useful supported zeolite membrane was reported in patent literature by Suzuki.[84] Since then various research groups have prepared different types of supported polycrystalline zeolite membranes. Table 9 lists pore structure and physical characteristics of several zeolites which have been extensively studied as the membrane materials in the past decade. The most commonly used supports for zeolite membranes are made of α-alumina and stainless steel. The supported zeolite membranes include a polycrystalline zeolite layer of about 5–30 μm in thickness. In this section, various methods and mechanisms for synthesis of the supported zeolite membranes will be reviewed first next, followed by a summary of structural, physical and permeation/separation properties of the polycrystalline zeolite membranes prepared in the past decade.

3.1 Zeolite Membrane Synthesis

In-situ Hydrothermal Synthesis Method

The most used preparation method is in-situ hydrothermal synthesis. Generally, synthesis solution or gel contains silicon, aluminum, sodium and water. Organic structure directing agents (SDAs, or formerly referred to as templates) may be required for synthesis of some zeolite membranes. The basic procedure in the in-situ hydrothermal synthesis is to bring a support in direct contact with the synthesis solution or gel and then to allow the growth of a zeolite film on the surface of the support under hydrothermal conditions. In some cases, zeolite membrane is formed inside the support pores. Experimental

Table 9. Pore Structure and Physical Characteristics of Common Zeolites Studied as the Membrane Materials

Oxygen Numbers at Window	Zeolite Name	Maximum Pore Size [Å]	Channel Directions	Thermal Stability [°C][a]/[°C][b]	Density [g/cc]	Porosity
8	LTA (NaA)	4.1	3	60/755	1.27	0.47
	CHA	3.7 × 4.2	3		1.45	0.47
10	MFI (ZSM-5, silicalite)	5.3 × 5.6	2		1.79	0.29
	FER	4.3 × 5.5	2		1.76	0.28
12	FAU (NaX, NaY)	7.4	3	660/770[c], 710/795[d]	1.31 (NaX), 1.27 (NaY)	0.50 (NaX), 0.48 (NaY)
	MOR	7.0 × 6.5	2		1.70	0.28
	LTL	7.1	1		1.61	0.32
	BEA	7.6 × 6.4	2			

[a]Temperature at which structural degradation is first observed by powder XRD.
[b]Temperature at which 50% degradation is observed by powder XRD.
[c]NaX(Si/Al = 1.25).
[d]NaY(Si/Al = 1.7).

MARCEL DEKKER, INC. • 270 MADISON AVENUE • NEW YORK, NY 10016

conditions, including the composition of synthesis solution or gel, support material, the manner how the support is in contact with the solution or gel, and hydrothermal synthesis conditions, should be carefully controlled so that the zeolite could nucleate and intergrow into a continuous film on/in the support. The supported zeolite membranes are then separated from the residual synthesis solution or gel, washed, dried and possibly calcined at a high temperature.

The majority of the zeolite membranes reported were of highly silicious MFI type zeolite. These MFI type zeolite membranes are formed in autoclave at 443 to 473 K under autogenous pressure. To remove SDA, which is required for synthesis of MFI type zeolite, membranes were calcined at 673 K to 823 K after hydrothermal synthesis. LTA (NaA) and FAU (NaX, NaY) type membranes could be prepared at 343 to 373 K under atmospheric pressure, and SDAs are not necessary. Preparation of several other zeolite membranes, such as MOR,[85,86] CHA (SAPO34),[87] P-type[88] zeolites, and ETS-4 titanosilicate molecular sieve[89] were also reported. Typical conditions for synthesizing several zeolite membranes are summarized in Table 10.

In many cases, in-situ synthesis of zeolite membranes was conducted in conditions similar to the zeolite powder synthesis. Typical phenomenon of zeolite powder synthesis is shown in Figure 14. Crystallinity of zeolites exhibits S shaped curve against synthesis time. There could be several hours at the beginning of synthesis with no detectable crystal formation. This period is called induction period, and nucleation occurs in this period. Similar phenomenon as powder formation is observed in zeolite A membrane formation. Kita et al.[90] used a gel having a molar composition of 2 Na_2O:2 SiO_2:1Al_2O_3: 120 H_2O for synthesis of zeolite A membranes. They immersed a substrate in the gel at 100°C for several hours. Transition behavior of support surface was observed by SEM. After 1 hour synthesis, the substrate was covered with gel and no crystals were observed, and after 3 hours, the substrate was totally covered with zeolite A crystals of 3 μm in sizes. These changes in surface morphology suggest that the zeolite film was formed with nucleation in the gel near the surface of the substrate. As zeolite membrane was prepared under non-equilibrium condition, synthesis time longer than six hours resulted in the formation of zeolite P, which has higher density than zeolite A.

Zeolite synthesis with nucleation is sensitive to experimental conditions such as synthesis solution/gel composition, pH and temperature. Furthermore, a certain amount of zeolite powder is generally formed during the zeolite membrane formation, while general powder synthesis condition is rarely adapted for membrane preparation. Therefore, finding the proper conditions to prepare desired zeolite membrane requires a lot of try-and-errors. Preparing a synthesis mixture from different reagent sources led to various results, even for almost same compositions. Researchers have studied the effect of alumina and silica sources on preparation of A type[91] and MFI type[3] zeolite membranes. Considering

Table 10. Typical Conditions for Synthesis of Various Zeolite Membranes by in-situ Hydrothermal Synthesis Methods

Zeolite	Composition (Na_2O:SiO_2:Al_2O_3:H_2O: templates)	Substrate	Temperature [°C]	Pressure	Time [h]	Calcined Condition	1st Author, Year	Ref.
Silicalite	0.05:1:0:80:0.1 (TPABr)	SS disk	170	autogeneous	48	500°C-20 h	Sano, 1995	[153]
Silicalite	2:6:0.005:573:1 (TPABr) 1.605:21: 0.105:988.5:1	α-, γ-alumina tube	170	autogeneous	15–24	480°C-8 h	Bai, 1995	[131]
Silicalite	0.053:1:0:14.2:0.15	SS disk	98–185	autogeneous	0.7–6 days	400°C-16 h	Bakker, 1996	[100]
ZSM-5	1.6:1:0:167:1.5 (TPABr)	clay	180	autogeneous	1–5 days	400°C-20 h	Geus, 1992	[130]
NaA	2:2:1:120:0	α-alumina tube	100	atomospheric	3.5	Not necessary	Kita, 1995	[90]
NaY	14:10:1:840:0	α-alumina tube	100–120	–	3–10	Not necessary	Kita, 1997	[151]

MARCEL DEKKER, INC. • 270 MADISON AVENUE • NEW YORK, NY 10016

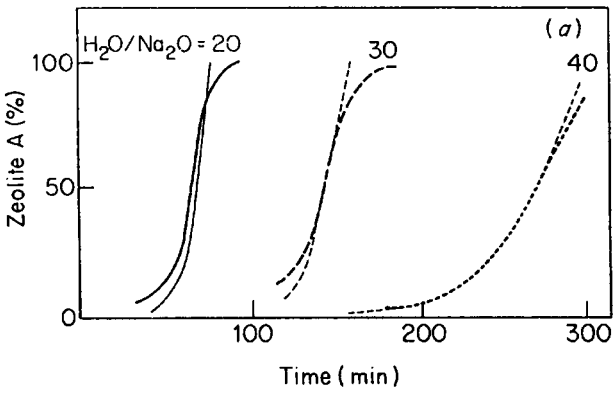

Figure 14. Crystallization curves of in hydrothermal synthesis of zeolite A (After Ref. [274]).

these results, regents generally used are $Al(OH)_3$ and Na_2SiO_3 for preparation of zeolite A and FAU membranes, while aerosol or colloidal silica and tetrapropylammonium (TPA-) bromide (TPABr) or TPAOH were used respectively as the silica source and SDA for preparation of MFI-type zeolite membrane.

Porous substrates (supports) having 0.1 to 10 μm pore diameter are usually used as the supports. α-alumina and stainless steel are the most used materials. Submicron MFI zeolite membranes have been also grown on the sol-gel derived γ-alumina or yttria doped zirconia membranes with pore diameter in the range of about 4 nm.[92] Substrate chemical composition sometimes affects the zeolite membrane preparation. Geus et al.[93] attempted to prepare MFI-type zeolite on several types of porous materials: clay, α-alumina, zirconia and metakaolin. Continuous MFI-type zeolite membrane was only formed on clay support. ANA type zeolite films formed on α-alumina substrate. Zirconia support is hardly dissolved in alkaline solution but MFI crystals were formed in discontinuous form. From these results, they concluded that the alumina dissolved from substrate helped the heterogeneous nucleation of MFI crystals. Dong et al.[92] could grow continuous MFI zeolite films on yttria stabilized zirconia support with oxygen vacancy defects but not on yttria doped zirconia without oxygen vacancy defects.

Substrate material interacts with or may even transport into the coated zeolite film since the zeolite membranes are prepared in alkaline solution.[94,95] Sano et al.[94] and Dong et al.[92] used two different materials as substrate to prepare MFI type zeolite membrane. Synthesis conditions used were the same for the two kinds of supports. Zeolite membrane formed on stainless-steel[94] or zirconia[92] support contains much lower aluminum (i.e., Si/Al ratio of ∞ on stainless steel), while the membrane formed on a porous α-alumina support

has much high aluminum content (Si/Al ratio of 300–400). Pan and Lin[95] found that aluminum can transport via solid state diffusion from the alumina support into the zeolite layer during the calcination step. At 650°C aluminum from the support can penetrate into the zeolite layer in the range from 2 to 5 μm from the interface within 6 hr. Aluminum from the support can also get into the framework of the zeolite layer via dissolution into the synthesis sol. The amount of aluminum transferred to the zeolite layer by the first mechanism depends respectively on calcination temperature and time, and that by the second mechanism depends on the aluminum solubility in the synthesis solution and hydrothermal synthesis conditions.

The position of substrate during synthesis is also an important factor. Figure 15 illustrates some typical positions of substrate reported in the literature. In case of using disk-shape substrate, typically the substrate is placed at the bottom, as shown in Figure 15(a).[83,88,97] Vroon[97] reported interesting results on the in-situ hydrothermal synthesis of silicalite films on porous alumina disk supports. When the porous disk support was first placed horizontally on the bottom of an empty autoclave which was then gradually filled up with the synthesis solution (by pouring the solution along the autoclave wall), they could obtain good quality silicalite membranes. However, continuous zeolite films could not be formed on the support when the synthesis solution was poured directly on the surface of the support disk or the support disk was immersed into the synthesis solution.

Dong and Lin[88] found that whether a continuous P zeolite film could be grown on the alumina support by the in-situ synthesis method depends on the position of support in the autoclave during synthesis. Only small patches of crystals were found scattering on the surface of the support when it was vertically placed in the autoclave during synthesis. Non-continuous film containing large irregular crystals was formed on the upper surface of the horizontally placed support. Continuous zeolite film could be grown only on the upper (polished) surface of the alumina support disc placed in a slanting position during synthesis. Kita et al.[90] also synthesized zeolite membranes with the substrate placed in a slanting position in the synthesis solution.

Disk-shaped substrates were also placed on the surface of the synthesis solution for in-situ synthesis of zeolite membranes, as shown in Figure 15(b).[98–100] Zeolite films were grown on the bottom of the disk substrates in contact with the synthesis solution. Tubular type substrate is generally placed vertically and the zeolite membranes were formed on the outer surface of substrates in the most cases. Noble and co-workers sealed one end of tube substrate and poured the synthesis solution inside to prepare zeolite membranes on the inner surface of the substrate, as shown in Figure 15(c).[101–103] Piera et al.[104] used multi-layered porous tube substrate, which has the smallest pore layer inside the tube. Immersing the substrate

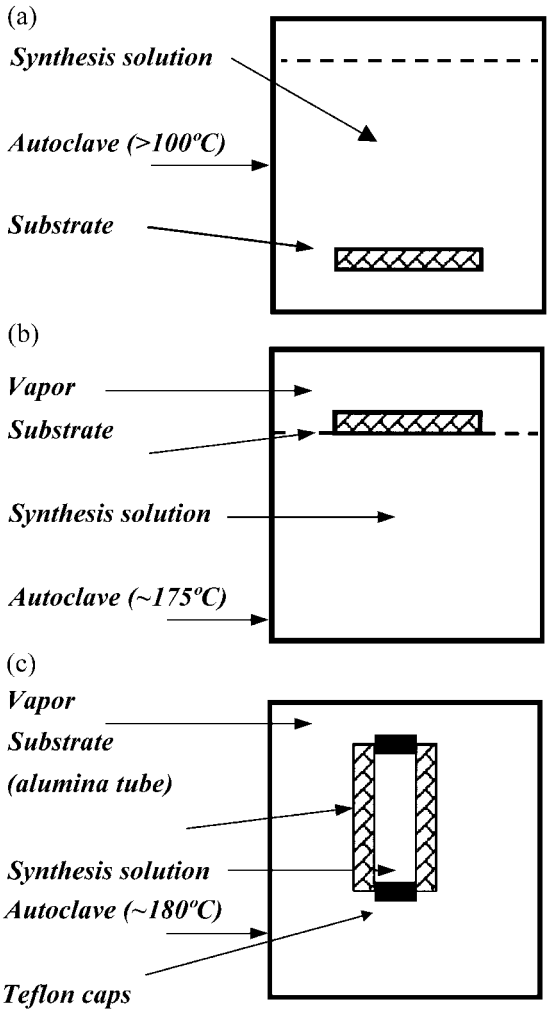

Figure 15. Schematic illustration of substrate positions and typical synthesis conditions during hydrothermal synthesis of zeolites: (a) substrate on the bottom of the synthesis solution, (b) substrate on the surface of the synthesis solution, (c) substrate tube filled with synthesis solution.

totally in the solution, they obtained continuous zeolite membrane inside the inner surface of the substrate.

As will be discussed later on the zeolite membrane growth mechanism, a heterogeneous growth mechanism is preferred for the formation of good

quality zeolite membrane by the in-situ synthesis method. The mechanism requires nucleation on the substrate surface followed by crystal growth to form a continuous zeolite film covering the support. To facilitate heterogeneous nucleation on the substrate surface, synthesis conditions and substrate position should be controlled or arranged in such a way that there is supersaturation in the region adjacent the surface of the substrate on which a zeolite film is to be formed. This explains why the in-situ synthesis method requires stringent synthesis conditions in order to obtain good quality continuous zeolite film. However, the relationship between the local supersaturation and zeolite membrane synthesis conditions is still unclear and almost all studies reported so far on in-situ zeolite membrane synthesis were based on the try-and-error experiments.

Recently microwave has been used in synthesis of zeolite powder.[105,106] Synthesis time was dramatically reduced by the microwave heating. For example, several hours are needed to crystallize zeolite A in the conventional hydrothermal synthesis. While by microwave heating, only 10 minutes are needed. Following similar direction, Kita et al.[107] and Xu et al.[108–110] prepared zeolite NaA and NaY membranes by microwave heating. The microwave synthesis of these zeolite membranes was conducted in the conditions similar to that of the conventional hydrothermal method except that the autoclave was placed in microwave field. Though microwave can heat up synthesis solution quicker than the conventional heating method, the synthesis temperature in the microwave heating was controlled to be similar to that of the conventional synthesis method in these studies. So the short synthesis time with microwave heating is not due to higher temperature but due to specific nucleation and crystal growth under microwave field which is still not well understood yet.

In the work of Kita et al.[90,107] the solution used contained $2Na_2O-2SiO_2-1Al_2O_3-120\sim360H_2O$ for zeolite NaA membrane and $22Na_2O-25SiO_2-1Al_2O_3-990\sim1980H_2O$ for zeolite NaY membrane. The compositions were similar to those used in the conventional hydrothermal synthesis. Hydrogel was heated from room temperature to 100°C within two minutes, and uniformly sized zeolite crystals were formed on substrate after five minutes. Compared to the general hydrothermal synthesis which required several hours of synthesis time,[90,107] they succeeded to reduce the required synthesis time. NaA membrane formed by microwave synthesis showed quite high water selectivity in pervaporation of ethanol–water mixture, similar to the membrane formed by the conventional hydrothermal synthesis. Xu et al.[108,110] also reported much quicker synthesis of NaA type zeolite membrane by the microwave method. Compared with the conventional hydrothermal synthesis method, they found that the A zeolite membranes prepared by the microwave method were thinner and consisted of smaller crystals, and therefore offer higher permeance.

Synthesis by Secondary Growth and Vapor Phase Transport Methods

The secondary growth method contains two steps. The first is to coat the substrate surface by zeolite seed crystals, and the second is to grow the seed layer to a continuous zeolite film by hydrothermal synthesis. In the first step, the zeolite seeds are coated on the substrate surface by either simple mechanical scrubbing the substrate surface with zeolite crystals[111,112] or dip coating the substrate with a zeolite–boehmite or pure zeolite sol.[95,113–115] In the dip-coating method, an important step is the preparation of a stable zeolite sol containing nanostructured zeolite particles. The procedure used for synthesis of the zeolite sol is similar to that used to prepare zeolite powder. But in preparation of zeolite sol the conditions should be controlled in such that only small zeolite crystals are formed and properly charged so they are stable in the aqueous phase. For example, Pan and Lin[95] reported synthesis of sililicalite sol by hydrothermal-treatment of the synthesis solution at lower tempearture as compared to synthesis of silicalite powder (120°C for 12 hr). The final sol used for dip-coating has a composition of 1 g silicalite, 0.14 g HPC (hydrooxy propyl cellulose, MW = 100,000 g/mol), 94 ml H_2O, with pH of about 10. Dip-coating process for coating the zeolite seed layer follows same procedure as used for preparation of mesoporous alumina membranes from boehmite sol as described earlier.

The aim of the second step in the secondary growth method is to allow the seeds to grow into a continuous film without intercrystalline void. In the secondary growth step, the substrate with zeolite seed layer is brought in contact with zeolite synthesis solution. This follows very much the same procedure as the in-situ synthesis method. Upon contact with zeolite synthesis solution, the seed crystals grow and eventually seal the intercrystal voids. New zeolite crystals may also form in the second growth step. Typical experimental conditions for synthesizing several different zeolite membranes in the second step of the secondary growth method are listed in Table 11. As compared with in-situ synthesis shown in Table 10, the secondary growth method requires much more dilute synthesis solution, lower synthesis temperature and shorter synthesis time. With the presence of the seed layer on the support surface, a continuous zeolite film can easily grow and cover the support under less stringent conditions as compared to the in-situ synthesis method.

For some zeolites, good quality membranes can be prepared only by the secondary growth method, not the in-situ synthesis method. Yamazaki and Tsutsumi[85,86] used clear solution to prepare zeolite A film on silicon and quartsz plates as well as on the quartz fiber. Substrates were set in upright position to prevent accumulation of crystals formed in solution by precipitation. They found that zeolite A crystals could be formed on the substrate without seed crystals, but to form a dense zeolite layer, seed crystals were

Table 11. Typical Conditions for the Synthesis of Zeolite Membrane and Film by Secondary Growth

Zeolite	Composition (Na_2O:SiO_2:Al_2O_3:H_2O:templates)	Substrate	Seed Size [μm]	Temperature [°C]	Pressure	Time [h]	Calcine Condition	1st Author, Year	Ref.
Silicalite	0:40:0:16800:12 (TPAOH):40g silicalite	Glass slide, silicon wafer	0.1	130	autogeneous	8	477°C-2 h	Lovallo, 1996	[113]
ZSM-5	7:20:0:1953:3 (TPABr)	α-Al_2O_3 disk	0.4, 2	110–150	Autogeneous	4–16	450–500° C-10 h	Lai, 1998	[280]
NaA	100:10: 1–3:2000:0	α-Al_2O_3 disk	1	80	atmospheric	5	Not necessary	Lovallo, 1996	[113]
NaA[a]	0.36:4.4:1: 706.2:4.1 ($(TMA)_2O$)	silicon wafer	<0.5	90		~3 days	–	Boudreau, 1999	[115]
NaA	90:9:1:5000:0	α-Al_2O_3 disk	1	80	atmospheric	5	Not necessary	Kumakiri, 2000	[111]
FAU	90:9:1:5000:0	α-Al_2O_3 disk	0.5	80	atmospheric	5	Not necessary	Kumakiri, 2000	[112]

[a]Zeolite film formed on dense substrate.

necessary. MFI zeolite membranes can be prepared by both the in-situ and secondary growth methods but seed layer is often required for preparation of A and FAU type zeolite membranes. Kumakiri et al.[111,118] could obtain zeolite A and FAU membranes on the substrates seeded respectively with zeolite A and FAU crystals from same synthesis solution under the same hydrothermal conditions for secondary growth. Their results clearly showed that under similar secondary growth conditions the type of the zeolite film formed on the substrate is determined by the structure of the zeolite in the seed layer.

Because of less stringent conditions required, the secondary growth method offers higher reproducibility in synthesis of good quality zeolite membranes as compared with the in-situ method. The secondary growth method is more preferred for large scale production of zeolite membranes. Furthermore, by controlling orientation of the send layer or controlling the synthesis condition during the secondary growth step, oriented zeolite films could be grown. Tsapatsis and co-workers prepared silicalite,[113] MFI zeolite,[119] zeolite L,[114] and zeolite A[115] membranes by the secondary growth method. By controlling the orientation of seed layer by the electrostatic deposition, they could obtain a dense and oriented zeolite film following the secondary growth step.[115] Starting with randomly oriented seed layers, they could also prepared zeolite membrane with high orientation by controlling the secondary growth synthesis conditions that give a faster crystal growth rate in a specific crystallographic direction (see Section 3.3).[113,115,119]

The secondary growth method can also be advantageously used to prepare zeolite membranes of better quality. Pan and Lin[95] recently reported secondary growth synthesis of silicalite membrane without using an SDA (TPAOH in this case). They could grow a mesoporous silicalite seed layer into a dense, continuous silicalite membrane by the secondary growth with template-free synthesis solution. Because SDA was not used in the membrane synthesis, no calcination for SDA removal was required for preparing the silicalite membranes. The unfavorable microstrcuture change associated with the SDA removal step[120] can be avoided. As a result, the silicalite membranes prepared by the SDA-free synthesis method offer better separation properties than the silicalite membranes prepared by the in-situ method.[95]

MFI zeolite and several other zeolite powders could be synthesized by vapor phase transport method.[121,122] Preparation of zeolite membranes by vapor phase transport was reported in the 90's.[122–126] Membranes of various types of zeolite, such as MIF, FER, MOR, FAU, EMT and beta, have been prepared by the vapor phase transport method. One of the advantages of the vapor phase transport method over the in-situ hydrothermal synthesis is that the former allows 100% conversion of reaction gel. With this method it is possible to obtain zeolite membranes with higher Si/Al ratio than hydrothermal synthesis.

The vapor phase transport method includes two steps. The first step is to cover the substrate by hydrogel containing silica, alumina and sodium. The second step is crystallization of the dry hydrogel in an autoclave with vaporized solvent, as shown schematically in Figure 16. Two different vapor phase transport methods were reported. One is to place water and SDAs at the bottom of autoclave, and feed them to the dry hydrogel by saturated vapor pressure at synthesis temperature. By this method, application of SDAs with low vapor pressure is difficult. SDA may not be consumed totally and could remain in the solution after synthesis. The other method is to prepare dry hydrogel containing SDAs and place only water in the bottom of autoclave.

Mastukata and co-workers[125,126] reported that the structure of the dry gel affects the structure and quality of the final zeolite membrane. They tried several conditions and pointed out the importance of preparing dense dry gel layer in synthesis of prepare dense zeolite membrane by the vapor phase transport method. The hydrogel placed on the substrate surface penetrated into the substrate pore before crystallization. Crystallization occurred in the hydrogel on the substrate as well as in the substrate pore. Nishiyam et al.[126] suggested that when zeolite crystals were formed inside the substrate pores more gel was soaked into the substrate as to fill the void among the zeolite crystals owing to

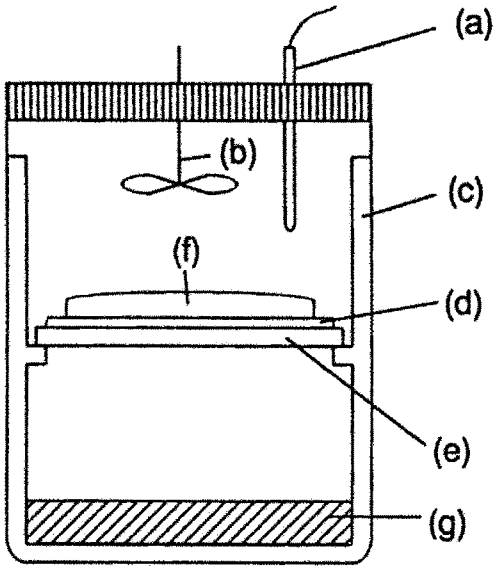

Figure 16. Schematic diagram of the autoclave for vapor phase transport synthesis: (a) thermometer, (b) stirrer, (c) Teflon-lined autoclave, (d) support, (e) screen, (f) drygel, (g) water/template (After Ref. [275]).

the capillary force. As a result, dense zeolite layer was formed inside the substrate pore. In contrast, zeolite layer formed on the substrate contained voids.

Post-treatments of Zeolite Membranes

Zeolite membranes prepared by various methods described above are of polycrystalline structure. In many cases, these zeolite membranes may contain a small amount of defects of macropore or mesopore sizes. Microporous intercrystalline gaps may exist too, as to be discussed in more detail in next section. These defects and intercrytalline gaps are referred here as the

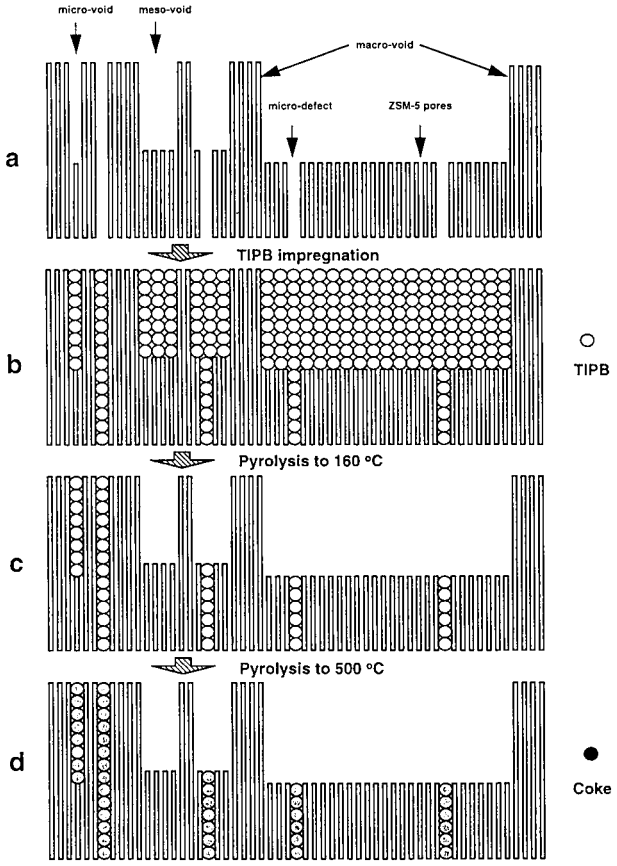

Figure 17. Schematic of coking process as post treatment of zeolite membrane (After Ref. [127]).

nonzeolitc pores. Several post treatments were reported to fill these non-zeolitic pores. Yan et al.[127] reported reduction of the size of the nonzeolitic pores by coking. The post-treatment process is schematically illustrated in Figure 17. First they prepared ZSM-5 membrane on α-alumina substrate. Then, tetraisopropylbenzene (TIPB) liquid was poured on the membrane. After TIPB liquid was impregnated completely into the zeolite membrane, the membrane was heated at 500°C for 2 hours to form coke in the intercrystalline region. TIPB molecules has kinetic diameter of 8.4 Å, larger than MFI type zeolitic pore size, so TIPB cannot enter inside the zeolitic pore but could only fill the nonzeolitc pores larger than the TIPB molecules. The post-treatment caused a significant reduction in the flux of iso-butane but not of n-butane or hydrogen as a result of the reduction in the intercrstalline region.

Nomura et al.[128] and Kumakiri et al.[111,112] conducted post-treatment of the silicalite and zeolite A membrane by counter diffusion chemical vapor deposition (CVD) (see Section 4 for more details of this method). Tetra-methyloxosilcate (TMOS) and tetraethyloxosilicate (TEOS) were used as the reactants. The molecules of these silica sources are larger than the zeolitic pores, so they are not expected to enter into the zeolitic pores. TMOS or TEOS was carried by nitrogen and fed from the zeolite membrane surface, while ozone and oxygen fed from the substrate side. TMOS or TEOS reacts with ozone and forms amorphous silica inside the nonzeolitic pores, reducing

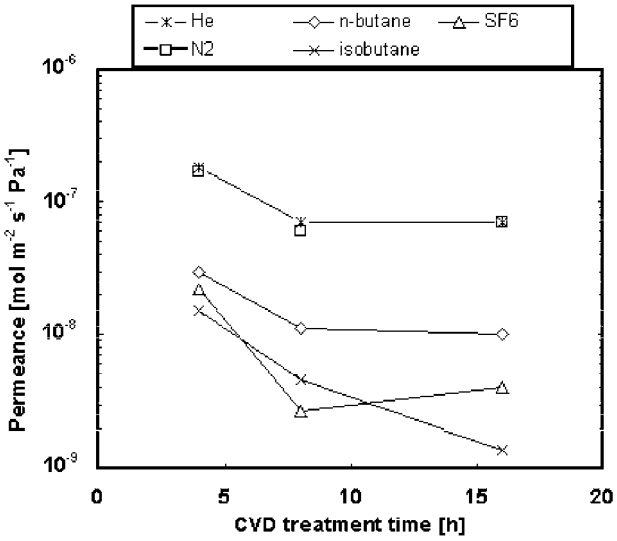

Figure 18. The effect of CVD modification on single gas permeance (Redrawn from Ref. [128]).

their pore sizes. When the non-zeolitic pore sizes become smaller than ozone, two reagents cannot meet, and the reaction stops. Figure 18 shows the single gas permeance obtained before and after CVD treatment on silicalite membrane. Permeance of SF_6, kinetic diameter 5.5 Å, decreased with prolonged CVD treatment time showing the reduction in the intercrystalline pore size.

Sano et al.[94] modified the silicalite membrane with silane coupling reagents and examined its effect on ethanol–water separation by pervaporation. Silane coupling reagents react with the silanol on the outer surface of silicalite crystal. FT-IR spectra of silicalite before and after the modification showed only a slight decrease in silanol group peak, indicating that most of the silanol groups within the zeolitic pores were not reacted. Although the reaction rate is low, the modification has increased the ethanol over water selectivity from about 5 to about 40 for the zeolite membrane.

3.2 Mechanisms of Zeolite Membrane Formation

In synthesizing a zeolite membrane the synthesis reactor contains two or three different materials: synthesis gel or solution, substrate and seed crystals. According to the influences of these materials on zeolite membrane synthesis, membrane forming mechanisms can be classified to five cases as illustrated in Figure 19. Homogeneous nucleation in synthesis gel/solution occurs in many studies reported on zeolite membrane preparation. This mechanism includes

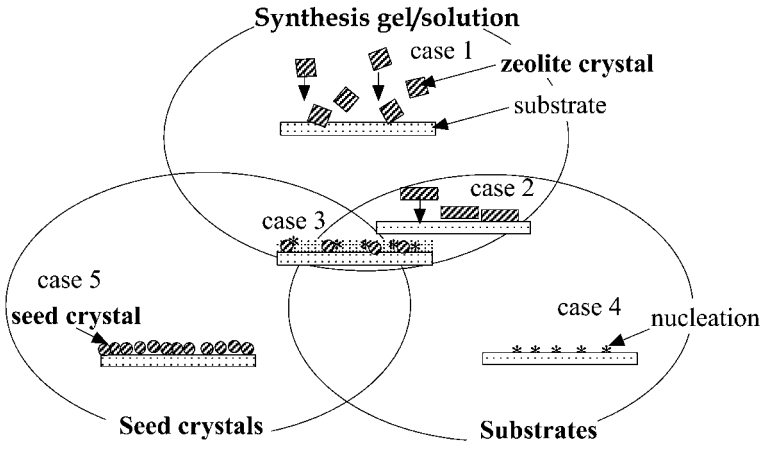

Figure 19. Classification of the mechanisms for zeolite membrane formation: Homogeneous nucleation and deposition of crystals (Cases 1–3), heterogeneous nucleation and crystal growth (Case 4), and seeded crystal growth (Case 5).

three cases (Cases 1 to 3 in Figure 19). In the first case (Case 1), zeolite layer is formed on the substrate surface by physical deposition of zeolite nuclei and crystals formed homogeneously in the synthesis gel/solution.[96,101] The driving force for the deposition can be gravity (when substrate is placed horizontally in the bottom of a autclave) or other physical attraction force between the particles and substrate surface. When solution is used, the crystals or nuclei in the solution are easy to move (due to the low viscosity of the solution) and get deposited on the substrate surface.

When deposition of the zeolite nuclei or crystals on the substrate surface is restricted or not evident, substrate surface may influence the membrane formation as schematically illustrated in Case 2 of Figure 19.[85] Yamazaki and Tsutsumi[116] prepared MOR membrane on stainless-steel filter and polytetrafluoroethylene (PTFE) plate using hydrogel. The substrates were placed at upright position to reduce the effect of accumulation of crystals formed in the gel. They suggested a membrane forming mechanism as illustrated in Case 2 in Figure 19. In the early stage of synthesis, secondary building units in synthesis mixture form dimmers. These dimmers align on the substrate with regular orientation, and form a (100) oriented film on substrate. The crystals shape on the substrate is prismatic, while crystals formed in gel has a rectangular shape. This difference is considered due to the hindrance during crystal growth on substrate. With prolonged synthesis time, small prismatic crystals formed in the hydrogel link to the rectangular crystals on the substrate, and the membrane becomes randomly oriented. Membranes formed on PTFE substrate follows the above mechanism. On the other hand, amorphous silica phase is first formed on the stainless-steel substrate, and obstructs the oriented attachment of dimmers. These differences may be due to the different electrical potential of substrates.

Seeded crystals are sometimes used to enhance the nucleation near the surface of substrate as illustrated in Case 3 in Figure 19. Kita et al.[90] explained formation of zeolite A membrane on the outer surface of tube substrate as below. The seeded crystals are dissolved first and an amorphous gel is formed on the substrate surface. Then, transformation of the gel into zeolite occurs and a zeolite membrane is formed on the substrate. As the membrane is prepared with nucleation and growth, polycrystalline zeolite membrane formed by this mechanism had a random orientation.

The Case 4 illustrated in Figure 19 is the formation of membranes by heterogeneous nucleation on/near the substrate surface, followed by crystal growth into a continuous zeolite layer covering the substrate. Generally, clear solutions are used for these syntheses.[88,92,98,99,130,132,133] These solutions contain much more water compared to the former three cases. For example, Koegler et al.[133] used synthesis solution containing 5–20 SiO_2:0.4–1.5 TPA_2O:2000 H_2O for ZSM-5 film preparation. They placed a disk-shape substrate at the top of autoclave to prevent deposition of zeolite crystals

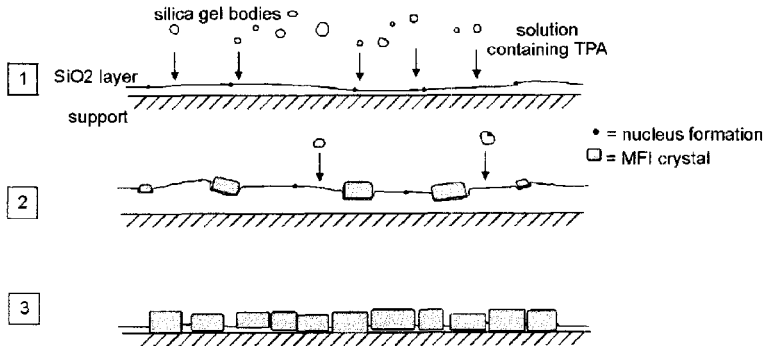

Figure 20. A three-step heterogeneous nucleation model for growing Si–ZSM-5 film on a support (After Ref. [133]).

homogenously formed in the solution.[98,133] Figure 20 shows more detail of this mechanism suggested by Koegler et al.[133] At the early stage of preparation, a thin gel layer is formed on the substrate surface although the solution is clear. Heterogeneous nucleation starts on/close to the interface of the gel and solution,[98,133] followed by crystallization and formation of zeolite film on the support. Heterogeneous nucleation was reported on synthesis of MFI[98,133] and LTA[98,132] films/membranes. In MFI-zeolite case, formation of an oriented mono-layer film was reported by Jansen et al.[98] and Koegler et al.[133] The film had orientation of (010) surface parallel to the substrate surface. They suggested that the preferred orientation of nuclei and preferred growth direction of a-, and c-axes in the plane of the interface of gel and solution were responsible for the formation of the oriented zeolite film.

The secondary growth mechanism for zeolite membrane formation is classified as Case 5 in Figure 19. As mentioned before, the seed layer of zeolite crystals could be deposited on the substrate by a physical means (such as dip-coating). Boudreau and Tsapatsis[115] proposed a model for the secondary growth of the seed layer, as illustrated in Figure 21. During the secondary growth hydrothermal synthesis step, seeded crystals grow at the early stage and an oriented zeolite layer is observed. With longer synthesis time, zeolite crystals could be formed homogeneously in the synthesis solution and deposited on membrane. These effects cause the disruption of orientation. Yamazaki and Tsutsumi[85] also presented a similar mechanism for seed growth assisted by the zeolitic components formed in the solution.

Kumakiri et al.[111] studied secondary growth on the seed layers of zeolite A and FAU zeolites. Clear synthesis solution of same composition was used for the secondary growth of the both seeded zeolites. The hydrothermal synthesis was conducted each time within the induction period to avoid formation of new crystals. The short-time secondary growth was repeated up to five times. In this

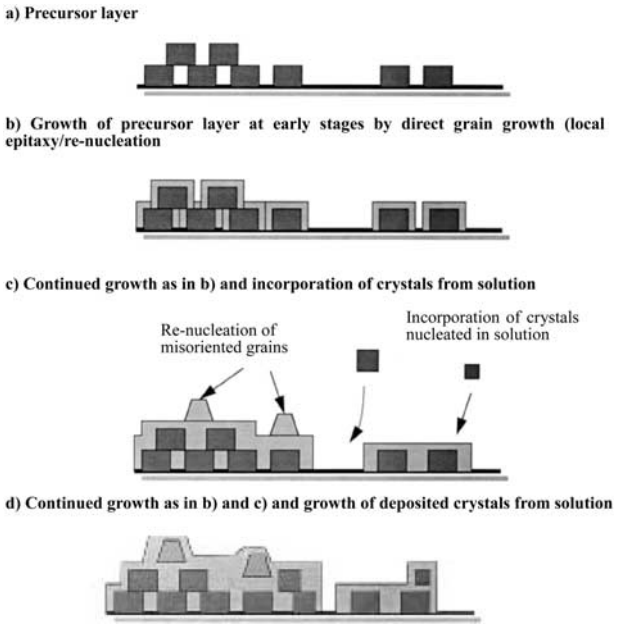

Figure 21. Mechanism of secondary growth of zeolite A film on support (After Ref. [115]).

way, only the crystals in the seed layer could grow. They obtained A and FAU zeolite membranes respectively on the A and FAU zeolite seeded layers. The fact that the zeolite membrane after secondary growth contains only the zeolite that is used as the seed indicating the effectiveness in avoiding the formation of crystals in the synthesis solution and deposition of these crystals on the substrate. TEM analysis confirmed growth of seed crystals till the intercrystalline gap became less than nano-meter size.[111] The water to ethanol selectivity increases with increasing number of the times of the secondary growth as a result of narrowing of the intercrytalline gaps of the seeded crystals by the secondary growth.

3.3 Microstructure of Zeolite Membranes

Zeolite Membrane Characterization

Zeolite membranes are commonly characterized by SEM, XRD and permeation/separation tests. The XRD patterns of most zeolite membranes

reported are the same as those of the zeolites in the powder form, supporting that the zeolite films are polycrystalline with the crystals randomly oriented on substrates. Orientation of crystals was reported in some cases.[98,115,133,134] Intercrystalline regions of a good quality zeolite membrane are generally too small to be distinguished by SEM observations. TEM was also used to study the microstructure of the zeolite membranes in nanoscale.[96,111,114,135,143] However, it is very difficult to observe the intercrystalline regions of zeolite membranes with high resolution TEM observations owing to low stability of the electron beam passing through zeolites. Si/Al ratio and its distribution along thickness were measured by EPMA,[83,85] TEM-EDS[135] and SEM-EDS.[92]

It should be pointed out that the above characterization techniques only provided very localized information about the characteristics of a zeolite membrane. The overall quality of the membrane cannot be determined by these methods. For example, penetrated defects or intercrystalline gaps could only be determined by permeation/separation tests. In case of membrane synthesized with SDAs, single gas permeance through membrane before SDA removal (calcination) can provide useful information about the presence of macroporous defects in the zeolite film.

Figure 22 shows helium permeance of an as-synthesized MFI membrane prepared by in-situ synthesis with an SDA (TPAOH), as a function of calcination

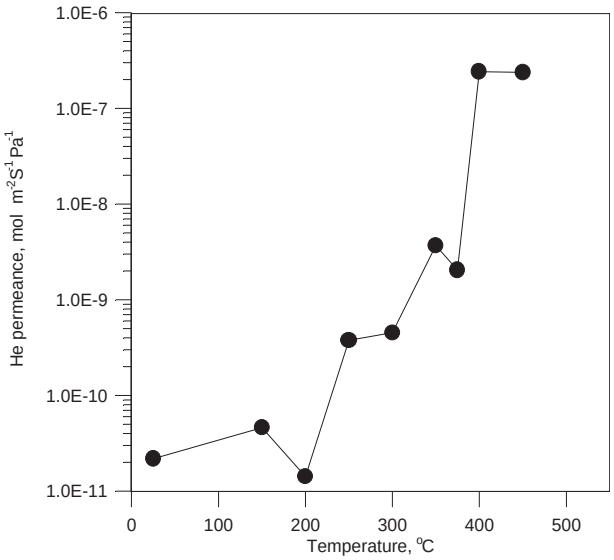

Figure 22. Helium permeance for the α-alumina-supported MFI zeolite membrane during the calcination process (After Ref. [120]).

Table 12. Structures of Selected Zeolite Membranes Prepared by Various Research Groups

Zeolite	Substrate	Substrate Pore Size [μm]	Preparation Methods	Crystal Size [μm]	Thickness [μm]	Performances	1st Author, Year	Ref.
Silicalite	SS disk	2	HS	20–100	460	Ethanol/Water PV $\alpha = 60$	Sano, 1992	[83]
MFI	SS Disk	–	HS	20–120	~50	n-C4/C1 Gas $\alpha = 50$ (25°C)	Geus, 1993	[93]
Silicalite	γ-Al_2O_3 tube	0.005	HS	10–15	~10	CH_3OH/H_2 VP $\alpha > 1000$	Jia, 1993	[101]
MFI	α-Al_2O_3	0.135–0.165	HS	0.2–0.7	2–5	n-C4/iso-C4 $\alpha > 10$ (200°C)	Vroon, 1995	[97]
Silicalite	Zirconia	~0.19	HS	0.4	0.5–0.75	H_2/CH_4 $\alpha = 13.2$ (25°C)	Dong, 1998	[88]
Silicalite	Glass slide, silicon wafer	–	SG	0.75	0.75 (oriented)	H_2/N_2 Ideal $\alpha = 60$ (185°C)	Lovallo, 1996	[113]

MARCEL DEKKER, INC. • 270 MADISON AVENUE • NEW YORK, NY 10016

MOR	α-Al_2O_3	0.1	DGC	~70	10	Benzen/p-xylene PV $\alpha = 160$ (22°C)	Matsukata, Nishiyama, 1996	[125]
NaA	α-Al_2O_3	1	HS	2–4	30	Water/ethanol PV $\alpha > 10000$	Kita, 1995	[90]
NaA	Glass slide	–	SG	0.3	~0.5 (oriented)	–	Boudreau, 1999	[115]
NaA	α-Al_2O_3	1	SG	2.2	5.4	Watre/ethanol PV $\alpha > 10{,}000$ (30°C)	Kumakiri, 2000	[118]
NaY	α-Al_2O_3	1.3	HS	–	20–30	Methanol/MTBE PV $\alpha = 5300$ (60°C)	Kita, 1997	[151]
FAU	α-Al_2O_3	0.1	SG	1.5	5.8	Water/ethanol PV	Kumakiri, 2000	[111]

HS: Hydrothermal Synthesis, SG: Secondary Growth.

temperature. Before calcination, zeolitic pores are filled with TPAOH and no helium should permeate through the zeolitic pores. The extremely low helium permeance (close to the low limit of the permeation apparatus) below 200°C indicates that the as-synthesized membrane is pinhole or defect free. SDA could be present in the intercrystalline regions. The temperature needed for removal of SDA from defect is lower than removal from zeolitic pore. Therefore, the slight increase in the helium permeance in 200–350°C shown in Figure 22 could be due to the removal of the SDA from the intercrystalline regions. Calcination at temperatures above 400°C removes the SDA from the zeolitic pores. As a result, the helium permeance increases substantially, as shown in Figure 22. A small amount of defects may be formed in the SDA removal step. These defects can not be detected by this method.

Another method to check the existence of defect is to measure the permeation flux of gas with molecules larger than the zeolitic pore. For this purpose, 1,3,5-triisopropyl benzene (TIPB) having kinetic diameter of 0.85 nm or SF_6 of 0.55 nm is used. If the large molecules will not permeate through the zeolite membrane, the membrane is considered to be free of defects with size larger than the permeating molecules. Another method is to compare ideal separation factor of a small molecule (such as hydrogen) with a large molecule, such as SF_6. A separation factor for the small molecule over the large molecule much larger than the value of the Knudsen separation factor (ratio of the squared-root of the molecule weight) indicates good quality of the membrane prepared. These techniques have been used by many research groups (e.g., Refs. [3,92,95,98,136,137]).

Physical Properties and Microstructure of Zeolite Membranes

Table 12 summarizes characteristics of representative zeolite membranes prepared by various groups. In general, zeolite membranes with smaller thickness, less intercrystalline gaps, and possibly oriented structure are preferred. Most zeolite membranes formed on porous substrates have polycrystalline structures and thickness in the range from 5–30 μm. The zeolite membranes with thickness less than 1 μm on substrates with submicron or mesopore sizes were also reported by several groups.[98,108,113,143] The thickness of most zeolite membranes is at least several times of the size of the zeolite crystals. The effective thickness of the zeolite film in which the crystallites are connected with minimized intercrystalline regions can be smaller than the thickness observed by SEM. Co-existing intercrystalline region possibly decreases the selectivity of the membrane. One approach to decrease the intercrystalline region is to form a zeolite membrane with large crystal having 20–100 μm

size.[93] In this sense, the number of intercrystalline region will decrease, though there is a limitation in decreasing the thickness of the membrane.

Oriented polycrystalline zeolite membranes were also reported recently by several groups. These include MFI type zeolite membranes with b-axis or c-axis normal to the support surface,[98,129,134] NaA zeolite membranes with (100) plane parallel to the support surface,[115] and LTL-type zeolite film with c-axis (channel direction) perpendicular to the substrate.[114] Several mechanisms for the synthesis of oriented zeolite membranes were proposed. The first involves the orientation in the early stage of synthesis, such as the successful attachment of crystals formed in the synthesis mixture by the in-situ hydrothermal synthesis method,[85,116,129] or ordered seed layer by the secondary growth synthesis method.[114,115] The second involves ordered structure formed during the zeolite film growth. That is, the fastest plane growth survives during the growth, resulting in a film consisting of the crystals of certain orientation on the surface.[134,138,139] For example, thick (12–18 μm) c-oriented MFI type zeolite membranes could be synthesized by 24-h growth at 175°C, a condition that MFI zeolite crystals grow faster in c-axis direction than the other two directions. In contrast, thin (2–3 μm) (h0h)-oriented MFI type zeolite membranes could be obtained by 120-h growth at 90°C.

Lin et al.[140] recently used microscope FTIR to study diffusion in large (about 50 μm) single silicalite crystal particles prepared by in-situ hydrothermal synthesis method. They found that these crystal particles consist of multiple crystallites with significant intercrystalline gaps through which gas molecules diffuse much faster than intracrystalline pores. It has become generally accepted that most good quality zeolite membrane contain both zeolitic pores defined by the zeolite framework and micropore sized intercrystalline pores.[120,137,141,142] Due to the polycrystalline nature of the zeolite membrane it is difficult to avoid formation of these intercrystalline pores.

The intercrystalline pores could be formed during film growth process. Local structure of the intercrystalline region was analyzed by TEM and some models on membrane densification process are presented based on the TEM observation and permeation results.[111,135,143] With TEM, Sasaki et al.[135] found that MFI zeolite layer formed in the substrate pores was dense and direct connection of grains was observed, while membrane formed on the support had intercrystalline gap of several nano-meter size. Kumakiri et al.[111] analyzed the microstructure of FAU membrane formed by the seed growth method. In this case no intercrystalline gap larger than nano-meter size was observed. These results suggested that intercrystalline pore could be diminished to the similar size as zeolitic pore size under a proper nucleation and growth condition.

The intercrystalline pores can also be formed in the zeolite membrane synthesized with a SDA during the subsequent calcination step for SDA

(template) removal. Figure 23 illustrates formation of the intercrystalline pores in the MFI type zeolite membrane on alumina support during the SDA (TPAOH) removal process. Due to good chemical reactivity of aluminum with silicalite crystallites, the MFI crystallite can be chemically bonded to the support surface during the in-situ synthesis and heating process of the calcination step (Figure 23). From 350 to 500°C, the SDA is removed and the MFI crystallites shrink. This may create tensile stress in the zeolite film if the bonding between the zeolite crystals is strong. With the strong chemical bonds already formed between the crystallites and support surface prior to the SDA removal, shrinkage most likely results in opening up the gap between the two well-contact crystallites (Figure 23) or enlarging gaps that existed prior to SDA removal. Cooling to room temperature is accompanied by expansion of the MFI crystallite and shrinkage of the alumina support (Figure 23). The intercrystalline gap becomes narrower but would will not return its original gap size because the zeolite crystallite after SDA removal at room temperature

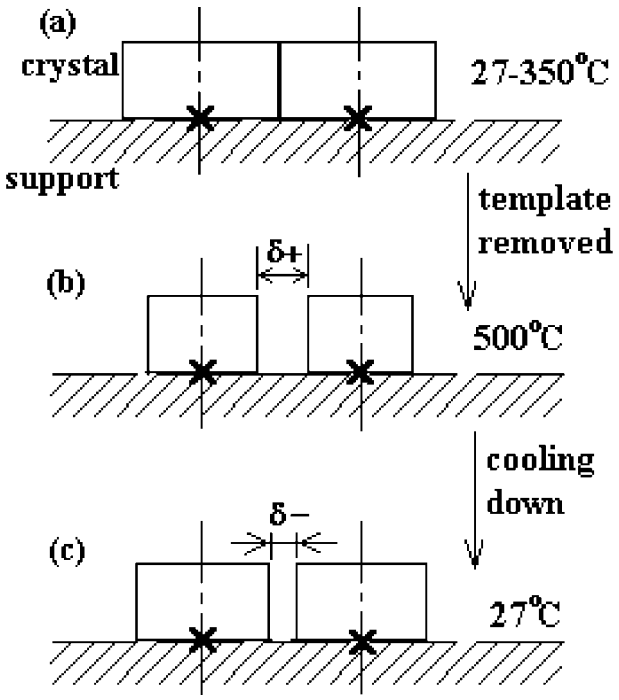

Figure 23. Schematic illustration of template removal associated microstructural development of zeolite film with strong bonds between the crystallite and support formed prior to template removal (After Ref. [120]).

is smaller than the as-synthesized zeolite.[120] Because of the unfavorable effects on the template removal step on the membrane microstructure, template-free synthesis of MFI type zeolite membranes has recently received increasing interest among the researchers working on zeolite membranes.[95,144,145]

The presence of the intercrystalline pores in a polycrystalline zeolite membrane, depending on their size and number, could affect the properties of the membrane for separation of molecules based on their intracrystalline diffusion properties. Xylene isomer separation is a good example to illustrate the extent of the intracrystalline pores in MFI type zeolite membranes. Table 13 lists the sizes of the xylene isomers and tri-isopropylbenzene (TIPB) molecules and their pervaporation fluxes through an MFI zeolite membrane prepared by the in-situ method. The negligible flux of TIPB indicates presence of minimum amounts of meso or macroscale defects or pinholes in the membrane. However, the membrane does not show expected molecular sieving properties for separation of xylene isomers. Binary p-/o- or p-/m-xylene pervaporation separation experiments on the same membrane show no separation between these isomers.[137] Due to the fouling of intracrystalline pores by xylenes, the flux data shown in Table 13 represent those through the microporous intercrystalline pores nonselective for xylene isomers.

However, zeolite membranes with microporous intercrystalline pores still offer good separation for gas molecules based on their sorption properties. Dong et al.[146] recently performed separation of simulated 8-component refinery gas containing: H_2(84.5%), CH_4(7.6%), C_2H_6 (2.5%), C_2H_4 (2.5%), C_3H_8 (0.75%), C_3H_6 (1.4%), n-C_4H_{10} (0.4%) and i-C_4H_{10} (0.3%) by an MFI zeolite membrane. The membrane was prepared by the same method and conditions as used for xylene pervaporation experiments listed in Table 13. The permeation experiments were conducted in feed pressures of 1–5 bar and at temperatures of 25–500°C. In all the experiments at different temperatures and pressures iso-butane permeance was so small that its concentration in the effluent of the permeate side was beyond the GC detection limit. Figure 24 shows gas

Table 13. Pervaporation Characteristics of Pure Xylene Isomers Through Silicalite Membranes (at 26°C)

Compound	Molecular Size (nm)	Viscosity 25°C (cP)	Pervaporation Flux (in 10 h) (10^{-2} kg/h.m^2)
p-xylene	0.585	0.61	>34
o-xylene	0.680	0.76	>27
m-xylene	0.680	0.60	>40
1,3,5-TIPB	0.84	~2.5	<0.08

(From Ref. [137].)

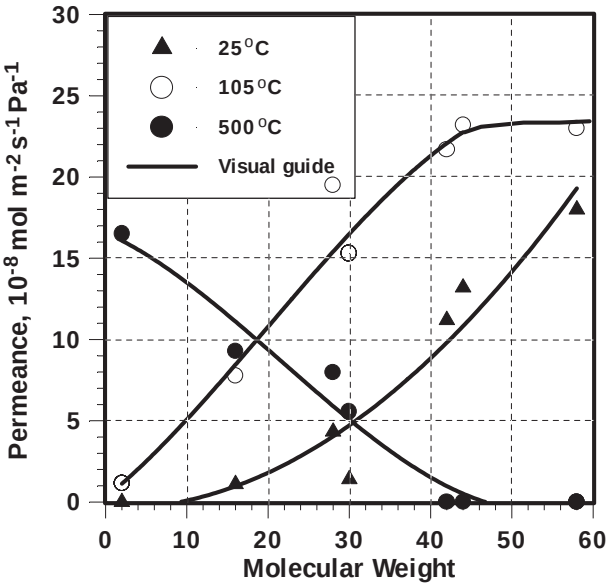

Figure 24. Permeance of the eight component hydrogen–hydrocarbon mixture (composition specified in the text) through a silicalite membrane (iso-butane not shown in the figure due to negligible flux) (After Ref. [146]).

permeance of these components (excluding iso-butane), as represented by their molecular weights, through the zeolite membrane. As shown in Figure 24, at low temperature (25°C) the gas permeance increases with molecular weight, with essentially zero hydrogen permeance. The permeance is consistent with affinity of the gas molecules with silicalite. The trend of the permeance versus molecular weight is however reversed at high temperature (500°C) at which the permeance decreases with increasing molecule weight, or decreasing intracrystalline diffusivity. At the high temperature hydrogen becomes more permeable than hydrocarbons.

3.4 Permeation Properties of Zeolite Membranes

Selected results for gas/vapor/liquid permeation and separation by various zeolite membranes are summarized in Tables 14–20. Zeolite membranes summarized in these tables include membranes of silicalite, ZSM-5, Y, A, SAPO-34, FAU and FER type zeolites. Most studies on gas permeation in zeolite membranes dealt with single gas or binary systems. Permeation and

separation data of selected gases for some zeolite membranes are reviewed next to illustrate general permeation properties observed experimentally for various zeolite membranes. These experimental results will be explained later with the help of theoretical models summarized in Section 5.

Gas/Vapor Permeation and Separation

Many researchers have studied single gas permeation through zeolite membranes, mostly of MFI type zeolites (e.g., Refs. [100–102,131,147–149]). For gas molecules smaller than the zeolitic pores of a zeolite membrane, the permeance of the species for the zeolite membrane does not necessary increase with decreasing molecule size, depending on the conditions (temperature and pressure) and membrane quality (intercrystalline region). Adsorption properties play a more important role in effecting permeation permeance. The temperature and pressure dependency of single gas permeance for zeolite membrane is also fairly complex. Details on the single gas permeation properties of zeolite and other microporous inorganic membranes will be discussed in Section 4 and 5.

In many cases, selectivity for mixture components is different from the ideal selectivity based on the permeation of single component. This is because the presence of one component affects the sorption and diffusion properties of the other components in the mixture. For example, blocking effect of component with stronger adsorption is observed in many cases. Gas separation of mixture by zeolite membranes was studied with multi-component of large and small molecules or molecules of strong and week adsorption ability. The n-butane and iso-butane separation by MFI zeolite membranes was studied by many researchers and Table 14 summarizes the representative results. When single gas was applied to the membrane, Bai et al.[131] observed larger permeation flux of iso-butane than n-butane, while most of the others observed opposite results. These are due to differences in microstructures of the zeolite membranes studied. Iso-butane has higher heat of adsorption, and might condense in the non-zeolitic pore. Owing to this preferable adsorption, membrane with large amount of non-zeolitic pores may show iso-butane permselectivity. In mixture gas separation, MFI membranes exhibit n-butane permselectivity. This permselectivity could come from the shape selectivity of the zeolite (diffusion properties)[150] and ability of n-butane to block i-butane (adsorption properties).[102]

Separation of hydrogen and n-butane mixture by zeolite membrane involves a binary gas mixture of a weak and a strong adsorbing component. Table 15 summarizes representative data of hydrogen and n-butane separation by zeolite membranes. Hydrogen has smaller size than butane; as a result,

Table 14. n-Butane and Iso-Butane Separation by Selected Zeolite Membranes

Zeolites	Substrate	Temperature [K]	n-C_4 Permeance Single/ Mixture [10^{-7} mol m^{-2} s^{-1} Pa^{-1}]	Selectivity Ideal/ Mixture (Composition n-:iso-)	Permeation Method	Membrane area [10^{-4} m^2]	Thickness [μm]	1st Author, Year	Ref.
Silicalite	γ-alumina tube	298	0.59/–	20/– (–)	Pressure drop	17	5	Bai, 1995	[131]
		583	12.3/–	0.6/– (–)					
ZSM-5	α-alumina disk	303	0.075/–	18/– (–)	Pressure drop, (vacuum)	2.0	10	Yan, 1995	[99]
		458	0.58/–	31/– (–)					
MFI	α-alumina disk	298	3.8/3.0	90/52 (1:1)	He sweep	1.9	~5	Vroon, 1996	[253]
		473	5.8/4.6	11/11 (1:1)					

MARCEL DEKKER, INC. • 270 MADISON AVENUE • NEW YORK, NY 10016

Silicalite	SS disk	295	0.42/–	58/27 (1:1)	He Sweep	–	50 ~ 60	Bakker, 1996	[100]
		403	–/–	–/23 (1:1)					
ZSM-5	α-alumina tube	303	20/–	10/– (–)	Ar sweep	≅18	10 ~ 20	Kusakabe, 1996	[282]
		373	1/–	50/– (–)					
ZSM-5	α-, γ-alumina, SS tube	340	–/0.29	–/33 (1:1)	Pressure drop	≅6	–	Coronas, 1998	[103]
		394	–/0.68	–/54 (1:1)					
		487	–/4.3	–/1.3 (1:1)					
Silicalite	SS disk	303	–	27/21 (1:1)	He sweep	2 ~ 3.1	30 ~ 50	Van De Graaf, 1998	[283]
		473		4.1/4.5 (1:1)					
MFI	α-alumina disk	295		–/71 (1:1)	He sweep	4	1 ~ 40	Xomeritakis, 2000	[119]
		295		28/39					

Table 15. Hydrogen and Butane Separation by Selected Zeolite Membranes

Zeolite	Substrate	Temperature [K]	H_2 Permeance Single/Mixture [10^{-7} mol m^{-2} s^{-1} Pa^{-1}]	Selectivity Ideal/Mixture (Composition H_2:n-, (iso-))	Measurement Method	Membrane Area [10^{-4} m^2]	Thickness [μm]	1st Author, Year	Ref.
Silicalite	γ-alumina tube	298	34/–	58/– (iso-C_4)	Pressure drop, Ar, SF_6 Sweep	17	5	Bai, 1995	[131]
		583	61/50	4.8/11.9 (iso-C_4)					
ZSM-5	α-alumina disk	303	0.62/–	8.3/– (–)	Pressure drop (vacuum)	2.0	10	Yan, 1995	[99]
		458	1.0/–	1.7/– (–)					
Silicalite	SS	295	2/–	4.8/0.008 (95:5)	He Sweep	–	50 ∼ 60	Bakker, 1996	[100]
ZSM-5	γ-, α-alumina tube	340	33/–	290/–	Pressure drop	10	25 ∼ 30	Coronas, 1997	[102]
		370	–/<0.1	–/0.09 (1:1)					
		463	44/–	13/–					
		560	–/30	–/2.8 (1:1)					
Silicalite	SS disk	303		3.3/0.02 (1:1)	He sweep	2 ∼ 3.1	30 ∼ 50	Van De Graaf, 1998	[283]
			–/–	72/1.6 (1:1) (iso-C_4)					
		336		6.9/0.01 (1:1)					
		473		1.7/0.9 (1:1)					
				9.4/6.9 (1:1) (iso-C_4)					

MARCEL DEKKER, INC. • 270 MADISON AVENUE • NEW YORK, NY 10016

single gas permeation of hydrogen was larger than that of butane. During the unsteady state permeation with the binary gas mixture, the permeation flux of both components changed with time in a peculiar way.[100] In the early stage of permeation, hydrogen permeated faster than butane and permeation flux increased with time. Gradually, butane started to permeate and hydrogen permeation was inhibited. As a result, hydrogen permeation showed maximum value. In the steady state, the membrane showed butane selectivity. These experimental observations could be explained by stronger adsorption of butane on the zeolite membrane pore. The adsorbed butane blocked the hydrogen permeation.[100]

Large research efforts particularly in Japan were denoted to studying zeolite membranes for carbon dioxide separation. Tables 16 and 17 show the carbon dioxide separation from methane or nitrogen by zeolite membranes. All three molecules are smaller than the zeolitic pore, and the ideal selectivity (the ratio of single gas permeance) is small. In mixture separation, carbon dioxide shows preferred permeation. This separation is caused by the preferential adsorption of carbon dioxide to zeolite membrane since carbon dioxide has strong polarity compared to nitrogen or methane. The stronger adsorption of carbon dioxide in the zeolite pores not only gives a higher permeance for carbon dioxide but also reduces the mobility of nitrogen or methane. However, the good selectivity observed at low temperatures disappears at high temperatures due to a decrease of the adsorption affinity of these molecules with zeolites.

Separation of an eight component simulated refinery gas mixture including hydrogen (~ 84 mol%) and light hydrocarbons ($C_1 - C_4$, $7.5 \sim 0.3$ mol%) by an α-alumina supported polycrystalline MFI zeolite membranes was studied by Lin and co-workers[146] over a temperature range of $25 - 500°C$ and a feed pressure range of $0.1 - 0.4$ mPa. The zeolite membrane shows excellent separation properties for rejection of hydrogen from the hydrogen/hydrocarbon mixture at low temperatures ($< 100°C$) (see Figure 24). At room temperatures and atmospheric pressure on both feed and permeate sides, hydrogen permeation rate is almost zero while the hydrocarbon permeation rate is in the range of $2 - 4 \times 10^{-4}$ mol/m^2.s^{-1}. The zeolite membrane outperforms the microporous carbon membrane in terms of both selectivity and permeance for hydrocarbons over hydrogen.

At high temperature (500°C) the zeolite membrane becomes perm-selective for hydrogen over hydrocarbons ($C_1 - C_4$) (see Figure 24). In the whole temperature range *iso*-butane is non-permeable (with a permeance below the GC analysis limit) through the zeolite membrane. The separation results of the zeolite membrane can be characterized by a solution–diffusion model considering competitive adsorption of hydrocarbons over hydrogen and configurational diffusion in the zeolite pores. The results demonstrate that the

Table 16. Carbon Dioxide and Methane Separation by Selected Zeolite Membranes

Zeolite	Substrate	Temperature [K]	CO_2 Permeance Single/ Mixture [10^{-7} mol m^{-2} s^{-1} Pa^{-1}]	Selectivity Ideal/ Mixture (Composition CO_2:CH_4)	Measurement Method	Membrane Area [10^{-4} m^2]	Thickness [μm]	1st Author, Year	Ref.
NaY	α-alumina tube	303	0.4/0.4	2/20 (1:1)	He sweep	1	20	Kusakabe, 1997	[148]
		403	2/2	5/5 (1:1)					
SAPO-34	α-alumina tube	300	0.24/–	19/30 (49:51)	Pressure drop	10	15	Poshusta, 1998	[87]
		470	0.1/–	2.3/3.4 (49:51)					
ZSM-5	γ-alumina tube	300	20/–	0.7/1.6 (1:1)	Pressure drop	10	–	Poshusta, 1998	[87]

Table 17. Carbon Dioxide and Nitrogen Separation by Selected Zeolite Membranes

Zeolite	Substrate	Temperature [K]	CO_2 Permeance Single/Mixture [10^{-7} mol m^{-2} s^{-1} Pa^{-1}]	Selectivity Ideal/Mixture (Composition CO_2:N_2)	Measurement Method	Membrane Area [10^{-4} m^2]	Thickness [μm]	1st Author, Year	Ref.
ZSM-5	α-alumina disk	381	0.26/–	2.3/–	Pressure drop (vacuum)	10	10	Yan, 1995	[99]
		458	0.19/–	3.7/–					
NaY	α-alumina tube	303	0.4/0.5	4/100	He sweep	1	20	Kusakabe, 1997	[148]
		403	2/	10/20					
SAPO-34	α-alumina tube	300	–/–	10/– (–)	Pressure drop	10	15	Poshusta, 1998	[87]

MFI-type zeolite membranes are promising for applications in separation processes for hydrogen concentration/purification from various hydrogen/hydrocarbon mixtures (at lower temperatures) and in membrane reactors for dehydrogenation reactions (at high temperatures).

Liquid Separations

Zeolite membranes have been studied for liquid separation by pervaporation and reverse osmosis processes. Most work of liquid separation by zeolite membrane was focused on pervaporation except for a recent work of Kumakiri et al.[112] who studied reverse osmosis separation of water–alcohol mixture by zeolite A membranes. Table 18 summarizes pervaporation results of water–hydrocarbon mixture by hydrophilic zeolite membranes. Kita reported quite high water selectivity of zeolite A membrane in various organic–water separation.[90,107,151] FAU membrane is also water selective, though the separation ability was lower than zeolite A membrane.[151] Compared to zeolite A membrane, the lower water selectivity in FAU zeolite membrane is due to its higher Si/Al ratio in the zeolite, making the membrane less hydrophilic.

Pervaporation separation of water–hydrocarbon mixture by zeolite A and FAU membranes synthesized by various preparation methods was also studied.[117,152] All membranes are water perm-selective. Same type of zeolite membranes prepared by different synthesis methods do not exhibit significant differences in pervaporation properties. It is known that the different preparation methods may cause a minor difference in the microstructure of the zeolite membranes (e.g., intercrystalline region). These results suggest that pervaporation properties are not sensitive to the microstructure of the zeolite membranes. This is quite different from the gas permeation properties of the zeolite membranes.

Table 19 summarizes the prevaporation properties of hydrophobic zeolite membranes. Silicalite membrane is permselective for alcohols over water, owing to its hydrophobicity as a result of high Si/Al ratio.[83,96,153] For pervaporation separation of acetic acid–water, silicalite membrane exhibits perm-selectivity for acetic acid while ZSM-5 membrane shows no separation.[94] Compared to Table 18, the hydrocarbon permeation fluxes through the hydrophobic zeolite membranes are similar to the water permeation flux through the hydrophilic zeolite membranes. However, the hydrophobic zeolite membranes exhibit much lower hydrocarbon to water selectivity than the water to alcohol selectivity offered by the hydrophilic zeolite membranes.

Results of pervaporation separation of organic mixtures by hydrophobic and hydrophilic zeolite membranes are summarized in Table 20. As shown, both hydrophobic and hydrophilic membranes exhibit permselectivity for

Table 18. Performances of Water Selective Zeolite Membranes in Pervaporation

Zeolite	Substrate	Synthesis Method[a]	Thickness [μm]	Feed Solution	Temperature [°C]	Water Flux [kg/m^2 h]	Selectivity [–]	1st Author, Year	Ref.
NaA	α-Al_2O_3 tube	HS	20 ~ 30	Water/Methanol (10 wt%)	50	0.57	2100	Kita, 1995	[90]
NaA	α-Al_2O_3 tube	HS	20 ~ 30	Water/Ethanol (10 wt%)	75	2.15	10000	Kita, 1995	[90]
NaA	α-Al_2O_3 tube	HS	20 ~ 30	Water/2-Propernol (10 wt%)	75	1.76	10000	Kita, 1997	[151]
NaA	α-Al_2O_3 tube	HS	20 ~ 30	Water/Acetone (10 wt%)	50	0.91	5600	Kita, 1997	[151]
NaA	Ceramesh sheet, carbon tube	HS	–	Water/2-Propanol (10 wt%)	25	0.13	8000	Jafar, 1997	[152]
NaA	Ceramesh sheet, carbon tube	HS	–	Water/2-Propanol (10 wt%)	70	0.79	4000	Jafar, 1997	[152]
NaA	α-Al_2O_3 disk	SG	~ 10	Water/Ethanol (90 wt%)	30	0.75	10000	Kumakiri, 2000	[284]
NaX	α-Al_2O_3 tube	HS	20–30	Water/Ethanol (10 wt%)	75	0.89	360	Kita, 1997	[151]
NaY	α-Al_2O_3 tube	HS	20–30	Water/Ethanol (10 wt%)	75	1.59	130	Kita, 1997	[151]
FAU	α-Al_2O_3 disk	SG	~ 10	Water/Ethanol (90 wt%)	30	0.2		Kumakiri, 2000	[284]

[a]HS—In-situ hydrothermal synthesis, SG—secondary growth.

MARCEL DEKKER, INC. • 270 MADISON AVENUE • NEW YORK, NY 10016

Table 19. Summary of the Pervaporation Results for Organic Selective Zeolite Membranes (Prepared by in-situ Hydrothermal Synthesis)

Zeolite	Substrate	Thickness [μm][a]	Feed	Temperature [°C]	Organic Flux [kg/m^2 h]	Selectivity [–]	1st Author, Year	Ref.
Silicalite	SS disk	400 ~ 500 (50 ~ 60)	Methanol/Water (1 mol%)	30	0.5	17	Sano, 1994	[141]
Silicalite	SS disk	400 ~ 500 (50 ~ 60)	Ethanol/Water (1 mol%)	30	0.2	64	Sano, 1994	[141]
Silicalite	SS disk	400 ~ 500 (50 ~ 60)	1-PrOH/Water (1 mol%)	30	0.07	90	Sano, 1994	[141]
Silicalite	SS disk	400 ~ 500 (50 ~ 60)	2-PrOH/Water (1 mol%)	30	0.04	45	Sano, 1994	[141]
Silicalite	SS tube		Methanol/Water (3.5 wt%)	23 – 32	1	7.2	Liu, 1996	[285]
Silicalite	SS tube		Acetone/Water (0.8 wt%)	23 – 32	0.2	250	Liu, 1996	[285]
Silicalite	SS disk	–	Acetic acid/Water (15 vol%)	30	0.038	2.6	Sano, 1997	[94]
ZSM-5	α-Al_2O_3 disk	–	Acetic acid/Water (15 vol%)	30	0.94	1	Sano, 1997	[94]

[a]Asymmetric membrane, data in parenthesis referred to the thickness of the inter growth layer thickness.

MARCEL DEKKER, INC. • 270 MADISON AVENUE • NEW YORK, NY 10016

Table 20. Summary of Organic Mixture Separation Results by Zeolite Membranes

Zeolite	Substrate	Synthesis Method[a]	Thickness [μm]	Feed	Temperature [°C]	Flux [kg/m^2 h]	Selectivity	1st Author, Year	Ref.
NaA	α-Al_2O_3	HS	20 ~ 30	Ethanol/ ETBE (10 wt%)	50	0.21	1200	Kita, 1997	[151]
NaX	α-Al_2O_3	HS	20 ~ 30	Methanol/ Benzene (10 wt%)	50	1.25	24	Kita, 1997	[151]
NaY	α-Al_2O_3	HS	20 ~ 30	Methanol/ Benzene (10 wt%)	50	0.62	1400	Kita, 1997	[151]
NaX	α-Al_2O_3	HS	20 ~ 30	Methanol/ MTBE (10 wt%)	50	0.26	320	Kita, 1997, 2001	[151,286]
NaY	α-Al_2O_3	HS	20 ~ 30	Methanol/ MTBE (10 wt%)	60	1.70	5300	Kita, 1997, 2001	[151,286]
silicalite	SS	HS		Methanol/ MTBE (50 vol%)	30–60	–	4–9	Sano, 1995	[153]
FER	α-Al_2O_3	VPT		Benzene/ p-xylene	30	0.2	600	Nishiyama, 1997	[126]

[a]HS—In-situ hydrothermal synthesis, VPT—vapor phase transport method.

MARCEL DEKKER, INC. • 270 MADISON AVENUE • NEW YORK, NY 10016

smaller molecule over the larger one. For FAU type zeolite membranes, NaY zeolite membranes exhibit higher methanol to MTBE or benzene selectivity than NaX zeolite membranes. NaY has a higher Si/Al ratio and is more hydrophobic than NaX. Therefore even in the organic mixture separation the hydrophobicity of the zeolite pores plays an important role in affecting the separation results.

Mitsui Engineering and Shipbuilding Co. in Japan developed a first large scale pervaporation plant using tubular NaA type zeolite membranes for solvent dehydration.[154,155] Due to its hydrophilicity, the NaA membrane is water perm-selective. The plant produces 530 L/hr solvents (ethanol, isopropanol, acetone etc) containing less than 0.2 wt% water, from the solvents with 10 wt% water. The pervaporation process is operated at 120°C. The tubular zeolite membranes are 80 cm long and 12 mm in outer diameter. The central part of the plant is a zeolite membrane unit consisting of 16 modules; each module is made of 125 NaA zeolite membrane tubes. Thus, this plant uses 2000 zeolite membrane tubes, with a total permeation area of about 60 m^2. It was reported that this zeolite membrane plant is cheaper than the polymer membrane one in terms of both capital and operation costs.

4. OTHER MICROPOROUS MEMBRANES

Many studies have been reported on synthesis and properties of a few other microporous inorganic membranes. Among these microporous membranes, carbon membranes have received most attention. Microporous, amorphous silica membranes could also be prepared by two methods very different from those described in the above two sections. Since the techniques for synthesis of mesoporous inorganic membranes are better established, it is not surprised to notice that in the past decade a large amount of work was published on preparing microporous inorganic membranes through narrowing the pore size of mesoporous membranes. In this section the microporous carbon and silica membranes will be reviewed first, followed by discussion of various methods used to modify mesoporous membranes. Some general characteristics of these microporous membranes will be summarized and compared with those of the microporous silica membranes prepared by the sol-gel method, and the zeolite membranes.

4.1 Synthesis of Carbon and Hollow Fiber Silica Membranes

High quality microporous carbon membranes in the hollow fiber geometry were first reported by Koresh and Sofer.[156–158] In the first paper on

this topic,[158] they reported good permeation and separation properties but gave little information about the synthesis of the microporous carbon membranes. The membranes were prepared by pyrolysis of polymer hollow fibers, probably consisting of poly(acrylonitrile).[159] Subsequently, several other research groups studied carbon molecular sieve membranes. Table 21 summarizes representative work reported on carbon membranes.

Preparation of the microporous carbon membranes usually includes two steps: synthesis of a polymeric precursor membrane in a desired geometry and conversion of the organic membrane into a carbon membrane in the same geometry. Most carbon membranes are prepared in the form of hollow fiber because the hollow fiber polymeric membranes can be readily fabricated.[158,160,161] Carbon molecular sieve membranes in other geometries were also prepared by converting thin polymer films supported on planar supports of porous graphite[162–165] or stainless steel,[159] and tubular supports of porous alumina[4,166,167,172] or stainless steel.[159,168,169]

The precursors used in making the carbon membranes are usually thermosetting polymers, including oxidized poly(acrylonitrile) (PAN),[160] poly(vinylidene chloride),[163] poly(imide),[161,164] polynuclear aromatic,[166] poly(furfuryl alcohol),[160,162,168] and penolic resin.[167] Hollow fibers of these polymers are prepared by the well established dry–wet spinning process.[170] Polymer thin films are first coated on the porous planar or tubular supports by dip-coating,[166] spin-coating[164,165] or spray-coating[168,171] of the solutions containing the polymer precursors. These polymer hollow fibers or films are then converted to carbons by pyrolysis at high temperatures. The quality of the polymer films at this stage should have a significant effect on the properties of the final carbon membranes after pyrolysis. It is expected that an even, flawless polymer film should be formed in order to obtain a carbon membrane without defects or pinholes larger than the micropores. However, few work has been reported on the relationship between the quality of an initial polymer film and the properties of the final carbon membrane derived from the film.

Pyrolysis (carbonation) typically takes place at an elevated temperature (about 400–1000°C) under vacuum or atmosphere of a non-oxidizing gas, such as helium or nitrogen. The organic polymer is converted to carbon by removing hydrogen, nitrogen and oxygen from the polymer precursor. The microstructure of a carbon membrane develops in the pyrolysis step. All microporous carbon membranes are amorphous, and the micropores are probably initiated by the small gaseous molecules channeling their way out of the solid matrix of the thin film during the pyrolysis. Since the pyrolysis is the most critical step in preparation of the carbon membrane, several research groups investigated the effects of pyrolysis conditions on the microstructure and permeation/separation properties of the final carbon membranes.

Table 21. Summary of Representative Work on Microporous Carbon Membranes

Polymer Precursor	Support Material and Geometry	Pyrolysis Conditions	Carbon Membrane Pore Size (nm)	Gas Separation Properties	Major Authors, Year	Ref.
Poly(vinylidene chloride)-acrylate	Flat and tubular porous graphite	1000°C in N_2	0.5–2	Surface flow, permselective to hydrocarbon	Rao and Sircar, 1993, 1996, 1999	[163,183, 184]
Acrylonitrile and methyl methacrylate	Supported, hollow fiber	600–950°C in air or N_2	7	No separation data	Linkov, 1994	[160]
Polyimide	Unsupported, hollow fiber	500–500°C, vacuum	0.3–0.6	O_2/N_2 selectivity of 8–13	Koros, 1995, 1996	[161,172]
Poly-furfuryl alcohol	Flat and tubular porous stainless steel	150–600°C in H_2	0.3–0.6	O_2/N_2 selectivity of 5–30	Foley, 1997, 1999, 2000	[168,171]
Polynuclear aromatic from pyrene and phenanthrene	Porous α-alumina tube	400–1050°C in deoxygenated N_2	2.4	Knudsen diffusion based selectivity	Morooka, 1998	[166]
Polyamic acid in N-methylpyrrolydone, phenolic resin (tubular support)	Flat macroporous graphites; Tubular alumina	550°C (or 700°C for tubes) in vacuum	<2 nm	O_2/N_2 and CO_2/CH_4 selectivities of 5 and 37 (or 150 on tubular support)	Fuertes and Centeno, 1998, 1998, 2001	[164,165, 167]

Geiszler and Koros[172] studied the effects of pyrolysis conditions, including purge gas for pyrolysis (helium, argon or carbon dioxide at various flow rates, and under vacuum) and pyrolysis temperature (550–800°C), on the gas permeation/separation properties of the hollow fiber carbon membranes prepared from polyimide hollow fibers. The membranes prepared under the flow of the purge gases mentioned above have a higher permeate flux and lower selectivity than the membranes prepared under vacuum. Reductions in the purge gas flow rate caused a decrease in the gas permeance of the carbon membranes. This appears to suggest that the presence of a purge gas or increasing purge the gas rate enhances the removal of the volatile byproducts (such as hydrogen, water, and carbon oxides) from the polymer film during pyrolysis, resulting in a more open microstructure of the final carbon membrane.

Carbon membranes pyrolyzed at higher temperatures has a less opening micropore structure with a higher carbon content and a lower gas permeance.[172] The permselectivity of the carbon membranes increases with increasing pyrolysis temperature.[172] Similar results were also obtained by Kusakabe et al.[166] on carbon membranes prepared from condensed polynuclear aromatics. It is easy to understand that carbonization (removal of noncarbon species) is enhanced at higher pyrolysis temperature. Low permeance and high perm-selectivity indicate a less opening pore structure of the carbon membrane obtained at high pyrolysis temperature. Kusakabe et al.[166] found that the micropore volume (determining the selectivity) increased but the mesopore volume (determining the permeance) decreased with increasing pyrolysis temperature. However, it is not clear how the pyrolysis temperature causes such a change in the microstructure of the carbon membranes during the pyrolysis step. Shiflett and Foley[168] found that carbon membranes obtained at higher pyrolysis temperature have a higher permeance and lower permselectivity. Their carbon membranes may contain no mesopores (as indicated by high oxygen to nitrogen selectivity) and therefore increasing pyrolysis temperature increases microporosity only.

Hollow fiber microporous silica membrane was prepared by the PPG Industries.[173] Preparation of this hollow fiber silica membrane was based on the phase separation phenomenon of glass[174] similar to that involved in preparation of the well known mesoporous Vycor glass membranes.[175,176] Preparation of the hollow fiber silica membrane starts with a melt of borosilicate consisting 20–60% boron oxide. The composition of the melt should be in such that two phases rich either in silicon or boron can be formed at a lower temperature. The melt is then extruded and attenuated at speed of about 150–7000 m/min to form hollow fiber at a high temperature. The hollow fiber is then quickly cooled down to a temperature below 400°C, and annealed at that temperature for a few minutes to a day to allow spatial redistribution of the two phases (boron oxide rich and silica rich phases). The boron oxide rich

phase is then leached out using a leaching agent, typically an acid (such as HCl) because boron oxide can easily dissolve in the acid. The leaching agent is finally removed from the silica skeleton, which remains to form the microporous silica membranes.

To succeed in preparing microporous silica membranes, it is important to control the size and connectivity of the leachable phase (boron rich phase). The connectivity of the leachable phase is in part determined by the glass composition. Annealing below 400°C could avoid nucleation of the leachable phase. In this case the size of the leachable phase is less than the size of the nucleus. Since the structure of the leachable (boron rich) phase determines the structure and size of the pores of a silica membrane, such small size of the leachable phase is essential to obtaining silica membranes with microporous sizes. Obviously, such a structure of the leachable phase makes the leaching process more difficult, requiring a longer leaching time. If the glass is annealed at a higher temperature (400–1000°C) for longer period of time, the leachable phase can nucleate to a nanometer size. Silica membranes of mesopore size (like Vycor membranes, with a pore diameter of about 4 nm) are obtained after removing the nanometer-scale leachable phase. Therefore, controlling the annealing conditions is the key to obtaining the silica membranes with a micropore size.

Other than the information provided in the patents authored by Hammel et al.,[173] no studies have been reported on detailed mechanisms of the synthesis of the microporous silica membrane by the phase separation method. This is in sharp contrast to the studies on the sol-gel derived microporous silica membranes. Way and Ma and their co-workers[177–179] independently studied the gas separation and permeation properties of the hollow fiber microporous silica membrane. This microporous silica membrane shows excellent gas separation properties, as to be reviewed next. Nevertheless, the major problem with this hollow fiber silica membrane is associated with its brittleness in comparison with hollow fiber carbon membranes. This makes it very difficult to handle the membranes, even for the laboratory experiments. This could partly be the reason for relatively few studies on this type of microporous silica membranes after they were invented about a decade ago.

4.2 Permeation Properties of Microporous Carbon and Silica Membranes

Table 22 compares the geometry of the hollow fiber silica membrane with the hollow fiber carbon membranes prepared by the different research groups. All the carbon and silica membranes summarized in Table 22 are microporous with a pore diameter smaller than 2 nm. Since it is difficult to measure the pore

Table 22. Comparison of Pore Size and Gas Permeance of Hollow Fiber Carbon and Silica Membranes

Membrane Material Producer/Reference	Carbon Koresh/Sofer, 1983[158]	Carbon Jones/Koros, 1995[161]	SiO_2 PPG, Bhandarkar et al., 1992[287]
Membrane Geometry			
ϕ_{out} (μm)	152	132	32
H_{Wall} (μm)	~6	35	~5
d_{pore} (nm)	<2	<2	<2
He Permeance and Flow through a 10 cm Long Fiber (Δp = 1 atm)			
He permeance 10^{-4} (cc/cmHg.cm^2.s)	~2	~0.2	~2
Surface area (cm^2)	0.48	0.41	0.1
Flow rate (cc/min)	0.21	0.18	0.04

size of microporous membranes,[7,180,181] the actual pore sizes of these microporous carbon and silica membranes were estimated at the range from 0.4 to 0.7 nm. The helium permeance of the carbon membrane prepared by Koresh and Sofer[158] is similar to that of the PPG silica membrane, but much larger than that of carbon membrane prepared by Jones and Koros,[161] obviously due to the thicker wall of the latter membrane. If normalized by the wall thickness, these microporous carbon and silica membranes have

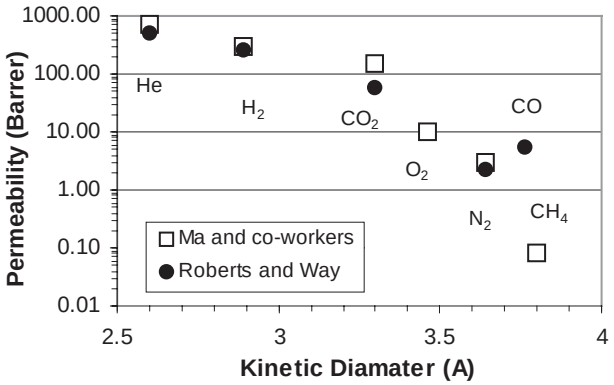

Figure 25. Single gas permeability versus gas molecular size for the PPG hollow fiber silica membranes reported by Way and Roberts[137] (at 70°C) and by Shelekhin et al.[178] (at 30°C).

Table 23. Activation Energy for Gas Permeation in Hollow Fiber Silica Membranes

Permeating gas	He	H_2	CO_2	O_2	N_2	CH_4
Kinetic diameter (Å)	2.6	2.89	3.3	3.46	3.64	3.8
Activation energy (kJ/mol)	2.54	/	4.22	14.9	14.9	18.9

(From Ref. [178].)

comparable helium permeability, indicating a similar pore structure of these three microporous hollow fiber inorganic membranes. The helium flow for a 10 cm long carbon fiber membrane is about 5 times that for the silica membrane of the same length due to smaller outer diameter of the silica membrane.

Two research groups studied independently permeation of single gases through the PPG hollow fiber silica membrane. Figure 25 shows permeation data of essentially same gases through the silica membranes studied by these two groups. As shown, the permeability (in Barrer, 1 Barrer $= 3.348 \times 10^{-16}$ mol/m.s.Pa) of these gases decreases with increasing kinetic diameter of the gas molecule. The data from these two groups agree quite well with each other considering the differences in the permeation temperature, experimental setup and conditions used in the two studies. Table 23 lists activation energy for permeation of these gases, obtained by regression of the Arrhenius equation with the permeability data at different temperatures, for the hollow fiber silica membranes.[178] The activation energy increases for the gases with increasing molecule size and decreasing permeability. These data suggest a possible molecular sieving mechanism for the microporous silica membrane.

Burggraaf and co-workers[25,34,35,38–40] measured permeance of several gases through the microporous silica membranes prepared by the sol-gel method. Table 24 lists the permeance data of some gases for the sol-gel derived silica membranes. These gases were also studied for the hollow fiber silica membrane for the sol-gel derived microporous silica membranes. As shown, the gas permeance, measured on the two sol-gel derived silica membranes, also decreases with increasing molecule size of the permeating gas.

Table 24. Gas Permeance (at 100°C) and Activation Energy for Permeation for the Sol-Gel Derived Microporous Silica Membranes[a]

Permeating gas	He	H_2	CO_2	CH_4
Kinetic diameter (Å)	2.6	2.9	3.3	3.8
Permeance (100°C) (10^{-7} mol/m^2.s.Pa)	28	19(22)	10(6.8)	~ 0
Activation energy (kJ/mol)	/	11(15)	6(10)	/

[a]Data in parenthesis are from Refs. [38–40] (permeance at 200°C).
(From Refs. [34,35].)

The permeance data of the two different sol-gel derived silica membranes agree reasonably well with each other. The activation energy for permeation of H_2 and CO_2 through the sol-gel derived silica membranes is larger than that through the hollow fiber silica membrane. Different from the hollow fiber silica membrane, the activation energy for permeation for the sol-gel derived silica membranes decreases with increasing gas molecule size.

Gas permeability for a microporous membrane is a product of diffusivity and solubility (adsorption equilibrium constant) of the gas in the membrane (see Section 5 for details). The activation energy for diffusion, not permeation, should be used to indicate how difficult a gas molecule moves in the micropores of a microporous membrane. Assuming a linear adsorption isotherm, the activation energy for diffusion (E_d) can be correlated to the activation energy for permeation (E_p) and heat of adsorption (q_{st}) by $E_d = E_p + q_{st}$. Note that q_{st} and E_d are respectively smaller and larger than zero so it is possible for one to obtain a negative value for the activation energy for permeation (E_p). de Lange et al.[38–40] measured heat of adsorption for H_2 and CO_2 on the sol-gel derived silica membranes. From the data of activation energy for permeation, E_d was calculated and the results are compared in Table 25 which gives E_d of about 21 and 32 kJ/mol respectively for H_2 and CO_2. Diniz da Costa[55] recently reported values of activation energy (E_d) for diffusion of He, H_2, CO_2, O_2, N_2 and CH_4 in a sol-gel derived silica membrane of about 14, 20, 22, 23, 24, 25 kJ/mol. As expected the activation energy for diffusion indeed increases with decreasing gas molecule size, indicating that larger molecules require more energy to move in the micropores. These data of the activation energy for diffusion are similar to those for gas diffusion in smaller pore zeolites (like A and MFI type zeolites with a pore diameter in the range of 0.4–0.6 nm). Therefore, the gas permeation data for the sol-gel derived microporous membranes suggest that the pore sizes of these membranes are in the same range as that of zeolites.

In comparison with the hollow fiber silica membrane with a thick membrane wall, very thin silica membrane can be formed on porous support by the sol-gel method. Recent advances in the sol-gel derived microporous

Table 25. Activation Energy for Diffusion and Heat of Adsorption in Sol-Gel Derived Silica Membranes

Permeating Gas	Kinetic Diameter (Å)	E_p (kJ/mol)	q_{st} (kJ/mol)	E_d^* (kJ/mol)
H_2	2.9	15	6.1	21.1
CO_2	3.3	10	22.3	32.3

(From Refs. [38–40].)

silica membranes include use of the support with smaller pore or smoother surface and coating of silica film under clean-room conditions.[48,67] The use of better quality support allows coating of ultrathin (down to 30 nm), defect free microporous silica film on the support. Clean-room coating avoids formation of pinholes in the thin silica film. As a result, these supported ultrathin microporous silica membranes offer significantly improved gas permeation and separation properties as compared to the hollow fiber microporous silica membranes or the sol-gel derived microporous silica membranes reported earlier. Figure 26 compares single gas permeance data of the sol-gel derived ultrathin microporous silica membranes reported recently[48,67] with those of the PPG hollow fiber microporous silica membrane. All the three microporous silica membranes show excellent gas separation properties, with an ideal separation factor for the small molecule (hydrogen) to the large one (methane) of about 10^4. But the sol-gel derived silica membranes exhibit gas permeance about two orders of magnitude larger than the hollow fiber membrane. Furthermore, the sol-gel derived microporous silica membranes are mechanically much stronger than the hollow fiber membrane, making the former more attractive for practical applications.

Much work has been done in searching for better polymeric membranes for separation of oxygen/nitrogen mixture because of its great industrial importance. Shiflett and Foley[182] recently reported microporous carbon membranes with nitrogen/oxygen separation properties better than all the polymeric membranes reported up to date. As described earlier, these carbon membranes were prepared by ultrasonic deposition of poly(furfuryl) alcohol on porous

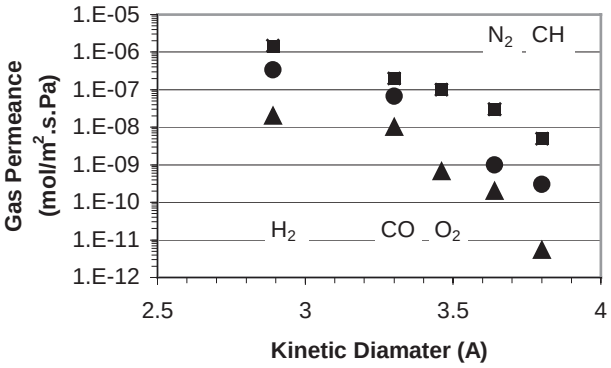

Figure 26. Comparison of single gas permeance of various gas molecules of different sizes through sol-gel derived microporous silica membranes (■—de Vos and Verveij;[48] ●—Tsai et al.[67]) and microporous silica hollow fiber membrane prepared by phase separation method (▲—Shelekhin et al.[178]).

inorganic support, followed by pyrolysis at 473–873 K under controlled conditions to convert the polymer layer to microporous carbon film. Table 26 compares the characteristics of the microporous carbon membranes with that of the sol-gel derived silica membranes. The carbon membrane gives an oxygen to nitrogen separation factor of about 30, the largest for any membranes reported at low temperatures. Both the kinetic and equilibrium factors may contribute to such a large separation factor.

However, the permeance of the carbon membrane is still too low, obviously due to the large membrane thickness. The separation power of the carbon membranes (both selectivity and permeance) can be substantially improved if the thickness of the membrane is reduced to the nanoscale range, such as that for the sol-gel derived microporous silica membrane listed in Table 26. This requires development of a delicate technique for formation of a continuous, defect/pinhole-free thin microporous carbon film on a porous support.

Flat and tubular carbon membranes with a surface flow mechanism were successfully developed by Air Products and Chemical Inc.[163,183,184] The pore sizes of these microporous carbon membranes (about 1 nm) are larger than the microporous carbon membranes described before (about 0.4–0.6 nm). The micropore adsorption and diffusion are the dominating mechanism for gas permeation through the microporous carbon and silica membranes discussed above. In contrast, both gas phase diffusion and surface flow contribute to the gas permeation through the microporous carbon membranes prepared by the Air Products with a larger pore size. This surface flow plays a significant role in controlling multiple-gas separation properties. When the carbon membrane is used to separate nitrogen, hydrogen and hydrocarbons, the hydrocarbons are strongly adsorbed on the hydrophobic surface of the internal pores of the carbon membranes. The fluxes of the adsorbed hydrocarbons, though possibly less mobile on the pore surface, can be very higher due to their higher concentration in the adsorbed phase. The adsorbed hydrocarbons may also hinder transport of nonadsorbing gas (such as nitrogen or hydrogen) in the gas phase, further enhancing the perm-selectivity for hydrocarbons over hydrogen or nitrogen.

The surface of the microporous silica membranes described above is hydrophilic due to the presence of the surface silanol groups. Crystalline silica (zeolite silicalite) has a hydrophobic surface and therefore their permeation/separation properties are expected to be similar to the hydrophobic carbon membranes. Dong et al.[146] prepared good quality microporous silicalite membranes and measured permeation and separation properties of the membranes with a eight component hydrogen and hydrocarbon gas mixtures, as described in Section 3. Table 27 compares the permeation and separation properties of the zeolite membrane with the microporous carbon membrane. Both silicalite

Table 26. Oxygen/Nitrogen Separation Properties by Microporous Carbon (at 25°C) and Silica (at 100°C) Membranes

Membrane Material	Pore Size d_p (nm)	Thickness L (μm)	O_2 Permeance J_{O2} (mol/m^2.s.Pa)	Separation Factor α_{O2/N_2}	1st Author, Year	Ref.
Carbon	~1	~15	5×10^{-11}	30	Shiflet, 2000	[168]
Silica	~0.5	0.03	1×10^{-7}	3–7	de Vos, 1998	[49]

Table 27. Comparison of Permeation and Separation Properties of MFI Zeolite Membrane[146] and Carbon Membranes[163] Under Similar Conditions

Gas Component	H_2	CH_4	C_2H_6	C_2H_4	C_3H_8	C_3H_6	n-C_4H_{10}	i-C_4H_{10}
Zeolite membrane[a]								
Mole fraction (%)	84.5	7.6	2.5	2.5	0.75	1.45	0.4	0.3
Permeance[b]	0	4.6	15.0	24.5	45.0	70.4	94.7	0
Carbon membrane[c]								
Mole fraction (%)	41.0	20.2	9.5	0	9.4	0	19.9	0
Permeability[d]	1.2	1.3	7.7	N/A	25.4	N/A	112.3	N/A
Permeance	0.16	0.17	0.86	N/A	3.3	N/A	14.8	N/A

[a]Zeolite membrane: $P_f = 0.372$ MPa atm, $P_p = 0.1$ MPa, $T = 25°C$, membrane thickness = 3 μm.
[b]Unit for permeance (10^{-9} mol/m^2.s.Pa).
[c]Carbon membrane: $P_f = 0.446$ MPa, $P_p = 0.108$ MPa, $T = 22°C$, membrane thickness = 2.5 μm.
[d]Reported permeability with unit in (Barrer).

MARCEL DEKKER, INC. • 270 MADISON AVENUE • NEW YORK, NY 10016

and carbon membranes are permselective for hydrocarbons over hydrogen. However, the zeolite membrane exhibits higher permeation flux and better selectivity than the carbon membrane. Furthermore, the carbon membrane loses its selectivity above the room temperature because the separation mechanism of the carbon membrane is based on the surface flow, which decreases rapidly with increasing temperature. In contrast, the hydrocarbon flux over the zeolite membrane is still higher than hydrogen flux at temperatures up to about 100°C. The permeation mechanism in the zeolite membrane is solution (adsorption) and diffusion, rather than the surface flow. This difference in transport mechanism explains the different results of these two hydrophobic microporous inorganic membranes.

4.3 Microporous Inorganic Membranes Prepared Through Pore Size Reduction

Microporous membranes of only a few materials can be fabricated by the direct synthesis methods, as summarized above. Substantial efforts were reported to prepare microporous membranes by modifying mesoporous inorganic membranes. Most work reported was focused on modifying 4 nm pore Vycor glass and sol-gel derived γ-alumina membranes. The Vycor glass membrane has a symmetrical wall of about 2 mm in thickness. The sol-gel derived γ-alumina membrane is normally about 4–5 μm in thickness, supported on 2 mm thick α-alumina. For the disk-shaped γ-alumina membranes, the α-alumina support has a symmetric pore structure with a pore diameter of about 0.2 μm. Tubular γ-alumina membranes are supported on multi-layer asymmetric α-alumina support with the upper most layer having the smallest pore size (about 0.2 μm in diameter). The support of the tubular γ-alumina membrane has a much lower mass transfer resistance than that used in the disk shaped γ-alumina membrane.

The basic idea to prepare microporous membrane through this route is to deposit an inorganic solid or large organic molecules in the pores of the mesoporous layer in order to reduce its pore size to smaller than 2 nm. Methods used to modify the ceramic membranes can be categorized into liquid phase approach and vapor phase approach. In both approaches, precursors are introduced into the pores of a porous ceramic membrane and a solid is formed in the pores and deposited on the internal pore surface of the membrane. In the liquid phase approach, a small amount of impregnating solution containing the solid precursor is sucked into the membrane pores by the capillary force. The precursor may be converted to a final deposit or an intermediate in the pores by a chemical reaction or after the solvent is dried. If the deposit is

not formed after the drying step, it is normally formed during a subsequent calcination step at a medium temperature (300–600°C).

Several studies were reported using the liquid phase approach to modify the mesoporous γ-alumina membrane with the aim of narrowing its pore size to improve the permselectivity. Miller and Koros[185] reported deposition of an organometallic compound, tetrahydrooctyl-1-trichlorosilane (TDFS) in the pores of a commercial tubular γ-alumina membrane. Ma and co-workers[186] impregnated Fe_2O_3 and Al_2O_3 in the same commercial tubular γ-alumina membrane. Uhlhorn et al.[25] attempted to improve the permselectivity and catalytic properties of the disk-shaped γ-alumina membranes by depositing Ag, MgO and V_2O_5. They used a reservoir method to coat a large amount of solid in the pores of the γ-Al_2O_3 layer. In this method, the precursor solution is soaked in both the support and the top-layer. Drying of the solvent takes place only on the surface of the γ-Al_2O_3 film. Because of the large amount of the solution contained in the α-alumina support, this method allows impregnation of large amount of solid in the thin γ-Al_2O_3 film. More recently, Lin et al.[187] reported deposition of CuCl on the disk-shaped and tubular γ-Al_2O_3 membranes in order to prepare membrane permselective for ethylene over ethane.

All these modified mesoporous γ-Al_2O_3 film membranes did not exhibit the features of a microporous membrane. Modification usually causes a significant reduction in gas permeance with slight improvements in gas selectivity. The modified membranes exhibit permselectivity closed or slightly better than that determined by the Knudsen permeation mechanism. For example, coating of CuCl resulted in about 10-fold reduction in gas permeance of the γ-alumina membrane but the modified γ-alumina membrane did not show improvement in ideal gas separation factor for ethylene over ethane.[187] The ethylene/ethane selectivity measured for permeation of the gas mixture for the modified membrane is about 10% higher than the unmodified membrane.[187] This improvement in the selectivity is not related to the reduction in pore size but due to the presence of the surface flow of ethylene on the CuCl modified γ-alumina pore surface. The difficulty to reduce the pore size of the mesoporous membranes to improve permselectivity will be explained in Section 4.4.

Chemical vapor deposition (CVD) is another approach commonly used to modify mesoporous membranes. The CVD can be operated in two ways to modify a mesoporous ceramic membrane. One way is to introduce the precursors in the opposite sides. This CVD process involves counter-diffusion of two vapor precursors in the membrane pores and CVD of a solid product on the pore surface,[188–190] as shown in Figure 27. This is basically a method extended from the electrochemical vapor deposition originally developed by Westinghouse for fabrication of solid oxide fuel cells.[191] Another way is to introduce vapor precursor or precursors from one side of membrane surface

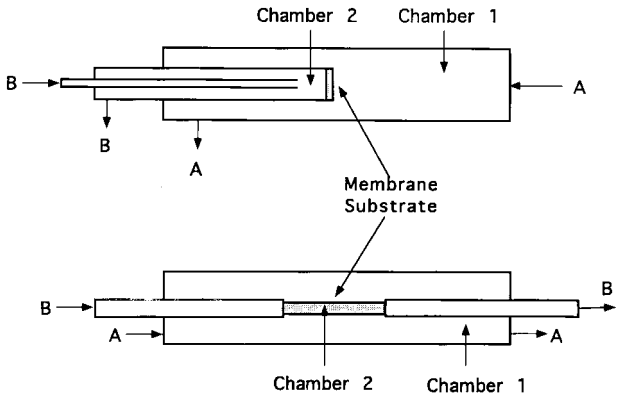

Figure 27. Schematic diagram for CVD modification of disk-shaped or tubular ceramic membranes (After Ref. [218]).

into the membrane pores and deposit (possibly after a chemical reaction) on the membrane pore surface.[189,192] This vapor phase method is very similar to the better-studied chemical vapor infiltration (CVI) method for fabrication of ceramic matrix composites.[193]

The CVD method was used to modify mesoporous membranes for a number of different purposes. Depending on the degree of deposition, the CVD modification could result in coating of a thin film on the internal pore surface of the mesoporous membrane to modify its surface chemical properties. With a proper selection of precursors, CVD for extended period of time may lead to the electrochemical vapor deposition to grow a thin dense films on the surface of the mesoporous membranes.[191,194–197] CVD was also used to deposit a thin microporous (or dense) silica in the mesoporous membrane.[188,192,198–200] This dense silica contains angstrom size framework opening (amorphous) and can be classified as microporous membrane. The attempts to narrow the pore size of the mesoporous membranes were also reported. In the next, we will first review those studies aimed at narrowing the membrane pore size by the CVD method.

Burggraaf and co-workers were the first attempting to narrow the pore size of mesoporous γ-alumina membranes.[201] In their work, the sol-gel derived 4 nm pore γ-alumina membrane disks were modified by counter-diffusion CVD of zirconia or yttria doped zirconia (YZ) using corresponding metal chloride vapor and oxygen/water vapor mixtures as the CVD precursors. The CVD reaction was performed at 800–1000°C and 1–10 mbar. Typical CVD time was about 20 min. YZ was deposited in a narrow region (about 0.5 μm) in the mesoporous γ-alumina layer of about 5 μm in thickness. The YZ

oxides deposited in the γ-alumina mesopore were small crystals (nucleus) detectable by XRD.

The CVD of YZ in the γ-alumina mesopore resulted in several fold reduction in the helium permeance, but did not show improvement in the ideal gas separation factor of helium to nitrogen. The data of single gas permeance versus average pressure[202] appeared to suggest a pore reduction of the γ-alumina layer by CVD. However, the pore size reduction was perhaps not sufficient in order to see a change in the gas permeation mechanism from Knudsen diffusion to microporous diffusion with improved permselectivity. Cao et al.[203] could verify the pore narrowing of the mesoporous γ-alumina layer by the same CVD process using the perm-porosimetry method.[204] Their study, however, showed the difficulty to control the deposition as to narrow the pores of the γ-alumina membranes to the micropore size range by CVD of yttria–zirconia. Long CVD time usually resulted in pore closure.

Liu and co-workers[205,206] reported pore narrowing of the commercial 4 nm pore γ-alumina membrane tube by CVD of silica using tetraethylorthosilicate (TEOS) and oxygen as the precursors. These two precursors, carried by helium and driven by a transmembrane pressure drop, passed through the membrane wall, from the tube side. The oxidation (decomposition) of TEOS in the pores of γ-alumina layer resulted in deposition of silica on the membrane pore wall. The deposition zone thickness was about 1.5 μm. Two types of silica-modified membranes, porous or dense, were obtained depending on CVD time, which varied from 15 to 300 min. The porous membranes were obtained by shorter CVD times. Pore size distributions of the active layer of the modified membranes were measured by the methods of permporosimetry and size exclusion of selected gases.[7] They reported that the CVD modification could reduce the pore size of the γ-alumina membranes down to about 0.4 nm.

Table 28 compares binary separation and permeation data of nitrogen and neopentane of the modified γ-alumina membranes of different pore size with the unmodified γ-alumina membrane. The CVD modification caused about 2 to 10 fold reduction in the pore size. The nitrogen permeance of the modified membranes is about 100 to 700 times lower than the unmodified membrane. This indicates that the CVD modification reduces not only the pore size but also the porosity. The modified membranes exhibit much higher nitrogen over neopentane selectivity. The activation energy for hydrogen permeation through the CVD modified membrane is in the range of 6–14 kJ/mol, significantly lower than that for dense silica membrane (about 35 kJ/mol).[188] These data also support that the CVD modified membranes reported by Liu and co-workers[205] are indeed microporous.

Morooka and co-workers[207,208] also modified 6–9 nm pore γ-alumina membrane by a similar CVD process as described above, using TEOS,

Table 28. Gas Permeation Properties of Unmodified γ-Alumina and those Modified by CVD of Silica

Samples	Average Pore Size (nnm)	N_2 Permeance ($\times 10^{-6}$ mol/m^2.s.Pa)	N_2/Neopentane
Unmodified	4.0	9.6	1.6
Modified (S42)	1.5–0.6	0.024	15.3
Modified (S47)	0.6–0.4	0.016	405

(From Ref. [205].)

phenyltriethoxysilane (PETS) and diphenyldiethoxysilane (DPDES), without oxygen precursor. Silica was formed on the pore mouth by decompostion CVD of the silicon precursors at 500–650°C, followed by calcinations at 400°C for 5 h to remove carbon residual. Depending on the precursor used, the silica modified alumina membranes were either dense (with pore size defined by the opening of the silica tetrahedral framework, in the range of about 0.2–0.4 nm) or microporous (0.5–1 nm). The modification only resulted in 3–5 fold reduction in hydrogen permeance. However, the modified membranes exhibited very good selectivity for the molecules of different sizes, with single gas permeance decreases with increasing molecular size in the order, helium > hydrogen > carbon dioxide > nitrogen > methane > propane > iso-butane and SF_6. The CVD modified membrane reported in this work has much smaller reduction in gas permeance but better selectivity compared to the similar silica modified membrane reported by Liu and co-workers.[205] This is because in the work of Sea et al.[208] CVD was conducted at higher temperature, resulting in deposition of a thinner silica film with smaller pore as compared to the work reported by Liu and co-workers.[205] More detailed analysis of the CVD process and the morphology of the deposit will be given in Section 4.4.

Dense glass of amorphous silica has been known for many years to be hydrogen permselective.[176,188] The glass contains fine pore openings defined by the framework of the randomly linked silica tetrahedrals. The sizes of the pore openings range from 0.2 to 0.4 nm, and small molecules, such as hydrogen can permeate through these openings. These dense glass membranes can be considered as a special microporous membrane. Due to its ultramicropore size, hydrogen permeability in these dense glass membrane is several orders of magnitude lower than the 4 nm pore Vycor glass membrane, with high activation energy for permeation (>30 kJ/mol). Molecules larger than hydrogen can hardly permeate through the dense glass membrane. Dense, amorphous titania, boron oxide and alumina also offer similar gas permeation/

separation properties. To increase the hydrogen permeation flux, many efforts were reported to prepare ultrathin silica layer on mesoporous ceramic membranes. Gavalas and co-workers were the first to use the CVD method to deposit such a silica film in mesoporous inorganic membrane.[188,209]

In the work of Gavalas et al.,[188] silica was deposited inside the 4 nm pore Vycor glass tubes by counter-diffusion CVD of silane (SiH_4) and oxygen (see Figure 27). In the same work, the authors also tried one-sided film deposition but this resulted in gas phase nucleation and deposition of a porous film on the Vycor wall. H_2 and N_2 permeation fluxes of the membrane measured as a function of temperature indicated that the permeation mechanism of H_2 was mainly by activated diffusion. Although the deposition reaction could be performed at relatively low temperature (450°C) and with fast rate (pore plugging completes in 10 min), the resulting membranes exhibited poor properties (decreased permeability and selectivity) at higher temperatures (>600°C) and in the presence of water vapor, probably because of densification and shrinkage of silica under these conditions.

In a subsequent work, the preparation of hydrogen permselective SiO_2, TiO_2, Al_2O_3 and B_2O_3 films by the hydrolysis of the chloride precursors $SiCl_4$, $TiCl_4$, $AlCl_3$ and BCl_3, supported on porous Vycor glass tubes, was studied experimentally.[210–212] Both counter-diffusion and one-sided reactant geometries were used in these experiments. This work was mainly carried out in order to prepare membranes with improved thermal stability as compared to pure silica membranes prepared previously by silane oxidation. Since the hydrolysis reactions could take place at high temperatures, c.a. 800°C, the stability of the membranes at this range would be assured. SiO_2 membranes could be prepared by either one-sided or opposing reactant geometry while TiO_2 and Al_2O_3 membranes could be formed only by the latter. This was attributed to the different reaction mechanism for SiO_2 formation, compared to that for TiO_2 and Al_2O_3. In the case of SiO_2, the reaction followed mainly heterogeneous mechanism so the manner of how the reactant was introduced was not important. In the case of TiO_2 and Al_2O_3 however, where homogeneous reaction kinetic is faster, one-sided introduction resulted in fast reactants depletion and thus negligible deposition in the pore walls. Higher H_2 permeabilities and selectivities were observed for SiO_2 membranes in this study.

CVD for silica membrane inside Vycor glass tubes made by oxidation of triisopropylsilane, $(C_3H_7)_3SiH$ (TPS), with oxygen in the opposing reactant geometry, was reported by Megiris and Glezer.[199] The prepared membranes had relatively higher H_2 permeability and selectivity. The evolution of the membrane microstructure consisted of initial pore narrowing near the TPS side and subsequent deposition of clusters of grains on this side, probably because of oxygen slip and reactions in the gas phase with TPS. From this study it was observed that the relative ratio of TPS to oxygen concentration

should be higher than a minimum value in order to achieve formation of selective membranes.

Similar work was reported by Okubo and Inoue[192] who performed silica deposition in order to introduce specific gas selectivity in porous Vycor glass tubes. In their work, tetraethoxysilane (TEOS) was introduced in the inner side of the Vycor glass tube and decomposed at 200°C to produce a thin silica deposit partially closing the pores close to the inner tube surface. Together with the CVD precursor, He and O_2 were introduced in the tube as well in order to continuously monitor the evolution of the permeability and selectivity of the membrane for these gases. The permeabilities of these gases decreased gradually with deposition time and obtained a plateau value even though precursor was still being fed in the system. The selectivity of the treated membrane remained initially constant and close to the Knudsen separation factor (3) but later increased relatively fast and stabilized to a value of 6. The above observations suggested that the CVD reaction proceeded to a level where pore closure was sufficient enough to constrict the permeation of large molecules like O_2 and TEOS, which explains the stabilization of the permeability of the membrane for He and O_2.

Prabhu and Oyama[213] modified mesoporous Vycor glass membranes by five different liquid and vapor deposition methods, including those reviewed above, and compared the results of hydrogen/methane separation by these modified membranes. They could not obtain good separation results for the membranes modified by some of the methods reviewed above due to the reproducibility problem. However, an interesting discovery reported in the paper was that the Vycor glass membrane modified by decomposition CVD of TEOS in inert gas at 873°C exhibited excellent permeation and separation results. The deposition of silica on the Vycor glass membrane only resulted in about 2 fold reduction in hydrogen permeance, but the hydrogen/methane separation factor increases from about 2.8 for the unmodified membrane to about 25,000 for the modified membranes. The authors suggested that the modification resulted in deposition of a thin layer of silica in the mouth of the pores of the Vycor glass membrane. This is expected from the theoretical analysis performed by Lin and co-workers at University of Cincinnati, as to be discussed in the next section, for the one-sided CVD at such high temperature.

The small thickness of the silica film deposited in the Vycor glass membrane explains minimum reduction in hydrogen permeance as compared to unmodified membranes. The high selectivity is related to the microstructure of the deposited silica, which is not clear at this stage. The deposited silica certainly does not have a microstructure which resembles the pore narrowing of Vycor. It is more likely that the silica formed by decomposition CVD at such high temperature has a more ordered structure with minimum defects. The pores are strictly defined by the silica tetrahedral framework opening, giving

rise to high hydrogen/methane selectivity. The lower activation energy (2 kJ/mol) for hydrogen permeation could indicate that heat of sorption of hydrogen is close to activation energy for hydrogen diffusion in the deposited silica. Based on the limited isotope exchange experiments Prabhu and Oyama[213] suggested a possible hydrogen atomic transport mechanism. This, unlikely for silica–hydrogen systems, remains to be validated by other experiments.

4.4 Characteristics of Membrane Modification Processes

Modification of mesoporous membrane, either by vapor or liquid phase method, is accomplished by deposition of a solid inside the membrane mesopores. In these methods the deposition occurs as a result of combined transport of precursor into the pores and reaction of the precursors to form a solid deposit inside the pores. If a cylindrical pore model is used to represent the microstructure of the mesoporous membrane being modified, the deposit usually distributes along the precursor transport direction in a manner shown in Figure 28. Macroscopically the results of the deposition can be characterized by deposition zone thickness, deposit location, and effective pore size (radius) of the deposition zone. The deposition zone thickness and pore size determine the permeance and selectivity of the modified membranes. The location of the deposit may have an effect on the mechanical properties of the modified membranes.[190]

Microscopically, the structure of the deposit can also affect the permeation and separation properties of the modified membranes. Two extreme cases of the microstructure of the deposit are shown in Figure 29.[214] In the first case, the pore of a mesoporous membrane is narrowed by a dense layer

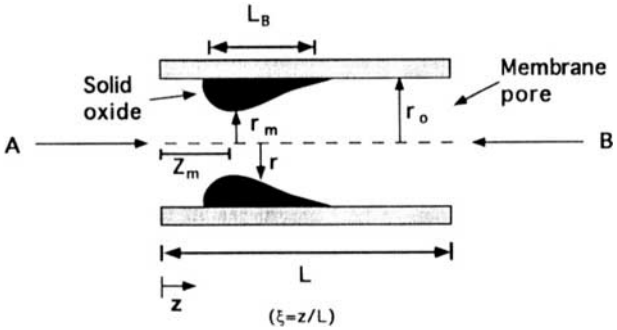

Figure 28. Schematic illustration of macroscopic characteristics of the solid product deposited inside a membrane pore by CVD (After Ref. [218]).

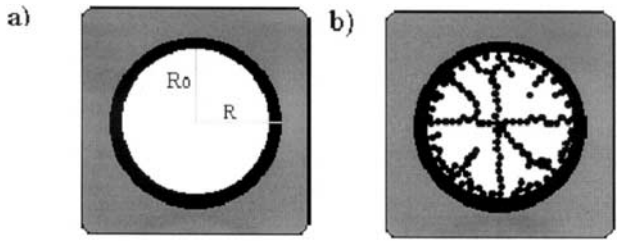

Figure 29. Schematic illustration of microscopic characteristics of the solid product deposited in a membrane pore (a) dense layer of deposit on the pore wall, (b) deposit of fractal structure in the pore (Modified from Ref. [214]).

deposited on the membrane pore wall. In the second case, the deposit has a structure more like branched polymer. Mesoporous ceramic membranes normally have a pore size distribution (PSD) and noncircular pore opening shape. Some ceramic membrane samples may contain pinholes or defects which constitute a small portion of the larger pores in the PSD for the membrane samples. These will also influence the characteristics of the deposit and final performance of the modified membranes.

All above major characteristics of the deposit important to the properties of the modified membrane are obviously determined by mechanism and conditions of the modification process. In the next, we will review the literature on quantitative understanding of these characteristics of the deposit and their relationship with the modification conditions. Since the CVD has been most extensively used to modify mesoporous membranes, most work in this area has been focused on modeling the CVD processes and comparison of the modeling results with the experimental data. Nevertheless, these results are applicable to other modification processes involving transport of precursors and reaction in the pores.

Theoretical modeling aimed at understanding the macroscopic characteristics of the CVD process for membrane modification followed the approach of phenomenological description of diffusion and reaction in porous media. Similar approach has been used to model another important process, chemical vapor infiltration (CVI), for fabrication of ceramic-matrix composites.[190,215] The CVI process involved infiltration of one or two precursors from the outer surface of a porous inorganic matrix by diffusion or viscous flow and reaction of the precursors in the pores. The solid product is deposited in the porous matrix. Different from the CVI, the CVD process for membrane modification is operated under the conditions that would give a deposition zone as small as possible. This makes modeling of the CVD process more difficult than the CVI process. Carolan and Michaels[216] were the first to model the CVD

process for membrane modification. Their mathematical analysis was based on a model considering counter-diffusion of the two reactants and reaction in the cylindrical pore. Lin and Burggraaf[190] and Brinkman et al.[217] later extended this model by considering the change of the pore geometry during CVD and using more realistic boundary conditions.

In these studies, deposition profiles (pore radius versus diffusion direction position) were calculated and examined under different conditions. Three parameters identified as most critical to the macroscopic characteristics are the Thiele modulus (ratio of reaction rate constant to diffusivity), relative gas phase concentration and intrapore diffusion coefficient of one reactant over the other. It was found that the Thiele module controls the deposition zone thickness and the concentration and diffusivity ratios affect the location of the deposit. The major limitation of these studies was that the models were solved for the cases with broader distribution of the deposit (larger deposition zone thickness) under the conditions of small Thiele modulus. These are not realistic for membrane modification because for this purpose the deposition zone as narrow as possible is desired. Xomeritakis and Lin[218,219] reported numerical solutions (by the finite element method) for the CVD model for membrane modification under the conditions of large Thiele modulus (narrow deposition zone). The simulation results show more clear effects of the Thiele moduli, pore closure rate constant, and reaction orders with respect to the two precursors, on the deposition results.

From the semi-analytical solution of the differential equation model for the CVD process,[218] Xomeritakis and Lin[219] later reported analytical expressions for the three parameters for the macroscopic characteristics of the deposit: the deposition zone thickness (L_B), deposition location (L_m) and pore narrowing rate (pore closure time) (t_{cl}) (referred to Figure 28 for their physical meanings). Table 29 lists such expressions for the deposition zone thickness and location of maximum deposition for three cases with different reaction orders with respect to the precursors A and B (see Figures 27 and 28 for the reactant feed configurations).

As shown by the expressions given in Table 29, in all three cases the deposition zone thickness decreases with increasing Thiele modulus. Since reaction rate constant is more sensitive to temperature than the diffusivity, the Thiele modulus increases with increasing temperature. Therefore CVD at higher temperature results in a narrower deposition zone in the membrane. As a result, membranes modified at a higher CVD temperature usually are more permeable than the membranes modified at a lower temperature. The location of the maximum deposition would be at the surface of the membrane exposed to precursor A if the reaction order with respect to precursor B is zero ($M = 0$) or the concentration of precursor B is in excess compared to the concentration of precursor A (quasi zero order for precursor B). This is the first case

Table 29. Analytical Expressions Correlating the Deposition Zone Thickness and Location of Maximum Deposition to the Major Parameters: Thiele Modulus (ϕ_A, ϕ_A), Deposition Reaction Rate B_o and Reaction Orders with Respect to Precursor A, N, and Precursor B, M

Reaction Orders	Deposition Zone Thickness	Location of Maximum Deposition	Evolution of Pore Radius at Location of Z_m with Time
N = 1, M = 0 (quasi-zero)	$\frac{L_B}{L} = \frac{4.605}{\sqrt{\Phi_A}}$	$\frac{Z_m}{L} = 0$	$t = \frac{1 - \phi_m}{B_o}$
N = 1, M = 1	$\frac{L_B}{L} = \frac{4.93}{\sqrt[3]{\Phi_A + \Phi_B}}$	$\frac{Z_m}{L} = \frac{\Phi_B}{\Phi_A + \Phi_B}$	$t = \frac{1.151 \cdot \left[1 - \left(\frac{5 + 16 \cdot \phi_m}{21}\right)^3\right] \cdot \Phi_A \cdot \Phi_B}{B_o \cdot (\Phi_A + \Phi_B)^{4/3}}$
N = 1, M = 2	$\frac{L_B}{L} = 6.405 \cdot \sqrt[4]{\frac{\Phi_A}{(\Phi_A + \Phi_B)^2}}$	$\frac{Z_m}{L} = \frac{\Phi_B}{\Phi_A + \Phi_B} + \frac{2}{15} \cdot \frac{L_B}{L}$	$t = \frac{1.00 \cdot \left[1 - (0.27 + 0.73 \cdot \phi_m)^3\right] \cdot \Phi_A^{5/4} \cdot \Phi_B}{B_o \cdot (\Phi_A + \Phi_B)^{3/2}}$

Parameter	N > 0, M > 0	N = 1, M = 0[1]
Φ_A	$\frac{2 \cdot \left(\frac{n_A}{n_S}\right) \cdot \left(\frac{L}{r_o}\right)^2 \cdot K \cdot (C_A^o)^{N-1} \cdot (C_B^o)^M}{a_{kA}}$	$\frac{2 \cdot \left(\frac{n_A}{n_S}\right) \cdot \left(\frac{L}{r_o}\right)^2 \cdot K \cdot (C_B^o)^2}{a_{kA}}$
Φ_B	$\frac{2 \cdot \left(\frac{n_B}{n_S}\right) \cdot \left(\frac{L}{r_o}\right)^2 \cdot K \cdot (C_A^o)^N \cdot (C_B^o)^{M-1}}{a_{kB}}$	…..
B_o	$\frac{\left(\frac{M_S}{\rho_S}\right) \cdot K \cdot (C_A^o)^N \cdot (C_B^o)^M}{r_o}$	$\frac{\left(\frac{M_S}{\rho_S}\right) \cdot K \cdot C_A^o \cdot (C_B^o)^2}{r_o}$

MARCEL DEKKER, INC. • 270 MADISON AVENUE • NEW YORK, NY 10016

shown in Table 29. For CVD reaction with nonzero reaction orders (the second and third cases in Table 29), the location of the maximum deposition moves towards the surface of the membrane exposed to precursor A if the concentration or the diffusivity of the precursor A decreases or that of the precursor B increases.

Lin and Burggraaf[189] and Xomeritakis and Lin[219] also compared the results of the mathematical model for the CVD process with the experimental results. They found that the model agreed fairly well with the experimental data for CVD modification of alumina membranes, such as maximum deposition location, deposition zone thickness, and pore closure time. These results of the theoretical analysis also provided useful guidance to control the macroscopic characteristics of the deposit in the porous membrane modified by the CVD. Theoretical analysis shows that deposition thickness as narrow as possible is essential to maintaining high permeance of a larger pore membrane after pore size reduction by a modification method. For a given deposition thickness, a pore size reduction is usually accompanied with a substantial decrease in the permeance. This can be illustrated next, as an example, by CVD modification of 4 μm thick γ-alumina membrane with deposition zone thickness the same as the γ-alumina layer.

If the γ-alumina membrane has circular cross-sectional pores and uniform pore size distribution and the deposition follows the heterogeneous mechanism shown in Figure 29(a), the ratio of the gas permeance for the membrane after reduction (pore radius R) to that for the unmodified membrane (pore radius R_o) can be correlated to the pore radius as $F/F_o = (R/R_o)^3$ (considering Knudsen diffusion permeation mechanism). This means that a two-fold reduction in pore size can cause an eight-fold decrease in gas permeance. If the deposition zone is much thinner, less reduction in gas permeance can be achieved with the reduction of the pore size to the same extent. In reality, however, the pore size reduction is accomplished at the expense of reducing gas permeance much more than what is predicted by $F/F_o = (R/R_o)^3$. These are clearly shown by the experimental results given in Table 28. Similar results were also found by other investigators.[185,189]

Lin and co-workers[202,220,221] were the first to address two other important factors that can affect the results of membrane modification: the pore size distribution and pore cross-section geometry of the membranes to be modified. The sol-gel derived γ-alumina membrane has a fairly uniform pore size distribution. However, the pores of the γ-alumina membrane have a slit-shaped cross-section,[23] as shown in Figure 30. The slit width determines the diffusivitiy (permselectivity) of a gas, while both the slit length and width contribute to the porosity (permeance). During a modification process, the solid may deposit on the pore surface in such a manner as to reduce the total internal pore surface area in order to minimize the surface energy. In the initial

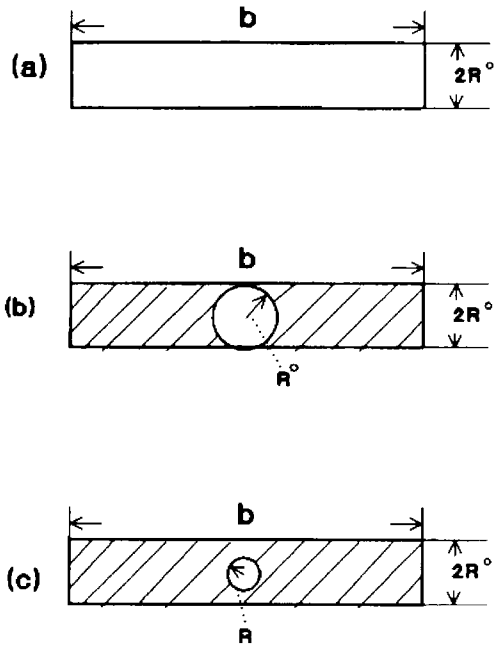

Figure 30. Schematic representation of a pore narrowing process for ceramic membrane with a slit-shaped cross-section pores (After Ref. [202]).

stage of the modification process the pore may be narrowed in the slit-length direction, until a circular or a near-circular pore with a pore radius equal to the half of the slit width is formed, as shown in Figure 30(b). Consequently, the effective pore size that affects the permselectivity may not change in the initial stage although the pore opening area (permeance) is significantly reduced. Further modification would result in a reduction in the effective pore size, as shown in Figure 30(c).

In the case shown in Figure 30, the relationship between the permeance reduction ratio and the pore size reduction ratio is $F/F_o = 1.57(R_o/b)(R/R_o)^3$.[202] For γ-alumina membrane with a typical slit length, b, of 25 nm and initial pore radius, R_o, of 2 nm, a two-fold reduction in the pore size is achieved at the expense of about 60-fold reduction in gas permeance, much more than the case with circular cross-sectional pore, as given above. These results are consistent with modification of γ-alumina membrane by CVD of silica,[205] zirconia[189] and organics.[185]

Many mesoporous membranes have a pore size distribution (PSD). Lin[220] used the population balance theory to study the effect of initial PSD

and deposition mechanism on the evolution of pore structure of ceramic membrane after CVD treatment. This study was based on an idealized deposit structure with a uniform deposit profile. Xomeritakis et al.[196] later extended the analysis considering more realistic deposit profile using the semi-analytical solution of the diffusion–reaction model for the CVD process described above. These theoretical studies show that the results of modification on the pore size change of a ceramic membrane are strongly determined by the initial pore size distribution and the pore narrowing kinetics of the modification process.

For a membrane having a pore size distribution with a large amount of smaller pores and a modification process with a heterogeneous deposition kinetic which gives a pore size independent pore narrowing rate, the modification could result in an increase in average pore size, unless the porosity (or permeance) of the membrane is substantially reduced. This is because the deposition kinetic favors narrowing and disappearance of the small pores, resulting in a swift of the average pore size to a larger value. It is very ineffective to narrow the average pore size of a membrane with a pore size distribution. The results also show that the average pore size of a ceramic membrane can be effectively reduced only if the membranes have a rather uniform pore size distribution or the modification process has a pore narrowing kinetic which gives a pore narrowing rate proportional to the pore size (dictated by the homogeneous reaction mechanism). These theoretical results are consistent with experimental findings on pore size reduction of ceramic membranes.[189,222]

The above review shows how pore size change of the membrane during modification by the methods described above depends on the deposition reaction kinetics and deposition conditions (temperature, concentration and substrate structures).[197,213,214] It is difficult to control the deposition extent or the pore size of the modification membrane by the modification methods described above. Furthermore, these methods do not allow microscopic (atomic) scale control of the structure of deposit. A cyclic CVD method, first used by Kim and Gavalas[223] for modifying Vycor glass membrane and later more systematically studied George and co-workers[224,225] who referred the method to as atomic layer chemical vapor deposition (ALCVD), provides the flexibility to deposit a solid in mesoporous ceramic membranes in a controlled manner. George and co-workers reported ALCVD modification of straight pore Anotec alumina[226,227] and tortuous pore γ-alumina membrane[228] for pore size reduction.

To apply ALCVD for membrane modification, the pore surface of the mesoporous ceramic membranes containing –OH groups is exposed to an aluminum or silicon vapor precursor (e.g., $AlCl_3$) which will be chemsorbed to form the intermediate species on the pore surface (e.g., $-O-AlCl_2*$). The

pores are then evacuated to remove all the aluminum or silicon precursor in the gas phase in the pores, and subsequently exposed to water vapor which reacts with the surface intermediate species to form one atomic layer of alumina or silica (e.g., –O–Al–OH). The pores of the membrane can be narrowed layer-by-layer in the manner shown in Figure 29(a) if the strict ALCVD method with 100% heterogeneous deposition mechanism is used for membrane modification. With ALCVD, the extent of pore reduction can be controlled by the cycles of CVD, rather than the CVD time and conditions.

However, the structure of the deposit obtained by the ALCVD is not desirable for membrane modification as the deposit is coated in the manner that can cause a substantial decrease in gas permeability through reduction in pore size or loss of the small pores. Recently Lin and co-workers[214,229] modified the ALCVD method by incorporating a certain degree of homogeneous deposition to decrease the pore size of mesoporous γ-alumina membranes in a more effective manner. They performed the modified ALCVD on the sol-gel derived γ-alumina by the two half reactions between H_2O and $Al(CH_3)_3$ (at 180°C) with the apparatus described earlier by Pan et al.[229] The membrane pores with surface –OH groups were exposed to $Al(CH_3)_3$ vapor at 26 mbar for 5 min (to form the surface intermediate species: $-O-Al-(CH_3)_2$*) and were evacuated to leave some residual $Al(CH_3)_3$ molecules (at 1 mbar) in the membrane pores. H_2O vapor was introduced into the membranes to react with the surface intermediates to form one atomic layer of alumina (heterogeneous deposition). It also reacted with the residual $Al(CH_3)_3$ molecules in the pore space to form solid alumina particles in the gas phase (homogeneous deposition). The solid particles were then deposited on the membrane wall. This completes one cycle of the modified ALCVD.

The unmodified and modified membranes were characterized by single gas helium permeation for reduction in gas permeance and permporosimetry for pore size of the modified zone. The results are summarized in Table 30. As shown in the table, the actual pore size of the 1 time CVD modified membrane estimated from the perm-porosimetry data is much smaller than what would be expected if the deposition process were truly ALCVD. If one assumes the deposit structure the same as shown in Figure 29(a), the helium permeance estimated using the actual pore size for the 1 time CVD modified membrane would be about 30 (10^{-8} mol/m^2.s.Pa), smaller than the experimentally measured one, 85 (10^{-8} mol/m^2.s.Pa) (see Column 2 in Table 30). This means that the CVD modification results in much more reduction in the pore size but less reduction in the porosity, as compared to those predicted using the ALCVD model. This is very desirable for membrane applications. The only possibility for this to occur is that the alumina deposit in the γ-alumina membrane pores has a fractal structure as shown in Figure 29(b). The subsequent CVD cycles (2 and 3 time CVD) did not appear to have caused as

Table 30. Pore Size and Permeation of Membranes Modified by Various CVD Cycles

1	2	3	4	5
Times CVD Modified	Measured He Permeance (10^{-8} mol/ m^2.s.Pa)	Pore Diameter Based on ALCVD (nm)	Calculated He Permeance (10^{-8} mol/ m^2.s.Pa)	Measured Pore Diameter from Perm-Porosimetry (nm)
0	130	3.6	130	3.6
1	85	3.3	100	2.2
2	35	3.0	75	1.9
3	20	2.7	54	1.8
4	10	2.4	37	$\sim$0.4

(From Ref. [214].)

much reduction in the pore size as compared to the first CVD cycle, as shown on the data given in Column 5 in Table 30. However, these pore size data (1.9 nm and 1.6 nm) should be treated with caution since the Kelvin equation may be no longer an accurate correlation to calculate the pore size from the vapor pressure of condensable gas in this pore size range.

The true atomic layer CVD requires complete heterogeneous reaction which produces a smooth layer on the wall of the γ-alumina membrane pores, as shown in Figure 29(a). This reduces not only the pore size but also more significantly the porosity of the membrane, which is undesirable for membrane modification. The modified ALCVD process may include homogeneous reaction which favors deposition with slight irregularities or protrusions. This is because by allowing a small amount of reactant (1 mbar of water or $Al(CH_3)_3$) to remain in the reaction chamber and hence in the γ-alumina pores after evacuation, some homogeneous reactions occurred in the pores of the γ-alumina membrane. However, the relatively small amount of remaining water and $Al(CH_3)_3$ vapor molecules allowed only for a relatively small amount of homogeneous reactions to occur.

5. MECHANISMS OF GAS PERMEATION THROUGH MICROPOROUS INORGANIC MEMBRANES

In the past decade, successful synthesis of a variety of good quality microporous inorganic membranes also promoted extensive experimental and theoretical studies on the mechanism of gas permeation through these microporous membranes. The theoretical studies were based largely on the

prior knowledge of adsorption and diffusion in zeolites. Gas permeation through microporous inorganic membrane is a process combining adsorption and diffusion. The permeation process even for the single gas permeation is complex involving a variety of phenomena. This section will review major theories reported in the past decade on gas permeation and diffusion in microporous inorganic membranes. The general trends of the experimentally measured permeation data will be summarized and explained with the help of the theoretical analysis.

5.1 Theory of Gas Permeation Through Microporous Inorganic Membranes

Microporous inorganic membranes reviewed in this paper include two groups of membranes with distinguishable macroscopic and mesoscopic structures: amorphous and crystalline membranes. The first group of membranes, including silica and carbon, are macroscopically uniform across the microporous film. The second group of membranes, represented by zeolite membranes, have a structure defined by the compact of small microporous crystallites with an intercrystalline boundary (or grain boundary or intercrystalline region). A strict theoretical treatment of gas permeation through the second group of membranes is more complex, requiring a consideration of diffusion and adsorption in both the intracrystalline and intercrystalline regions. Nevertheless, essentially all the studies on the theories of gas permeation through microporous membranes reported so far assumed a macroscopically homogeneous microporous film. In these theories diffusion and adsorption in the polycrystalline film are treated as in a single crystal film.

During permeation of a gas through a microporous membrane three major steps occur each representing a flow resistance: mass transfer (diffusion) from the bulk gas phase through a stagnant gas film adjacent to the membrane surface, mass transfer across the surface in which the gas molecules change from a gaseous state to a state within the porous material, and diffusion through the bulk of the microporous material. The desorption and diffusion through a stagnant gas film also occur in the permeate side. The surface reaction (sorption) and diffusion steps mentioned above play an important role in gas transport through microporous membranes. Their relative importance depends on membrane material characteristics such as pore size, sorption strength, and gas properties such as molecular size, shape and concentration.[3,230,231]

Neglecting the transport resistances in the fluid phase and at fluid–membrane interface, gas permeation through a mesoporous or macroporous membrane includes viscous flow, molecular diffusion and Knudsen diffusion. The theory governing the transport in these large pore membranes is the

Dusty–Gas model.[232,233] For gas permeation through microporous membranes, these mechanisms do not apply and the transport is dominated by microporous (configurational) diffusion. However, if a microporous membrane contains defects or pinholes of larger than 2 nm, the overall permeance and separation properties are determined by both microporous and macroporous/mesoporous transport mechanisms.

Stefan–Maxwell equation, a theory similar to the Dusty–Gas model, has been proposed by Krishna[234–236] to describe transport in microporous material. The application of this theory for gas permeation through microporous inorganic membranes was first reported by Kapteijn et al.[237,238] For n-component diffusion in microporous membrane, this theory gives the following implicit equation describing the flux for gas species i, J_i:

$$\frac{-\theta_i}{RT}\nabla\mu_i = \sum_{\substack{j=1 \\ j\neq i}}^{n} \frac{\theta_j J_i - \theta_i J_j}{q_{sat}\rho D_{ij}} + \frac{J_i}{q_{sat}\rho D_{iz}} \qquad \text{for i} = 1, 2, \ldots \text{n} \tag{4}$$

In Eq. 4 μ_i and θ_i are the chemical potential and the occupancy for species i in the membrane, with $\theta_i = q_i/q_{sat}$ where q_i and q_{sat} are respectively the amount adsorbed based on membrane weight (mol/kg) for species i and for all species ($\Sigma\theta_i = 1$), ρ is the density of the membrane (kg/m^3), D_{ij} is the Stefan–Maxwell diffusivities describing the interchange between species i and j in the membrane, and D_{iz} is called the corrected diffusivity representing interaction between species i and membrane.

The chemical potential gradient can be correlated to the concentration gradient by:

$$\nabla\mu_i = \frac{RT}{\theta_i}\sum_{j=1}^{n}\Gamma_{ij}\nabla\theta_j \qquad \text{for i} = 1, 2, \ldots \text{n} \tag{5}$$

with the thermodynamic correlation factor defined by:

$$\Gamma_{ij} = \theta_i \frac{\partial \ln P_i}{\partial \theta_j} \qquad \text{for i,j} = 1, 2 \ldots \text{n} \tag{6}$$

Calculation of the thermodynamic correlation factor requires the equilibrium relationship between the concentration in the membrane and the partial pressure of the permeating gas:

$$\theta_i = f(p_1, p_2, \ldots p_n) \qquad \text{for i} = 1, 2, \ldots \text{n} \tag{7}$$

The above relationship is also referred to as the adsorption isotherm of the permeating gas on the membrane material.

The implicit flux equations, Eq. 4, can be solved to give the following explicit flux equations in n-dimensional matrix notation (for one dimensional diffusion in the rectangular coordinate):[236]

$$(J) = -\rho[B]^{-1}[\Gamma]\frac{d(\theta)}{dz} \tag{8}$$

with matrix [B] given by:

$$B_{ii} = \frac{1}{D_{1z}} + \sum_{\substack{j=1 \\ j\neq i}}^{n} \frac{\theta_j}{D_{ij}}, B_{ij} = -\frac{\theta_i}{D_{ij}} \qquad \text{for i, j} = 1, 2, \ldots \text{n} \tag{9}$$

For steady state permeation through a microporous membrane, Eq. 8 gives a set of n first order differential equation with flux (J) independent of the position z. Simultaneous solution of Eq. 8 will give n equations correlating the permeation fluxes of various species to the membrane thickness, concentrations of the permeating gas on the both surfaces of the membrane, diffusivities, and other membrane and adsorption equilibrium constants. The above expressions for binary system will be given later.

For single component permeation through a microporous membrane, the above equations are reduced to:

$$J = -\rho D_c \Gamma \frac{dq}{dz} \tag{10}$$

At the steady state, the single gas permeance through a microporous membrane can be obtained by integrating the above equation as:

$$F = \frac{\phi}{L(P_f - P_p)} \int_{q_f}^{q_p} D_c \Gamma dq \tag{11}$$

where q_p (permeate) and q_f (feed) are the concentrations of the permeating gas at $z = L$ and $z = 0$, respectively, P_f and P_p are respectively feed and permeate side pressures, ϕ is a constant accounting for the membrane porosity and totuosity factor, L is the membrane thickness, and D_c is the corrected diffusivity (same as D_{1Z}). The above equation correlates the permeance to the diffusivity, sorption equilibrium properties, membrane thickness and the upstream and downstream pressures. For a constant diffusivity and linear adsorption isotherm ($q = KP$, $\Gamma = 1$), the above equation is deduced to:

$$F = \frac{\phi}{L}(D_c \times K) \tag{12}$$

where K is sorption equilibrium constant (or solubility). This equation is the same as that derived from the well-known solution–diffusion model for gas permeation through dense polymer membranes.[170]

5.2 Modeling Single Gas Permeation

In modeling single gas permeation through a microporous membrane, the membrane is assumed to be defect- or pinhole-free. If a microporous membrane contains a considerable amount of defects and pin-holes (mesopores and macropores), one should consider gas permeation through the defects, governed by the viscous flow and Knudsen diffusion. The Dusty–Gas model gives the following equation relating single gas permeance through these defect pores to pressures and temperature by:[202]

$$F = \alpha + \beta \frac{P_f + P_p}{2} \tag{13}$$

where the first and second terms represent contributions by the Knudsen flow and viscous flow respectively as:

$$\alpha = 1.06\left(\frac{1}{L}\right)\left(\frac{\varepsilon}{\tau}\right)\frac{r_p}{\sqrt{RTM_w}} \tag{14}$$

$$\beta = 0.125\left(\frac{1}{L}\right)\left(\frac{\varepsilon}{\tau}\right)\frac{r_p^2}{\eta RT} \tag{15}$$

In Eqs. 14 and 15 the unit of α and β are respectively mol/m^2.s.Pa and mol/m^2.s.Pa^2, ε, τ and r_p are porosity, totuosity factor and pore radius (m) of the membrane defects, and η and M_w are the viscosity (kg/m.s) and molecular weight (kg/mol) of the permeating gas.

Eqs. 13 clearly show the dependency of the single gas permeance through membrane defects or pinholes on temperature, feed and permeate pressures, membrane pore structure, and permeating gas properties (viscosity and molecular weight). For example, the permeance is proportional to $T^{-1/2}$ for Knudsen mechanism, and to $T^{-3/2}$ for viscous flow mechanism (viscosity being proportional to $T^{1/2}$). For a microporous membrane with defects and pinholes, the total flow measured includes flow through the defects, Eq. 13 and that through the micropores described next. If a single gas permeation properties through a microporous membrane can be well described by Eqs. 13, the membrane very likely contains a large amount of macroporous or mesoporous defects and pinholes. Then the quality of the membrane is poor.

For a good quality microporous membranes without macroporous/mesoporous defects, single gas permeance can be obtained by integrating Eq. 11. The final equation would correlate the permeance to the diffusivity, membrane parameters, feed and permeate pressures, and adsorption equilibrium constant. The integration requires information about adsorption equilibrium and diffusivity. Equilibrium of adsorption of gases in microporous materials has been well studied, and many adsorption isotherms are available.[78,239,240] The representative adsorption isotherm for single gas adsorption in microporous membrane is the Langmuir isotherm:

$$\frac{q}{q_s} = \theta = \frac{KP}{1+KP} \tag{16}$$

where K is the Langmuir adsorption constant (Pa^{-1}), θ the (relative) occupancy. With $\Gamma = \partial \ \mathrm{lnP}/\partial \ \mathrm{lnq}$, and using the Langmuir isotherm, we can find that the thermodynamic factor is given by:

$$\Gamma = \frac{1}{1-\theta} \tag{17}$$

Gas diffusion in microporous materials has been studied experimentally for several decades.[71] However, the major advances in theoretical understanding gas diffusion in microporous materials were reported in the 1990's.[241–243] The theoretical studies provided a correlation relating the diffusivity of a single species in microporous material to the temperature, relative size of the gas molecule to the material pore, and gas molecular loading in the microporous material. The multi-component diffusivities in microporous materials, in principle, can be predicted from single gas diffusivity data.[162,255]

According to Xaio and Wei,[242] the diffusion coefficient in micropores can be given by the following general expression

$$D = g_d \lambda u \exp\left(\frac{-E_d}{RT}\right) \tag{18}$$

where u is velocity of the diffusing molecules, λ is the diffusional free length, g_d is probability factor, and E_d the activation energy for diffusion. Two different diffusion regimes are possible depending on the temperature: the surface diffusion at low temperatures and the gas translation (GT) diffusion at high temperatures.

At low temperatures an adsorbed phase is present in the pores of the membrane where the diffusion takes place by molecules jumping between the

adsorption sites. This diffusion is denoted as surface diffusion and its diffusivity (D_s) can be derived from Eq. 18 as

$$D_S = g_d \lambda^2 u(\theta) \exp\left(\frac{-E_d}{RT}\right) \tag{19}$$

where E_d is the energy barrier on the internal pore surface.

If the temperature is increased, the amount adsorbed will decrease and above a certain temperature no well-defined adsorbed phase will be present in the membrane micropores. The molecules inside the pores to diffuse from site to site have to overcome an energy barrier imposed by the pore structure. This diffusion is denoted as gas translation (GT) diffusion and its diffusivity can be derived from Eq. 18 as:

$$D_{GT} = g_d d_p \left(\frac{8RT}{\pi M}\right)^{1/2} \exp\left(\frac{-E_d}{RT}\right) \tag{20}$$

where E_d is the energy barrier in the micropore. Eqs. 19 and 20 can be used to predict the corrected diffusion coefficient of non-polar molecules, such as branched paraffins and benzene in microporous material.[242,243]

Substitution of Eqs. 16 and 17 in Eq. 11 and integration, assuming D_c is independent of the concentration q, yields an explicit expression for the single gas flux through microporous membrane in the Langmuir regime:

$$J_S = \rho.\varepsilon.q_s \frac{D_c}{L}\left(\frac{1+KP_f}{1+KP_p}\right) \tag{21}$$

or

$$J_S = \rho.\varepsilon.q_s \frac{D_c}{L}\left(\frac{1-\theta_p}{1-\theta_f}\right) \tag{22}$$

Under the conditions of linear adsorption isotherm ($KP \ll 1$), Eq. 16 is reduced to the linear relation: $q = KP$ (with $K = q_s b$) (Henry's regime). In the Henry's regime the flux is given by:

$$J_S = \rho.\varepsilon.q_s \frac{D_c}{L} K(P_f - P_p) \tag{23}$$

The temperature dependency of J_i is introduced using the following van't Hoff-type relation for K and Arrhenius relation for D_c for the surface diffusion regime as shown before in Eq. 19.

$$K = K_o \exp\left[\frac{Q_a}{RT}\right] \tag{24}$$

$$D_c = D_{co} \exp\left[\frac{-E_d}{RT}\right] \tag{25}$$

where Q_a is the (isosteric) heat of adsorption and E_d is the activation energy for diffusion in the micropores.

The temperature dependence of the flux can be found by substituting Eqs. 24 and 25 in Eq. 21 for Langmuir regime or in Eq. 23 for Henry's regime with $KP < 1$ to yield respectively:

$$J_S = \frac{\rho.\varepsilon.q_s}{L} D_{co} \exp\left(-\frac{E_d}{RT}\right) \times \ln\left[1 + K_o P_f \exp\left(\frac{Q_a}{RT}\right)\right] \ (Langmuir\ regime) \tag{26}$$

$$J_S = \frac{\rho.\varepsilon.q_s}{L} K_o D_{co} \exp\left[\frac{Q_a}{RT} - \frac{E_d}{RT}\right] P_f \ (Henry's\ regime) \tag{27}$$

In deriving the above two equations the permeate pressure (P_p) is assumed to be zero.

At relatively high temperatures or for gas molecules having weak interaction with micropores, GT diffusion is dominant. In this case the diffusivity is better described by using Eq. 20. In the GT regime a certain fraction of the total concentration in the micropores is desorbed from the internal surface to the ''gaseous phase'' in the pore system (q_g) while the rest resides on the pore wall (q_a). The single component flux for the GT diffusion is obtained by substituting Eq. 20 for D_c, and q_g for q in Eq. 11, noting that $\Gamma = 1$ and $q_g = P/RT$ as determined from the ideal gas law.[231,242,243] This leads to the following expression in the case of $RT > Q_a$:

$$J_{GT} = \frac{\rho \varepsilon g_d d_p}{L} \left(\frac{8}{\pi MRT}\right)^{1/2} \exp\left(\frac{E_d}{RT}\right) P_f \tag{28}$$

For large values of Q_a and K and $RT \leq Q_a$, the molecules are desorbed in the gaseous phase in the micropore but are not desorbed outside the microporous material. This means that after desorption within the micropores $q_g > P/RT$ for which $q_a = q_{sat}\, KP/(1 + KP)$ and $q_g \approx q_a \exp(-\Delta E_d/RT)$, and with Eqs. 13 and 20 and for $KP < 1$ (Henry regime), one obtains:

$$J_{GT} \approx \frac{\rho \varepsilon g_d d_p}{L} \left(\frac{8RT}{\pi M}\right)^{1/2} q_{sat} K_o \exp\left(\frac{Q_a - \Delta E_d - E_d}{RT}\right) P_f \tag{29}$$

where ΔE_d represents the desorption energy of gas from the pore wall into the gaseous phase in the micropore.[231]

In the work of Xiao and Wei[242] the two different diffusion mechanisms (surface or solid vibration diffusion and gas translation diffusion) were used separately to describe gas diffusion in microporous under different conditions. Bakker et al.[254] and Burggraaf[231] extended the theory by assuming that these two transport mechanisms are additive, that is, at a given temperature and loading both the surface diffusion and gas translation diffusion contribute to the total mass transport through the membrane. They proposed that the total gas permeance through a microporous membrane is:

$$J = J_S + J_{GT} \tag{30}$$

where J_S and J_{GT} are respectively described by Eq. 26 or Eq. 27 and Eq. 28 or Eq. 29.

The above flux equations are simplified ones neglecting downstream pressure and concentration dependency of the diffusivity. In practice it is not difficult to derive more accurate equations that correlate the permeation flux to various parameters considering all these effects. It is obvious that the permeability of single gas depends on both adsorption and diffusion properties. The adsorption isotherm should be measured experimentally. It is possible to predict the diffusivity including the activation energy for diffusion using the theory proposed by Xiao and Wei.[242] Recent development in molecular simulation of adsorption and diffusion of single gases in zeolites also made it possible to predict the permeability directly although so far only limited work in this area has been reported.[245] Nevertheless, Eq. 30 (with Eqs. 26–29) shows a clear dependency of single gas permeation flux (or permeance) on feed pressure, temperature and other properties of membrane and permeating gas.

For example, temperature affects gas permeance by influencing both adsorption and diffusion, as illustrated in Figure 31. Increasing temperature always lowers the concentration gradient (driving force) and enhances mobility (diffusivity) of the permeating species. For permeating gas with a linear adsorption isotherm, the permeance (or flux) can increase or decrease monotonously with temperature, depending on whether heat of adsorption (Q_a) is smaller ($<$) or larger ($>$) than activation energy for diffusion (E_d), as shown by Eq. 27. For nonlinear adsorption isotherm (like Langmuir isotherm), gas permeance monotonously increases with increasing temperature if $Q_a < E_d$, as shown by Eq. 26. However, for the Langmuir adsorption isotherm it is possible that gas permeance increases, reaches a maximum, then decreases with increasing temperature if $Q_a > E_d$, as shown in Figure 31 (fine-dashed curve). This is because the reduction in the average concentration gradient (or driving force) is less significant in the lower temperature range than at high temperatures. For GT diffusion, the permeance always increases with temperature,

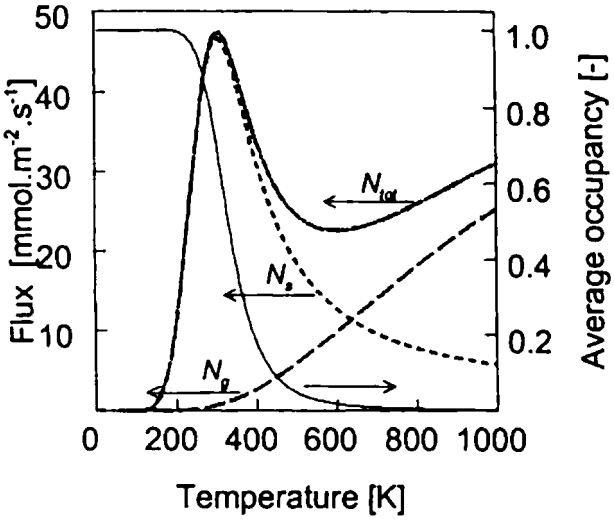

Figure 31. Temperature dependency of single gas permeance through a zeolite membrane ($Q_a = 25$ kJ/mol, $E_d = 15$ kJ/mol) (After Ref. [150]).

as shown in Figure 31 (coarse-dashed curve). If the additive theory, Eq. 30, is correct, the two dashed curves in Figure 31 can be combined. Therefore, it is possible to observe a maximum and a minimum in the curve of the temperature dependency of single gas permeance through a microporous membrane, as shown in Figure 31 (solid curve).

5.3 Experimental Single Gas Permeation Data

Many groups reported experimental data of gas permeation through microporous inorganic membranes. Instead of giving an exhausted review of these data, we only summarize here the major trends observed experimentally about the single gas permeation through microporous inorganic (mainly zeolite) membranes with emphasis on comparison of theoretical models with experimental data. It should be noted that single gas permeation measurements can be conducted by several configurations, including steady-state Wicke–Kallenbach and unsteady batch methods, with or without sweep gas (carrier gas).[245,246] Strictly speaking only single gas permeation data measured by the steady-state Wicke–Kallenbach method without sweep gas can be used to compare with the theoretical single gas flux equation given above. In theory, with a sweep gas (either in the permeate or feed or both sides) the single gas

permeation system should be treated as a binary system. Permeation flux measured by the unsteady state method often does not correspond to the same concentration gradient (driving force) as in the steady state with the same feed and permeate pressures.

The theoretical analysis given above suggests that single gas permeation flux can be predicted from the diffusion and adsorption isotherm data measured independently, or diffusivity can be calculated from the permeation flux data if the adsorption isotherm is known. Kapteijn et al.[238] measured permeation fluxes of several alkanes and alkenes through a 40 μm thick silicalite membrane and corresponding adsorption isotherms of silicalite powders prepared under the same conditions as the membrane. The diffusivity data for methane, ethane, propane, ethylene and propene calculated from the permeation flux data are close (within a factor of 2–3) to the mean diffusivity data measured by other methods. Considering a large discrepancy in the diffusivity data measured by different methods,[71] this agreement can be considered acceptable.

Vroon[97] measured adsorption isotherms of methane and n-butane on silicalite membrane. The data are regressed by the Langmuir equation, Eq. 16, and the values of parameters are listed in Table 31. Coupling these equilibrium data with diffusivity data on single silicaltie crystals measured by other group, as listed in Table 31, Vroon[97] calculated gas permeation flux using model Eq. 21. The predicted flux data are compared with the experimental permeation flux data (measured by the steady state Wicke–Kallenbach method), as shown in Figure 32. Fairly good agreement is obtained for the methane, but for n-butane the model over-predicts the flux data at lower pressures.

The above two studies show that there is a reasonable agreement between the flux (or diffusivity) data measured directly from the polycrystalline silicalite membranes and the flux (or diffusivity) data predicted from (or measured on) the silicalite crystal particles. However, the exact agreement between the data measured on membrane and crystal particles should not be

Table 31. Sorption Equilibrium and Diffusivity Data of Methane and n-Butane at 298 K on Silicalite Membrane

Gas	Langmuir Parameter (Pa^{-1})	Sorption Capacity (mol/m^3)[a]	Diffusivity (m^2/s)[a]	Heat of Sorption (kJ/mol)	Activation Energy of Diffusion (kJ/mol)
Methane	3.8×10^{-6}	2.2×10^{3}	0.7×10^{-10}	20	14
n-butane	8.0×10^{-3}	2.2×10^{3}	1.0×10^{-12}	38	25

[a]Sorption data measured by Ref. [97] and diffusivity data from Ref. [288].

expected because of the following reasons: 1) the diffusivity measured on zeoltie particles may not necessarily be the same as the macroscopically averaged diffusivity of a polycrystalline zeolite membrane; 2) permeation of a gas through a polycrystalline zeolites membrane may involve mechanism other than the micropore diffusion, such a Knudsen or viscous flow through pin-hole or defects and a possible unidentified microporous transport mechanism through the crystalline boundary (intercrystalline region); 3) permeation through membrane may also include other transport resistances such as adsorption and diffusion on membrane surfaces; and 4) single gas permeation data are often measured under the conditions that the single gas permeation equation does not apply (e.g., the sweep gas was used in single gas permeation measurements in both studies reviewed above), and in most experiments the permeate side pressure can not be well defined. Given these reasons and the fact that there is a large discrepancy in the diffusivity on zeoltie particles measured by different methods,[71] it became more important to focus on how various parameters affect gas permeation through zeolites membranes, rather than the comparison between the membrane and particle data.

Experimentally data showing feed pressure dependency of single gas permeation through microporous inorganic membranes have been reported in several studies.[100,231,237,244,248–253] Figure 33 shows dependency of single gas permeation flux on feed pressure for several light hydrocarbons through a silicalite membrane. In general, permeation flux of less-adsorbing gases (like methane in Figure 32) depends more linearly on the feed pressure. For strongly-adsorbing gases the relationship between the permeation flux and feed pressure becomes more liner at high temperature because the adsorption capacity decreases as temperature increases. Thus, this linear relationship translates into a pressure independent permeance of these gases through zeolites membranes. For strongly-adsorbing gases, especially at low temperatures the permeation flux exhibits a nonlinear dependency on the feed pressure, as shown in Figure 34. In this case the permeance decreases with increasing feed pressure.

These types of feed pressure dependency for single gas permeation can be explained by the permeation flux Eqs. 21 and 23. For weakly-adsorbing gases, or strongly-adsorbing gases but at high temperatures, the adsorption isotherm can be described by linear Henry's equation. As a result, the permeation flux depends linearly on feed pressure, as shown by Eq. 23. The adsorption isotherms of strongly-adsorbing gases in microporous material are generally of Langmuir type, characterized by a sharp increase in adsorption loading at lower pressures and gradual approaching to the saturated capacity as pressure further increases. This type of nonlinear adsorption isotherm would give a gas permeance which decreases with increasing feed pressure. Eqs. 21 and 23 were derived by assuming a diffusivity that is independent on

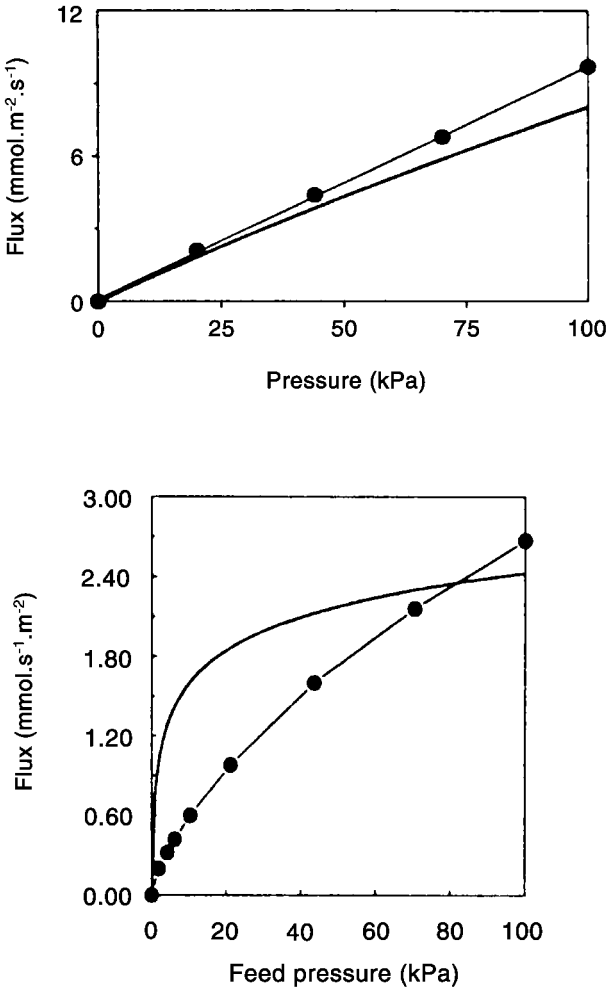

Figure 32. Comparison of measured and calculated permeation flux for methane (top) and n-butane (bottom) through silicalite membranes (permeate pressure about zero) (After Ref. [97]).

the adsorbate loading.[71] It is known that zeolitic diffusivities can increase or decrease with the adsorbate loading. The fact the Eqs. 21 and 23 can be used to describe experimentally observed feed pressure dependency of single gas permeation flux for many microporous inorganic membranes indicate that

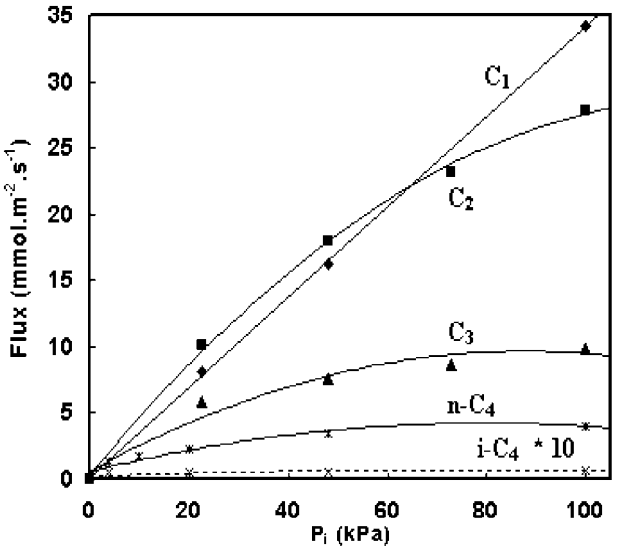

Figure 33. Feed gas pressure dependency of gas permeation flux through silicalite membrane for light alkanes at 295 K (Redrawn from Ref. [100]).

the pressure dependency of sorption equilibrium, not the diffusivity, has a stronger influence on pressure dependency of the gas permeance. It should be pointed out that increase of single gas permeance with feed pressure has been reported for microporous silica,[38–40] MFI zeolites,[251] and SAPO-34[252]

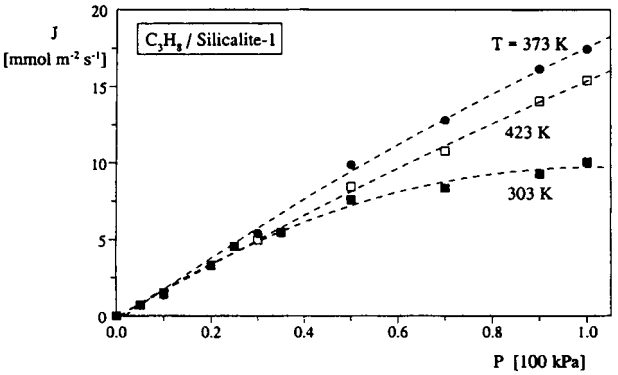

Figure 34. Feed gas pressure dependency of propane permeation flux through silicalite membrane at different temperatures (After Ref. [254]).

membranes. Such pressure dependence is not consistent with the adsorption isotherm observed for the microporous membrane materials, and is more likely a result of the contribution of viscous flow through membrane pinholes (see Eq. 13).[249,251]

Few experimental data are available in the literature showing direct effects of downstream (permeate) pressure on permeation flux (or permeance) for microporous inorganic membranes. This is because most single gas permeation experiments were performed with a sweep gas in the permeate side in which the exact partial pressure of permeating gas is difficult to control. For linear adsorption isotherm a small variation in the permeate pressure will not affect the pressure dependency of permeation flux or permeance, as shown by Eq. 23. However, for highly nonlinear adsorption isotherms, especially those of type II with large K value, the permeation flux is more sensitive to the permeate pressure than the feed pressure, as shown by Eq. 21. This is because the permeate pressure is much lower than the feed pressure and for many microporous materials and adsorption amount increases sharply with pressure in the low pressure range. In most permeation experiments the thin microporous film faces the feed side and the thick macroporous support the permeate side. The support resistance would result in a higher permeate pressure for the microporous film than observed in the downstream of the whole membrane composite. This would give a much lower permeation flux than expected from the downstream pressure.[131] The pressure drop across the support changes with experimental conditions, so do the effects of the support on the permeation flux.

Various temperature dependencies of single gas permeance have been experimentally observed for gas permeation through microporous membranes. Depending on the adsorption equilibrium properties (heat of adsorption and adsorption isotherm shape), activation energy of surface diffusion, concentration dependency of diffusivity, membrane quality, and experimental conditions (temperature range, upstream and downstream pressures), the following five types of temperature dependencies have been observed experimentally: 1) permeance increases monotonously with temperature, 2) permeance decreases monotonously with temperature, 3) permeance increases and then decreases with temperature, 4) permeance decreases and then increases with temperature, and 5) permeance shows a minimum at lower temperature and maximum at high temperature. A summary of experimental data showing various temperature dependencies is given in Tables 32–36. As discussed in Modeling Single Gas Permeation, such five temperature dependencies can be explained by the theoretical model shown in Figure 31. In fact, the solid curve shown in Figure 31 include all the five cases depending on the temperature range selected. Next we will discuss briefly temperature dependency of selected systems.

Table 32. Summary of Experimental Data on Microporous Inorganic Membranes Showing Monotonous Increase of Permeance with Temperature

Membrane Type	Permeant	Temp. Range (K)	Feed Pressure (kPa)	1st Author, Year	Ref.
Zeolite/α-Alumina	i-C4	298–473	100	Vroon, 1996	[253]
Silicalite-1/Stainless steel		193–623		Bakker, 1996	[100]
Silicalite/γ-Alumina	o, m, p-Xylene, Ethylbenzene, Toluene, Benzene p-Xylene, o-Xylene	380–480		Baertsch, 1996	[147]
ZSM-5/γ-Alumina		353–430	8.4/component	Gump, 2001	[289]
Silica-Polyimide/ γ-Alumina	He, N_2, CO_2	300–625		Kusakabe, 1996	[282]
Silica/γ-Alumina	H_2	300–873	1.8, P = 1.5	Sea, 1996	[207]
Mordenite/Alumina	H_2, He, C1	290–400	301, ΔP = 200	Nishiyama, 1997	[126]
ZSM-5/α-Alumina	n-C4, I-C4	298–480	222, ΔP = 138	Gump, 2000	[247]
ZSM-5/Stainless Steel	n-C4				
	i-C4		138, ΔP = 138		
H-ZSM-5/Alumina/ Stainless steel	SF_6	298–550	ΔP = 138	Flanders, 2000	[259]
	SF_6, DMB, TMP[a]	298–600			

[a]TMP: Trimethylpentane.

Table 33. Summary of Experimental Data on Microporous Inorganic Membranes Showing Monotonous Decrease of Permeance with Temperature

Membrane Type	Permeant	Temp. Range (K)	Feed Pressure (kPa)	1st Author, Year	Ref.
Zeolite/α-Alumina	C1	273–473	100	Burggraaf, 1998; Vroon, 1996	[230,253]
ZSM-5/α-Alumina	C1, CO_2	290–470	270, $\Delta P = 138$	Poshusta, 1999	[251]
SAPO-34/α-Alumina	H_2, CO_2, He, N_2	298–470	270, $\Delta P = 138$	Poshusta, 2000	[252]
SAPO-11/α-Alumina	o-Xylene, Benzene	353–430	8.4/component	Gump, 2001	[289]
H-ZSM-5/Stainless steel	CO_2	298–550	$\Delta P = 138$	Flanders, 2000	[259]
MFI Zeolite/Alumina	H_2	323–723	125	Ciavarella, 2000	[263]

Table 34. Summary of Experimental Data on Microporous Inorganic Membranes Showing Increase and then Decrease of Permeance with Temperature

Membrane Type	Permeant	Temp. Range (K)	Feed Pressure (kPa)	1st Author, Year	Ref.
Silicalite/Stainless steel	C1, C2, n-C4	193–623	100	Bakker, 1996	[100]
MFI Zeolite/α-Alumina	C2, C3, n-C4	298–473	100	Vroon, 1996	[253]
Silicalite-1/Stainless steel	C3, n-C4	270–625	101	Van De Graaf, 1998	[283]
Zeolite/α-Alumina	C2, C3, n-C4, i-C4, H_2, CO_2	273–473	100	Burggraaf, 1998	[230]
ZSM-5/Stainless Steel	i-C4	298–480	138 (w/sweep)	Gump, 2000	[247]
B-ZSM-5/γ-Alumina	p-xylene	353–430	2.1/component	Gump, 2001	[289]
MFI Zeolite/Alumina		323–723	125	Ciavarella, 2000	[263]
H-ZSM-5/Stainless steel or /Alumina	n-C6	298–600	$\Delta P = 138$	Flanders, 2000	[259]

MARCEL DEKKER, INC. • 270 MADISON AVENUE • NEW YORK, NY 10016

Table 35. Summary of Experimental Data on Microporous Inorganic Membranes Showing Decreases and then Increases of Permeance with Temperature

Membrane Type	Permeant	Temp. Range (K)	Feed Pressure (kPa)	1st Author, Year	Ref.
Silicalite/ Stainless steel	N_2, H_2, He(/Ne), Ne, Ar	190–680	101	Bakker, 1997	[100]
	He, Ne	200–600	101	Van De Graaf, 1999	[250]
Mordinite/Alumina	N_2, O_2, CO_2	290–400	301, $\Delta P = 200$	Nishiyama, 1997	[126]
Ferrierite/Alumina	H_2, He, C1, N_2, O_2, CO_2				
Silicalite/α-Alumina	C1, CO_2	290–470	270, $\Delta P = 138$	Poshusta, 1999	[251]
H-ZSM-5/Alumina or /Stainless steel	CO_2, N_2, H_2 DMB	298–550	$\Delta P = 138$	Flanders, 2000	[259]
ZSM-5/Stainless steel	i-C4	298–480	222, $\Delta P = 138$ 138 (w/sweep)	Gump, 2000	[247]

Table 36. Summary of Experimental Data on Microporous Inorganic Membranes Showing Permeance with a Maximum at Lower Temperature and Minimum at High Temperature

Membrane Type	Permeant	Temp. Range (K)	Feed Pressure (kPa)	1st Author, Year	Ref.
Silicalite-1/SS	–C1, C2, C3, n-C4, SF_6, CO, CO_2, Kr, Xe	190–680	101	Bakker, 1997	[100]
	–C1, C2	270–625	101	Van De Graaf, 1998	[283]
H-ZSM-5/SS	$-N_2$	298–550	P = 138	Flanders, 2000	[259]

For permeation in the Henry's regime, permeation of methane through silicalite membranes decreases with temperature. Vroon et al.[253] found that methane permeance decreased from 9.8×10^{-8} mol/m^2.s.Pa to 6.4×10^{-8} mol/m^2.s.Pa when the temperature increased from 298 K to 347 K. This agrees with the Eq. 27 for gases having ($Q_a > E_d$). Vroon et al.[253] reported values of $Q_a = 20$ kJ/mol and $E_d = 14$ kJ/mol for methane. However, for ethane, propane, n-butane the permeation increases with temperature. This trend has been shown for hydrocarbons in silicalite membranes by Kapteijn et al.[238,248] and Bakker et al.[254] Hydrogen (H_2) gas permeation through silicalite membranes decreases with temperature up to around 300 K[254] after which it starts to increase. Hydrogen has ($Q_a > E_d$) confirming the permeation decrease in the Henry's regime.[253] The increase flux with temperature can be described by considering the combined surface and GT diffusion contribution to the total flux. Neon and Argon exhibit a similar behavior as H_2. He and Ne are weakly adsorbing gases and their permeation through a microporous membranes depends on the amount of gas adsorbed in membrane pores. Helium, which permeates by counter diffusion against a feed gas, is hindered more by stronger adsorbed molecules and to move through the gas phase of the pores it needs sufficient space.

Figures 35 and 36 show single gas permeance through silicalite membranes as a function of temperature. Several groups have reported the presence of maximum and minimum in the permeation as function of temperature for linear hydrocarbons (methane, ethane, propane, and n-butane), inorganic gases (CO, and CO_2), and noble gases (Kr and Xe). Other gases exhibit only a minimum in the permeance like He (against Ne), N_2, H_2, Ne, and Ar, as shown in Figure 36. The maximum is described by the equilibrium

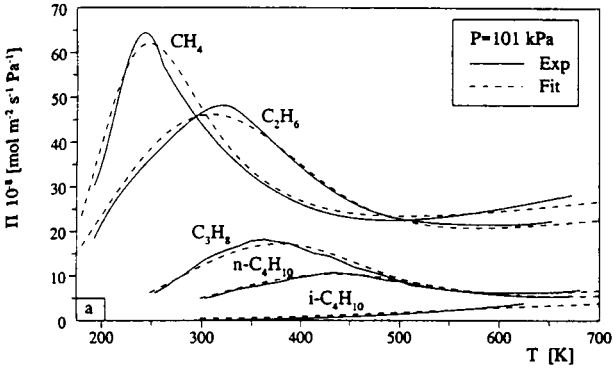

Figure 35. One component permeance of CH_4, C_2H_4, C_3H_8, nC_4H_8 and iC_4H_{10} through a silicalite membrane at feed pressure of 101 kPa as function the temperature (190 to 680 K) (After Ref. [254]).

adsorption and surface diffusion. At relatively low temperatures the surface diffusion is dominant and the diffusivity increases with temperature. Above a given temperature the equilibrium amount adsorbed in the membrane pores decreases, causing a decline in permeation flux after which an increase in the flux is observed as shown in Figure 35. This behavior might be explained by the combination of surface and GT diffusion. The sequence of the maximum of the permeation follows the equilibrium amount adsorbed, i.e., the higher the q_{sat} the lower the temperature at which the maximum occurs.[254]

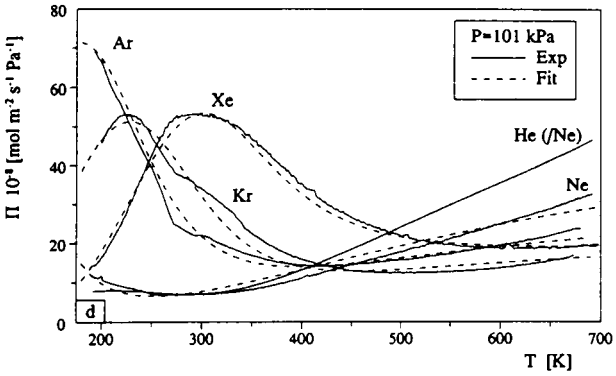

Figure 36. One component permeance of noble gases He, Ne, Ar, Kr, and Xe through a silicalite membrane at feed pressure of 101 kPa as function the temperature (190 to 680 K) (After Ref. [254]).

Eqs. 18 and 22 predict the maximum in the permeation as a function of temperature. This is caused by the non-linear sorption term.[242,243] Values of the temperature of maximum (T_m) shift depending on the feed pressure values. Shelekhin et al.[241] defined a temperature T_{iso} below which permeation is dominated by surface diffusion characterized by an increase of flux with temperature. At temperatures above T_{iso} the permeation is dominated by GT diffusion for which flux decreases with increasing temperature for the compounds having ($Q_a > E_d$). So the only way to create minimum in the flux is a combination of the surface diffusion model and the GT model.

However, some gases like i-butane show a different temperature dependence of permeance temperature when compared to other gases like n-butane. For this gas no maximum nor minimum is observed. This is because for i-butane the contribution from surface diffusion is much smaller than the contribution from gaseous diffusion due to its adsorption and diffusion properties. Also it was observed that n-butane permeates faster than i-butane because i-butane is more strongly adsorbing than n-butane. This trend has been confirmed by Vroon et al.,[253] Bakker et al.,[254] for silicalite membranes, and by Yan et al.[99] for ZSM-5 membranes.

Permeation in Faujasite-type (NaY) membranes shows the same trends observed on silicalite membranes. Kusakabe et al.[256] have found that permeance of CO_2 and N_2 through (NaY) membranes greatly increased with increasing temperature over the range of 0–40°C. This is in agreement with the Henry's regime results discussed before. However, in the 40–400°C temperature range the permeance initially increases and then decreases generating a maximum in the permeance curve. This observation agrees with the Langmuir regime as expressed by Eq. 26.

The effects of molecular sizes on single gas permeance through amorphous microporous membranes were discussed in Sections 2 and 4. Similar effects are also observed on the crystalline zeolites membranes. Figures 37 and 38 show permeation flux or permeance of molecules of various sizes through a silicalite membrane[230] and three SAPO-34[252] membranes at lower temperatures. For molecules with sizes much smaller than the zeolites pore sizes ($\sim$0.55 nm for silicaltie and $\sim$0.40 nm for SAPO-34), the size of permeating gas does not have a clear effect on gas permeance. For molecules with sizes close to the zeolites pore size, the gas permeance decreases sharply with increasing molecular size. The permeation theory shows that single gas permeation depends on both adsorption and diffusion properties of the permeating gas associated with the zeolites. At low temperatures, adsorption properties, which do not depend much on the molecular sizes of smaller molecules, play a more important role in gas permeation through microporous membranes. Thus, one should not expect a clear molecular size effects on permeation of small molecules through microporous membranes.

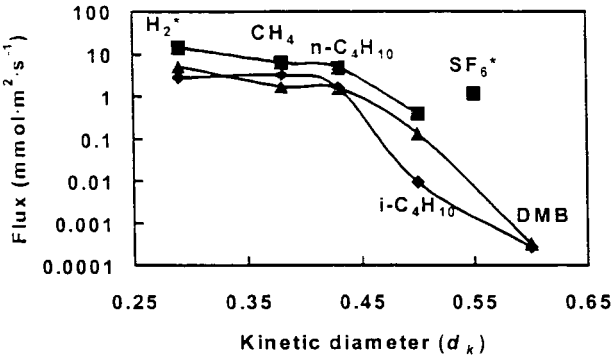

Figure 37. Single gas permeation flux of various gases through a 3 μm thick silicalite membrane at temperatures of 298 K (◆) and 473K (▲ ■) and feed pressure of 33 kPa (◆ ▲) and 100 kPa (■) (After Ref. [230]).

The adsorption of gas in zeolites becomes negligible at high temperatures. Under such conditions, permeation is determined by the diffusivity of the gas permeating in membrane pores. Bakker at al.[254] found that diffusivity in silicalite is almost constant for molecules with a kinetic diameter up to 0.3 nm (corresponding to kinetic diameter to pore diameter ratio of 0.55). Above this value the corrected diffusivities decrease strongly with the molecule size. Hence, one should expect to observe clear decrease of single gas permeance

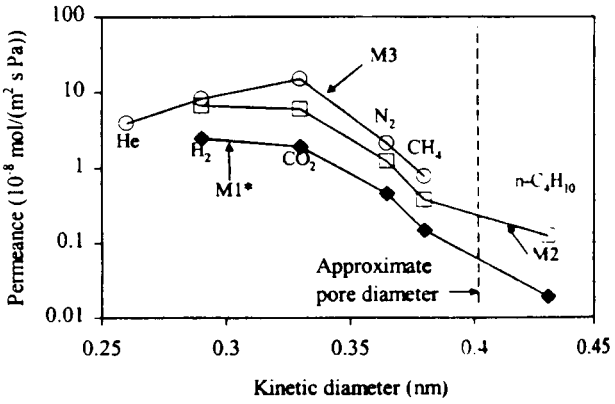

Figure 38. Room temperature permeance of single gas through three 5–10 μm thick SAPO-34 membranes (M1, M2, M3) at a feed pressure of 270 kPa and transmembrane pressure drop of 138 kPa (After Ref. [252]).

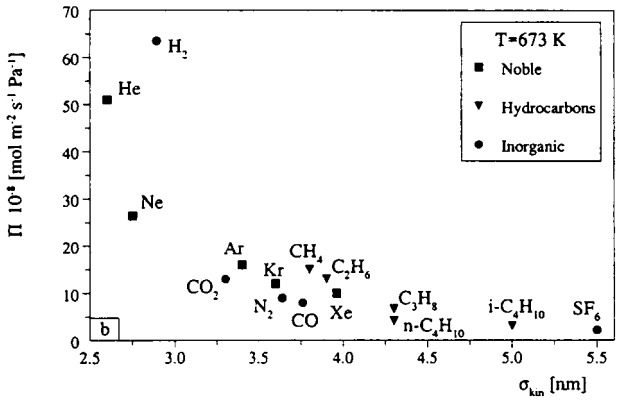

Figure 39. One component permeance for the different gases though a 50–60 μm thick silicalite membrane at 673 K (After Ref. [254]).

for good quality micorporous membrane with increasing size of the molecules. Figure 39 clearly shows such effects of molecular sizes on gas permeance through a silicalite membrane at high temperature.

5.4 Binary-Mixture Gas Permeation Through Microporous Membranes

The expression for multi-component gas permeation through microporous membrane is given by Eqs. 8 and 9. To derive the specific flux equations for each species requires knowing multi-component adsorption isotherms and various diffusivities. The following multi-component Langmuir adsorption isotherm equation has been used to model multi-component permeation through zeolites membranes:[236,238,248–250,257]

$$\theta_i = \frac{q_i}{q_{s,i}} = \frac{K_i P_i}{1 + \sum_{i=1}^{n} K_i P_i} \tag{31}$$

For binary system neglecting inter-molecular interaction where D_{ij} is absent, the following flux equations can be obtained by combining Eqs. 8, 9 and 31:[234,236,249,250,257]

$$J_1 = -\rho q_{s,1} \left(\frac{D_1}{1 - \theta_1 - \theta_2} \right) \left\{ (1 - \theta_2) \frac{\partial \theta_1}{\partial z} + \theta_1 \frac{\partial \theta_2}{\partial z} \right\} \tag{32}$$

$$J_2 = -\rho q_{s,2}\left(\frac{D_2}{1-\theta_1-\theta_2}\right)\left\{(1-\theta_1)\frac{\partial\theta_2}{\partial z}+\theta_2\frac{\partial\theta_1}{\partial z}\right\} \tag{33}$$

Other models taking into account the interactions between the permeating gases are given by Van de Graaf et al.[249,250]

Eqs. 32 and 33 are the simplest form of flux equations for multi-component gas permeation through microporous membranes. A steady-state mass balance would give a constant flux (J_1 and J_2) across the membrane. Integrating Eqs. 32 and 33 should yield equations correlating the permeation flux to diffusivities and surface coverage (θ) for both species at membrane feed and permeate surfaces, which can be converted to feed and permeate pressures using Eq. 31. With Eqs. 32 and 33, Van de Graaf[249,250] predicted the permeation of binary gas mixtures of methane, ethane and propane through silicalite membranes using single component adsorption equilibrium isotherm and diffusivity data. The model results agree fairly well with the experimental data for these binary systems in which both components exhibit comparable sorption affinities with silicalite. The model could not predict well the permeation of binary mixture of a fast, weakly adsorbing component and a slow, strongly adsorbing component, but the model gives improved prediction when adsorbate–adsorbate interaction is considered.

Unlike single gas permeation, for multi-component system even for the simplest case (Eqs. 32 and 33) it is very difficult to obtain explicit expression that correlates the steady state permeation flux of each species to the feed and permeate partial pressure and temperature. Numerical methods were used to integrate Eqs. 32 and 33 for permeation flux.[236,249] For multi-component permeation of more than two components, a strict formulation using Stefan–Maxwell approach becomes less attractive because of the mathematical complexity and unavailability of proper correlations for various diffusivities. Simplified models,[146,258] though less accurate, might be more convenient for examination of the effects of various parameters on the permeation and separation of multi-component system by the membrane. Experimental study is far more effective to understand multi-component permeation through microporous membranes since multi-component permeation experiments can be readily conducted.

The experimental results of multi-component permeation through inorganic membranes are usually analyzed by comparing the separation factor based on the permeance of each component in the presence of others to the ideal separation factor based on the single gas permeance values. Multi-component separation factor has been defined by the following two ways:

$$\alpha_{i,j} = \frac{(Y_i/Y_j)}{(X_i/X_j)} \tag{34}$$

$$\alpha_{i,j} = \frac{F_i}{F_j} = \frac{J_i/\Delta p_i}{J_j/\Delta p_j} \tag{35}$$

where Y and X is molar fraction in the retentate and permeate, Δp is transmembrane partial pressure difference based on the effluent composition. Eq. 34 is a more strict definition although both definitions have been used in the literature and often do not give much different results. It should be noted that multi-component separation factor depends not only on the thermodynamic and transport properties of the membrane/fluid–mixture system but also on the configuration of the permeation cell and the flow conditions of the permeation measurement. Separation factors obtained from mixtures for microporous membranes in most cases are not same as the ideal separation factors (permselectivity) obtained from the ratio of single gas permeance. At higher temperature and lower concentrations the mixture separation approaches the ideal separation factor.[230]

Several groups reported experimental data on permeation and separation of a large number of binary gas mixtures through zeolites (mainly silicalite) membranes.[104,144,147,237,238,244,248–251,259–264] Some of the binary gas and liquid separation data for zeolite membranes have been summarized in Section 4. Burggraaf[230] classifed the gas mixtures into three categories: weakly (W)—weakly (W) adsorbing gases, weakly (W)—strongly (S) adsorbing gases, and strongly (S)—strongly (S) adsorbing gases. Representative experimental results on binary gas permeation/separation through microporous membranes are summarized according to these categories in Tables 37–39. The general trends are discussed next.

Table 37. Summary of Experimental Data on Weak–Weak Binary Gas Permeation Separation Through Microporous Membranes

Membrane Type	Gas Mixture	Temp. Range (K)	Feed Pressure (kPa)	1st Author, Year	Ref.
Silicalite/ α-Alumina	H_2/C1	298–473	50/50	Keizer, 1998	[262]
	N_2/O_2		80/20		
Silicalite/ Stainless steel		200–650	101	van den Broeke, 1999	[257]
SAPO-34/ α-Alumina	H_2/C1, H_2/N_2, $C1/N_2$	300–470	50/50	Poshusta, 1999	[251]

Table 38. Summary of Experimental Data on Weak–Strong Binary Gas Permeation Separation Through Microporous Membranes

Membrane Type	Gas Mixture	Temp. Range (K)	Feed Pressure (kPa)	1st Author, Year	Ref.
Silicalite/ Stainless steel	H_2/CO_2, H_2/n-C4	300–600	50/50	Kapteijn, 1994	[237]
				Bakker, 1996	[100]
	C1/C2	298–630		Van De Graaf, 1998	[283]
		273–373		Van De Graaf, 1999	[250]
	C1/C3				
	N_2/CO_2, C1-CO_2	200–675		van den Broeke, 1999	[257]
	C1/C2	300–525			
	H_2/n-C4	300–675			
Zeolite/α-Alumina	C1/nC4	298–473	50/50	Vroon, 1996	[253]
				Vroon, 1998	[291]
	H_2/i-C4	323–723	125	Ciavarella, 2000	[263]
Silicalite/α-Alumina	H_2/CO_2, H_2/C3, H_2/n-C4	298–473	50/50	Keizer, 1998	[12]
	C1/n-C4		50/50, 5/95		
	C1/i-C4		95/5		
	C1/Benzene		50/50		
	C1/p-xylene		91/9, 99/1		
			99.4/0.6		
	O_2/CH_3OH, O_2/C_2H_5OH	300–425	108	Piera, 1998	[104]
ZSM-5/α-Alumina	C1/CO_2	290–470	50/50	Poshusta, 1999	[251]
SAPO-34/α-Alumina	C1/CO_2, N_2/CO_2, H_2/CO_2	300–470		Poshusta, 2000	[252]

Table 39. Summary of Experimental Data on Weak–Strong Binary Gas Permeation Separation Through Microporous Membranes

Membrane Type	Gas Mixture	Temp. Range (K)	Feed Pressure (kPa)	1st Author, Year	Ref.
Zeolite/α-Alumina	n-C4/i-C4	298–473	50/50	Vroon, 1996	[253]
				Vroon, 1998	[291]
ZSM-5/Stainless steel			138	Gump, 2000	[247]
ZSM-5/Alumina					
	n-C6/2,2-DMB[a]	350–400	50/50	Gump, 1999	[142]
Silicalite/α-Alumina	n-C2/C_2H_4, n-C3/C_3H_6	292[c]	50/50	Kapteijn, 1994	[244]
	n-C4/i-C4	295[c]	50/50	Bakker, 1996	[100]
	n-C4/i-C4	298–473	50/50	Keizer, 1998	[12]
	n-C6/2,2-DMB[a]		8/16		
	C_3H_8/C_3H_6		45/55		
	Benzene/cyclohexane		4.5/4.5		
	p-xylene/o-xylene	298–473	0.31/0.26		
		380–480		Baertsch, 1996	[147]

B-ZSM-5/γ-Alumina		353–430	2.1/2.1	Gump, 2001	[289]
	p-xylene/Ethylbenzene, p-xylene/toluene, m-xylene/ethylbenzene				
SAPO-11/α-Alumina	o-Xylene/Benzene	353–430	8.4/8.4	Gump, 2001	[289]
Silicalite/Stainless steel	n-C4/iC4, C_2H_4/C_3H_6	298–630	50/50	Van De Graaf, 1998b	[283]
	C3/n-C4	300–675	101	Van den Broeke, 1999	[283]
	n-C4/I-C4		50/50		
Silicalit/TiO_2/ Stainless steel		300–480	101	Gora, 2001	[292]
		300–573	101	Nishiyama, 2001	[293]
H-ZSM-5/Alumina or /Stainless steel	n-C6/2,2-DMB[a], n-C6/TMP[b]	298–550	50/50	Flanders, 2000	[259]

[a]DMB = Dimethylbenzene.
[b]TMP = Trimethylbenzene.
[c]Transient.

The gas permeance of air and binary mixture of nitrogen and oxygen through silicalite membrane under different temperatures has shown to be almost similar to the pure component permeance.[230] This is attributed to that both N_2 and O_2 are weakly adsorbates and have similar adsorption and diffusion properties in silicalite. In general, for a combination of W–W adsorbing gases the separation factors approach the ideal or permselectivity values but are usually somewhat lower, whereas the permeance values in the mixture are somewhat decreased with respect to single gas permeance.[230]

For a mixture of a fast, weakly adsorbing component and a slow, strongly adsorbing component (W–S mixture), the flux of weakly adsorbing component can be significantly reduced by the presence of the strongly adsorbing component as compared to the single gas permeation. For example, for carbon dioxide–nitrogen (S–W) mixture, if the amount CO_2 (S) in the feed is increased the binary flux of CO_2 increases in an almost linear way and a clear reduction was observed for the binary flux of N_2 (W).[257] As a consequence, the separation factor increases with the amount of CO_2 in the feed. This effect is shown in Figure 40. The separation factor of the CO_2–N_2 mixture is two to three times higher than the ideal separation factor. This behavior can be explained by the effect of competitive adsorption on the binary permeation. The same trend has been seen for the CO_2–CH_4 mixture. However, the separation factors for CO_2–CH_4 are smaller than those of CO_2–N_2 because methane is more strongly adsorbed in silicalite than nitrogen.

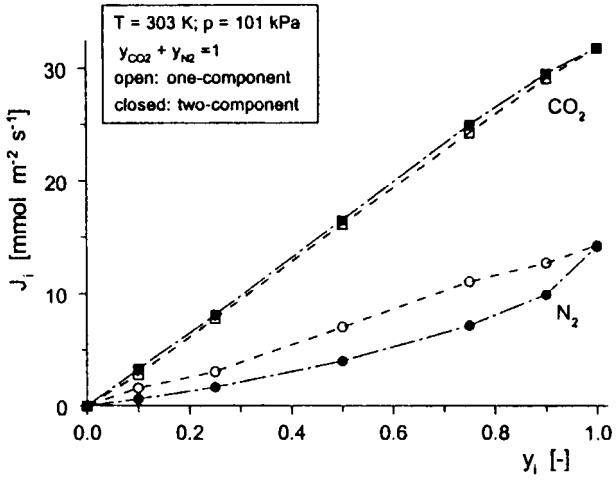

Figure 40. Comparison between the one and two component permeation fluxes for CO_2 and N_2 through silicalite membrane as a function of the feed composition (101 kPa and 303 K) (After Ref. [257]).

There are some differences in temperature dependency between S–W mixture permeation and single gas permeation. For a single-component permeation the maximum in permeance of CH_4 occurs at a lower temperature than the maximum of CO_2 because CH_4 is weakly adsorbed compared to CO_2. However, in the mixture the CH_4 maximum occurs at a slightly higher temperature than the maximum of CO_2.[257] Obviously the permeation of weakly adsorbed gas (methane) is affected by the presence of CO_2 up to a certain temperature above which there is no longer any competitive adsorption and CO_2 and CH_4 are permeating independently. Ethane (S) and methane (W) binary mixture flows through silicalite membrane as a function of temperature have also shown the same trend obtained for carbon dioxide–methane mixture. The permeance of ethane is hardly affected by presence of methane as compared to the single-component results, while methane flux is reduced significantly by ethane. The separation factor at a given pressure decreases with increasing temperature and at a given temperature it decreases with increasing pressure.

For separation of n-butane–H_2 (S–W) mixture using supported silicalite membrane, a maximum in the permeation curve is observed for the S component (n-butane) in the mixture. Similar maximum was observed for their single gas permeation curves. When the temperature increases the permeation values become equal and finally cross each other, with the W component (H_2) becoming faster permeating. So the separation factor $\alpha > 1$ for S–W mixture at low temperatures and then $\alpha < 1$ at high temperature.[237,244] This can be explained by the preferential adsorption of the S component, which blocks the voids and excludes the other component at low temperatures. At higher temperatures the concentration of (S) component decreases much more strongly than (W) component and the blocking effect decreases and then vanishes, leading to higher separation factor for the (W) component. At this stage the mixture starts to behave in a way similar to a mixture of two (W) components.

Increasing ethane (S) feed partial pressure increases the (S–W) separation factor. As the temperature increases, the extent of methane (W) flux reduction by ethane (S) is diminished, and so the selectivity toward ethane (S) decreases. At high temperatures the separation factor is almost independent of the pressure, indicating a transition of the transport mechanism from surface diffusion to gas translational diffusion with no significant interaction between the two components at high temperatures. In this condition, they will permeate independently.[257]

Separation of binary mixtures with molecules of different kinetic diameters having one small molecule, e.g., O_2–N_2, H_2–CH_4, H_2–CO_2, and CH_4–nC_4H_{10}, using silicalite membranes[161] shows that the permeance and separation factor of the components compared to the single component follow

the same trend as for the W–S binary mixture obtained by van den Broeke et al.[257] and Van de Graaf et al.[249,250] Keizer et al.[262] also reported permeance of CH_4 as function of temperature in presence of benzene, p-xylene, and 2,2-dimethylbenzene (DMB) through silicaltie membrane. The CH_4 permeance is reduced by a factor of 200, 600, and 1700 respectively compared to the single-component permeance. This strong reduction is caused by blocking of the pore entrance on the external surface by the large molecules. In all cases the CH_4 permeance increases sharply with temperature until the permeance is almost equal to the single component one. This is attributed to desorption of the large component molecules from the external surface with increasing temperature.

The permeation and separation results for binary S–S mixture or large molecules are more complex. Funke et al.[260] reported permeation of binary mixture of hexanes and octanes through silicalite membranes. They found that the permeances of the hydrocarbons in mixtures can not be predicted from the single–compound permeances. The permeance of one species can be increased or decreased by the presence of another species. Gump et al.[142] and Flanders et al.[259] reported separation of C_6 isomers by ZSM-5 zeolite membranes. They found that the temperature dependency of gas permeance in the mixture is similar to that in single component system, but the permeance of the more bulky C_6 (2,2-dimethylbutane, DMB) is significantly reduced by the presence of linear C_6 (n-hexane), resulting in a higher n-hexane to DMB separation factor in the mixture than the ideal separation factor. In contract, Keizer et al.[262] found that the flux of n-C_4H_{10} in a mixture of C_4H_{10}/iso-C_4H_{10} is about half the value of the single component flux while the iso-C_4H_{10} in the presence of C_4H_{10} is hardly reduced. In this situation the occupancy of both components is high both inside the pores and at the external surface. However, iso-C_4H_{10} is bulkier than C_4H_{10}, and it can block pore-mouth and limits diffusion of C_4H_{10}.

Several groups studied separation of xylene isomer by zeolites membranes.[147,261,262] The kinetic diameter of p-xylene and o-xylene is respectively about 0.58 and 0.68 nm. The diameter of the p-xylene is about the same as the pore size of MFI zeolite and that of o-xylene is significantly larger. Keizer et al.[262] reported that the flux of o-xylene is very small and that of p-xylene is hardly influenced by the presence of the other component. At high temperature separation by size exclusion can be observed because the o-xylene cannot enter the membrane pores and no strong preferential sorption or blocking by the o-xylene occurs at the membrane surface. However, p- to o-xylene gas separation factor for the silicalite membranes reported are quite different among the various research groups. For example, Baertsch et al.[147] reported no selectivity for p- to o-xylene while Keizer et al.,[262] Xomeritakis and Tsaptsis[261] reported the p- to o-xylene separation factor in the range of

2–25, and Sakai et al.[265] reported a maximum p- to o- or m-xylene separation factor of about 250.

The complexity for S–S binary gas separation by microporous membranes is due to strong interaction between permeating molecules which is not well quantified. This interaction affects both adsorption equilibrium and diffusivities of the permeating species. The hydrocarbons that are strongly adsorbed by the microporous zeolites membranes are usually large molecules. The steric hinderance and the quality of the zeolites membrane can affect the separation results. For example, Gump et al.[142] found that the bulky 2,2-dimethylbutane (DMB), as a single component, permeates through mainly non-zeolitic micropores. In the n-hexane–DMB binary mixture, the DMB permeance is reduced because the non-zeolite pores can be blocked by the prefertial n-hexane adsorption. This gives a n-hexane to DMB mixture separation factor larger than the ideal separation factor.

5.5 Multi-component Gas Permeation

Multicomponent permeation through the microporous zeolite membranes has largely been limited to pervaporation (e.g., Refs. [266,267]). This is not surprised as the zeolite membranes have now been used commercially for removal of water from organic mixture by the pervaporation processes, as discussed in Section 3. Up to date data on the permeation of gas mixtures containing more than two components for microporous membranes are very limited although practical applications of the zeolite membranes most likely involve multicomponent systems. Funke et al.[260] studied the permeation of binary and ternary vapor mixtures containing *n*-octane, *iso*-octane, and *n*-hexane. They reported that the permeances of the components are influenced strongly by the presence of other components in the feed. They concluded that multiple component gas permeation through a zeolite membrane is not predictable based on either single gas or binary gas permeation data. Yang et al.[258] investigated gas separation properties of silicalite membranes with feed containing 25% hydrogen, 50% methane, 20% ethane, and 5% propane. They found that the permeance of hydrogen in the mixture permeation is several orders of magnitude smaller than the pure hydrogen permeance. Arruebo et al.[268] studied separation of synthetic natural gas (methane: 83.6–83.6%, ethane, 7.5–7.7%, propane: 2.0–1.9%, and balanced amounts of higher hydrocarbons) by silicalite membrane for removal of heavy hydrocarbons from natural gases. They found that higher hydrocarbons are more perm-selective to methane at room temperature.

Rao and Sircar[163] reported pure gas permeability of hydrogen and four hydrocarbons and the permeability of the same gas mixture as the feed through

Table 40. Comparison of Pure and Mixture Gas Permeance Through Microporous Carbon Membranes

Component	Mixture Composition %	Permeability of Mixture (P_f = 4.4 amt)	Pure Gas Permeability (P_f = 1.17 atm)
H_2	41.0	1.2	130
CH_4	20.2	1.3	660
C_2H_6	9.5	7.7	850
C_3H_8	9.4	25.7	290
C_4H_{10}	19.9	112.3	155

At 295.1 K, unit for permeability: barrer.
(From Ref. [183].)

a microporous carbon membrane of about 2.5 μm in thickness. The results of pure and mixture permeability are compared in Table 40. For pure gas permeation, the permeability incrases with increasing adsorption affanity of the permeating gas with the carbon. This mechanism is similar to that of the hydrophobic silicalite membrane, as explained above. The permeabilities of all the five species with gas mixture as feed are smaller than the pure gas permeability. However, the reduction in the gas permeability for the less adsorbing species is more signficant than the more adsorbing species. For example, the butane to hydrogen selectivity is 1.2 in the pure gas permeation but is 94.4 for the mixture permeation. This is also similar to what is found for the hydrophobic zeolite membrane. Table 40 also shows that butane permeabiltiy in the mixture is smaller than pure butane permeability. Since the partial pressure of butane in the feed in the mixture is similar to that in the pure gas permeance, this result indicates that the presence of less adsorbing gases also reduces permeation of the more adsorbing species.

Table 41. Separation Factors of Silicalite Zeolite Membrane Prepared by In-Situ Crystallization Method with Template

T (°C)	H_2 84.5%	CH_4 7.6%	C_2H_6 2.5%	C_2H_4 2.5%	C_3H_8 0.75%	C_3H_6 1.45%	n-C_4H_{10} 0.4%	i-C_4H_{10} 0.4%
25	0	1.6	5.8	11	21	53	69	0
105	0.2	1.5	3.9	6.8	7.0	18	7.7	0
200	1.3	0.5	0.4	1.3	1.9	2.2	0	0

(From Ref. [95].)

Dong et al.[146] studied separation of an eight component mixture of hydrogen–light hydrocarbons simulating a refinery gas by silicalite membrane under wide temperature (25–500°C) and feed pressure (1–5 atm) ranges. The composition of the gas mixture is given in Table 41. Figures 41 and 42 show permeation fluxes of total hydrocarbons and hydrogen versus temperature at different feed pressures (1 atm permeate pressure with helium as the sweep). The temperature dependences of these multi-component system as shown in Figures 41 and 42 resemble a hydrocarbon–hydrogen binary system. The permeance of hydrocarbons increases, and after reaching a maximum, decreases with temperature. For non-adsorbing gas (hydrogen), the gas permeance increases monotonously with temperature in the temperature range studied. The permeation flux increases with increasing feed pressure. The values of the separation factor of various species of the eight component mixture for the silicalite membrane are listed in Table 41. As shown by the Figure 3-13 and Table 41, at low temperature (< 100°C) the silicalite membrane shows a high selectivity for hydrocarbon over hydrogen. However, at high temperature (500°C) the silicalite membrane becomes permselective to hydrogen over hydrocarbons. At low temperature the permeance of the various species increases with increasing adsorption affinity of the species with silicalite. The difference in the diffusivity

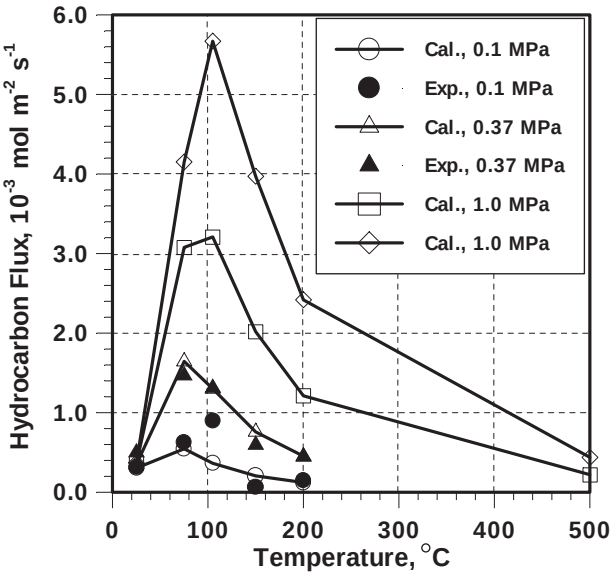

Figure 41. Hydrocarbon permeation fluxes of an eight component feed (Table 41) through a silicalite membrane at different temperatures and feed pressures (closed symbols are experimental data and solid liens are model results) (After Ref. [146]).

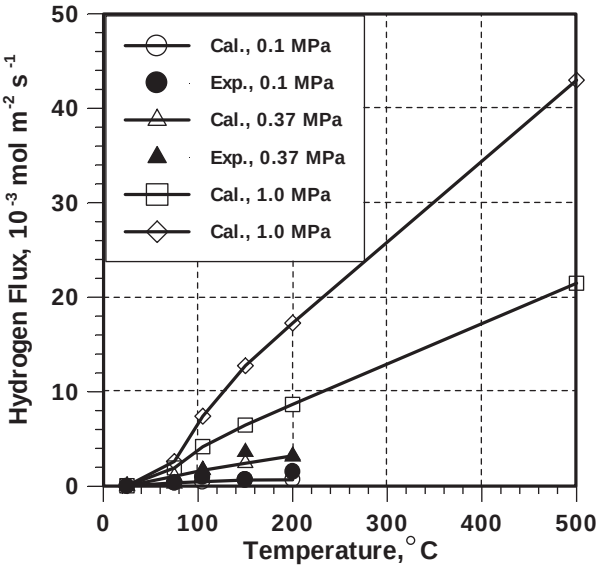

Figure 42. Hydrogen permeation flux of an eight component feed (Table 41) through a silicalite membrane at different temperatures and feed pressures (closed symbols are experimental data and solid liens are model results) (After Ref. [146]).

of various species has a less influence on the permeance. At high temperatures the difference in the amount adsorbed in the zeolites between various gas species becomes negligible. Therefore diffusion dominates the gas permeance through zeolites membranes. Thus, at high temperatures the permeance decreases with increasing size of the permeating gases. The adsorption–diffusion model for binary system as described above can be used to explain these results.

Rigorous theoretical modeling of multicomponent permeation and separation through microporous inorganic membranes is very complex and has not been reported. However, two research groups have reported simplified models which treat the multicomponent system as a binary one with one component being the nonadsorbing gas (hydrogen) and all other hydrocarbons grouped as the adsorbing gas. Yang et al.[258] postulated that the presence of the adsorbing molecules form a potential energy barrier for the diffusion of the non-adsorbing species, and the permeance of the non-adsorbing species (e.g., hydrogen) in the presence of the adsorbing species, F, is reduced, with respect to its pure gas permeance, F_o, as:

$$F = F_o \exp\left(-\frac{\sum E_{0,j}\theta_j}{RT}\right) \tag{36}$$

where $E_{o,j}$ is the potential energy barrier of the pure adsorbing gas j at its conditions of saturated adsorption and θ_j is the coverage of the adsorbing species j. $E_{o,j}$ is calculated from the slope of the plots of lnP vs θ of the pure gas adsorption isotherm on zeolite. With known adsorption isotherms for the adsorbing species, Eq. 36 was used to predict hydrogen permeance in the mixture from the pure hydrogen permeance for a silicalite membrane, and good agreement was obtained between the predicted and experimentally measured data.

Dong et al.[146] presented a simplified model based on a somewhat different concept for multi-component permeation through zeolites membranes. Again, the simplified model treats the multi-component system as a binary one with all hydrocarbon compounds in the simulated gas mixture lumped into one component, i.e., hydrocarbon (HC) and hydrogen as the second component. The HC passes through the membrane via adsorption–diffusion mechanism, while hydrogen diffusion is non-adsorptive. The permeation fluxes can be described by:

$$J_{HC} = D_{HC} \cdot \frac{\Delta C_{HC}}{\mathrm{L}} \tag{37}$$

$$J_{H2} = D_{H2} \cdot \varepsilon \cdot \frac{\Delta P_{H2}}{RT\mathrm{L}} \tag{38}$$

where D_{HC} and D_{H2} are diffusivity of HC and H_2 in the zeolite membrane, respectively, C_{HC} is the amount of adsorbed HC per unit volume of the zeolite membrane, and P_{H2} is partial pressure of hydrogen and l is the membrane thickness. They assumed that the diffusivity and solubility of hydrogen in the pores filled with HC is negligible and therefore in Eq. 38 fraction of zeolite pores free of hydrocarbons, ε, can be related to the fraction of zeolite pores filled by HC, θ_{HC}, as $\varepsilon = 1 - \theta_{HC}$.

The fraction of zeolite pores filled by HC is related to HC partial pressure by the Langmuir equation:

$$\theta_{HC} = \frac{C_{HC}}{C^*_{HC}} = \frac{K_{HC} \cdot P_{HC}}{1 + K_{HC} \cdot P_{HC}} \tag{39}$$

where C^*_{HC} is the saturated amount of HC that can be adsorbed on the zeolite. The constant K_{HC} and the diffusivities for HC and H_2 can respectively be correlated to temperature by the von't Hoff and Arrhneius type equations, Eqs. 24 and 25, which include pre-exponential constants and heat of adsorption or activation energy for diffusion. These constants were obtained by regressing the permeation data at different temperatures and feed pressures. The comparison of the model results and experimentally data are shown in Figures 41 and 42. The model agrees fairly well with the experimental data.

Furthermore, the model allows prediction of the permeance of gas separation at higher feed pressures.

5.6 Effects of Membrane Microstructure on Gas Separation

Limited studies reported in the past few years have shown that the microstructure of a polycrystalline zeolite membrane and structural change of the zeolite in the membrane can affect gas permeation and separation properties of the zeolites membrane. It is difficult to quantify the microstructure of a polycrystalline zeolite membranes though attempt to do so was recently reported.[269] One would expect that zeolite crystallite size and shape, crystal orientation in the film, and intercrystalline pore size and shape should be among the key parameters that define the microstructure of a zeolite membrane. As discussed before, a good quality polycrystalline zeolite membrane often includes both the zeolitic pores and microporous non-zeolite pores.[270] In most cases gas permeates through both types of micropores. Gas permeation through this type of zeolite membrane is similar to microporous silica membrane with a pore size distribution. The separation properties of this membrane are controlled by the adsorption properties, especially at low temperatures. For the membrane shown in Table 41, the separation factor of the various hydrocarbons increases with increasing carbon number (except for iso-butane).

The presence of microporous intercrystalline pores, depending on their sizes, can affect mixture separation results by a zeolite membrane. Sano et al.[141] studied ethanol–water separation by a silicalite membranes with intercrystalline pores estimated to be about 1 nm in sizes. They suggested that the non-zeolitic pores are less ethanol permselective than zeolitic pores. Silanol modification of the silicalite membranes decreased the intercrystalline pore sizes and enhanced the hydrophobicity of the non-zeolitic pores. Thus, the modified silicaltie membranes showed an improved selectivity. Gump et al.[142] reported results of separation of n-hexane and DMB mixture by a ZSM-5 membrane. Although single gas permeation fluxes of the two components were similar, DMB permeation flux was dramatically decreased by the existence of n-hexane in mixture gas separation. The n-hexane selectivity decreased with increasing temperature, owing to the decrease in adsorption ability. At high temperatures (e.g., 398 K), increasing n-hexane partial pressure in the feed resulted in an increase in the selectivity. They suggested that n-hexane condensed in the intercrystalline pores of considerable sizes and blocked the DMB permeation.

Pan and Lin[95] recently prepared silicalite membranes by the secondary growth method without template. These silicaltie membranes contained less or no intercrystalline pores since no template removal step responsible for the

formation or enlargement of the intercrystalline pores was required in membrane preparation by this method. Thus, these zeolite membranes should contain primarily the zeolitic pores. The gas permeance of the template-free silicaltie membrane is 3–4 times lower than that of the similar silicaltie membrane prepared with template due to smaller amount of the intercrystalline pores in the former. Table 42 gives the separation properties of the template-free silicaltie membrane. Compared with data given in Table 41, this membrane exhibits separation properties different from the silicalite membrane synthesis with the template (Table 41). In this case the average pore size of this zeolite membrane is more close to the sizes of the most hydrocarbons listed in Table 41. Thus, the separation properties of this membrane are determined mainly by the diffusivity of the hydrocarbons. The zeolitic diffusivity of hydrocarbons in the zeolitic pores decreases with increasing carbon number. Therefore for this membrane the separation factor decreases with increasing carbon number of the hydrocarbon, as shown in Table 42.

As mentioned before, several groups studied separation of xylene isomer by MFI type zeolites membranes but the results reported are quite different. Xomeritakis and Tsaptsis[261] reported the p- to o-xylene separation factor in the range of 2–25, and Sakai et al.[265] reported a maximum p- to o- or m-xylene separation factor of about 250. The silicalite layers of the zeoltie membrane prepared by Xomeritakis and Tsaptsis were thick (about 20–30 μm), oriented, and in an asymmetric structure with a thin dense silicalite region on the top of the silicalite layer. The silicalite membranes reported by Sakai et al.[265] were self-supporting (without a support) and 60–130 μm in thickness. These structures of the silicalite membranes may avoid or minimize the enlargement of the intercrystalline gaps caused by the template removal during zeolite membrane synthesis. In contrast, most alumina supported thin silicalite membranes prepared by the in-situ synthesis method (e.g., Refs. [137,147]) do not offer good separation properties for xylenes due possibly to the presence of microporous intercrystalline pores with pore size larger than the o- or m-xylene molecules.

Table 42. Separation Factors of Silicalite Membrane Prepared by Secondary Growth Method Without Template (with the Simulated Refinery Gas as the Feed, see Table 41)

T (°C)	H_2	CH_4	C_2H_6	C_2H_4	C_3H_8	C_3H_6	n-C_4H_{10}	i-C_4H_{10}
25	0	26	9.1	5.8	0	0	0	0
105	0.6	2	1.5	2.4	0	0	0	0
200	3.5	0.4	0.4	0.4	0	0	0	0

The microstructure of polycrystalline zeolite membrane may change with temperature. Dong et al.[120] reported that the lattice volume of supported silicalite in the alumina or zirconia supported silicalite membrane decreases with increasing temperature whereas the volume of the support (alumina or zirconia) expands as temperature increases. It is reasonable to expect that the intercrystalline pores become larger at higher temperatures. However, no study has been reported on the effects of such microstructural change with increasing temperature on gas permeation and separation properties of the polycrystalline membranes.

Microporous zeolite membrane, especially at the upstream surface, can be highly loaded with the adsorbed species during permeation due to high partial pressure of the permeating gas in the feed. When the size of the adsorbed gas molecules is close to the zeolite pores, the presence of the guest molecules may cause a change in the phase structure and pore size of the zeolite membrane. Such a change has been found on the p-xylene–silicalite and benzene–silicalite systems.[271–273] Silicalite without guest molecules is in a monoclinic structure, and, with a slight change of lattice to an orthorhombic structure, can take up to 4 molecules of p-xylene or benzene per unit cell. Higher loading of the guest molecules is accompanied with a change in the lattice to another orthorhombic structure with larger a and c lattice parameters.[272,273] The channel sizes of the silicalite at higher loading of the guest molecules is larger than that at lower loading.

Xomeritakis and Tsapatsis[261] found that the o-xylene alone permeated much slower through a silicalite membrane than p-xylene. The o-xylene permeance in the o-xygene/p-xylene mixture (at the feed partial pressures larger than 0.15 kPa or larger than 25% saturation pressure) is 6 times as high as the pure o-xylene permeance. It is very likely that the high loading of p-xylene has caused phase change of the silicalite crystals, allowing o-xylene to diffuse faster through the silicalite pore channels. It should be pointed out that very few studies have been reported on the crystalline structural change of microporous inorganic materials with guest molecules present in the crystalline pores, and the effects of these structural changes on gas adsorption, diffusion and permeation properties. These properties are however important for membrane applications and more study in this is expected in the future.

6. CONCLUDING REMARKS

Significant progress has been made in synthesis of various types of microporous amorphous or crystalline inorganic membranes. Microporous silica membranes can be routinely prepared by the sol-gel methods. Hollow-

fiber microporous silica membranes can be fabricated by the phase separation method. But the brittleness of these hollow-fiber silica membranes might have limited their practical applications. The hydrothermal stability of the microporuos silica membranes should be improved in order to apply these membranes in industrial processes at high temperatures. Microporous carbon membranes can be prepared by several different pyrolysis methods from polymer precursors. The carbon membranes exhibit excellent gas separation properties, especially for nitrogen and oxygen gas mixtures.

Significant efforts have been reported in the past decade on polycrystalline microporous zeolites membranes. Good quality zeolite membranes can be prepared by several methods, including in-situ synthesis, secondary growth and vapor phase transportation. Synthesis of over ten different type zeolite membranes of various pore sizes has been reported in the literature. It is agreed that the good quality zeolite membranes are devoid of mesopore and macropore sized pinhole and defects but may contain microporous intercrystalline gaps. The presence of these microporous intercrystalline gaps very often does not affect separation properties for molecules with sizes smaller than the zeolitic pores. Preparation of zeolite membranes without intercrystalline pores is essential to achieving gas separation properties based on the molecular sieving mechanism.

All the microporous inorganic membranes show similar gas separation and permeation properties. These microporous membranes exhibit fascinating permeation and separation properties few people expected a decade ago. Gas and liquid separation properties of these microporous inorganic membranes are determined by mechanisms of preferential adsorption, selectively configurational diffusion or molecular sieving. Gas permeation through these microporous inorganic membranes is an activated process, and can be predicted by the gas diffusion theory developed in the last decade for microporous materials. The Stephans–Maxwell equations are the basis of macroscopic transport equations governing gas permeation and separation through these microporous membranes.

The extensive research in the microporous inorganic membranes in the past decade has already led to large scale commercial applications of these membranes in industry. Tubular NaA type zeolite membranes have been used in Japan for solvent dehydration. Due to its hydrophilicity, the NaA membrane is water perm-selective. A typical zeolite membrane separation plant could produce 530 L/hr solvents (ethanol, isopropanol, acetone etc.) containing less than 0.2 wt% water, from the solvents with 10 wt% water. Each plant uses 2000 zeolite membrane tubes of 80 cm long and 12 mm in outer diameter, with a total permeation area of about 60 m^2. The first decade of the new millennium will see more industrial applications of various microporous inorganic membranes.

ACKNOWLEDGMENTS

One of the authors (YSL) would like to acknowledge support from various funding agencies, in particular, the National Science Foundation, Exxon Education Foundation, Amoco and Japan Society for Promotion of Science, for the research in his group on microporous inorganic membranes.

REFERENCES

1. Koros, W.J.; Ma, Y.H.; Shimidzu, T. J. Membr. Sci. **1996**, *120*, 149.
2. Hsieh, H.P. *Inorganic Membranes for Separation and Reaction*; Elsevier: Amsterdam, 1996.
3. Burggraaf, A.J.; Cot, L. *Fundamentals of Inorganic Membrane Science and Technology*; Elsevier: Amsterdam, 1996.
4. Naheiri, T.; Ludwig, K.A.; Anand, M.; Rao, M.B.; Sircar, S. Sep. Sci. Technol. **1997**, *32*, 1589.
5. Casanave, D.; Ciavarella, P.; Fiaty, K.; Dalmon, J.A. Chem. Eng. Sci. **1999**, *54*, 2807.
6. Hsieh, H.P.; Bhave, R.R.; Fleming, L.L. J. Membr. Sci. **1988**, *39*, 221.
7. Nakao, S. J. Membr. Sci. **1994**, *96*, 131.
8. Huang, P.; Xu, N.P.; Shi, J.; Lin, Y.S. J. Membr. Sci. **1996**, *116*, 301.
9. Tsuru, T.; Hino, T.; Yoshioka, T.; Asaeda, M. J. Membr. Sci. **2001**, *186*, 257.
10. Leenaars, A.F.M.; Keizer, K.; Burggraaf, A.J. J. Mater. Sci. **1984**, *19*, 1077.
11. Asaeda, M.; Du, L.D. J. Chem. Eng. Jpn. **1986**, *19* (1), 72.
12. Keizer, K.; Uhlhorn, R.J.R.; Vanvuren, R.J.; Burggraaf, A.J. J. Membr. Sci. **1988**, *39*, 285.
13. Uhlhorn, R.J.R.; Veld, M.H.B.J.H.I.; Keizer, K.; Burggraaf, A.J. J. Mater. Sci. Lett. **1989**, *8*, 1135.
14. Yoldas, B.E. Am. Ceram. Soc. Bull. **1975**, *54*, 296.
15. Chang, C.-H.; Gopalan, R.; Lin, Y.S. J. Membr. Sci. **1994**, *91*, 27.
16. Brinker, C.J.; Scherer, G.W. *Sol–Gel Science*; Academic Press: London, 1990.
17. Lin, Y.S.; Chang, C.H.; Gopalan, R. Ind. Eng. Chem. Res. **1994**, *33*, 860–870.
18. Lin, Y.S.; de Vries, K.J.; Burggraaf, A.J. J. Mater. Sci. **1991**, *26*, 715–720.
19. Lin, Y.S.; Burggraaf, A.J. J. Am. Ceram. Soc. **1991**, *74*, 219–224.
20. Gopalan, R.; Chang, C.-H.; Lin, Y.S. J. Mater. Sci. **1995**, *30*, 3075.
21. Gopalan, R.; Lin, Y.S. Ind. Eng. Chem. Res. **1995**, *34*, 1189.

22. Zuter-Hofman, J.M. Chemical and Thermal Stability of Modified Mesoporous Ceramic Membranes. Ph.D. Thesis, University of Twente: The Netherlands, 1995.
23. Leenaars, A.F.M.; Burggraaf, A.J. J. Colloid Interface Sci. **1985**, *105*, 27.
24. Leenaars, A.F.M. Preparation, Structure and Separation Characteristics of Ceramic Alumina Membranes. Ph.D. Thesis, University of Twente: The Netherlands, 1984.
25. Uhlhorn, R.J.R.; Veld, M.H.B.J.H.I.; Keizer, K.; Burggraaf, A.J. J. Mater. Sci. **1992**, *27*, 527.
26. Nair, B.N. Structure Property Relationships in Silica Sols, Gels and Molecular-Sieving Membranes. Ph.D. Thesis, University of Tokyo: Japan, 1998.
27. Nair, B.N.; Keizer, K.; Okubo, T.; Nakao, S.-I. Langmuir **2000**, *16* (10), 4558.
28. Asaeda, M.; Kitao, S. *Proceedings of the 2nd International Conference on Inorganic Membranes*; 1991; 295.
29. Asaeda, M.; Okazaki, K.; Nakatani, A. Ceram. Trans. **1992**, *31*, 411.
30. Asaeda, M.; Yamamichi, A.; Satoh, M.; Kamakura, M. *Proceedings of ICIM3*; Ma, Y.H., Ed.; 1994; 315.
31. Asaeda, M. *Proceedings of the 29th Society of Japan Chemical Engineering Congress, Japan*; Sep. 25, 1996.
32. Asaeda, M. *Proceedings of 1999 International Conference on Membranes, Toronto*; 1999.
33. Asaeda, M.; Yamasaki, S. Sep. Purif. Technol. **2001**, *25*, 151.
34. Uhlhorn, R.J.R.; Keizer, K.; Burggraaf, A.J. J. Membr. Sci. **1992**, *66*, 271.
35. Uhlhorn, R.J.R.; Zaspalis, V.T.; Keizer, K.; Burggraaf, A.J. J. Mater. Sci. **1992**, *27*, 538.
36. Brinker, C.J.; Hurd, A.J.; Schunk, P.R.; Frye, G.C.; Ashley, C.S. J. Non-Cryst. Solids **1992**, *147 and 148*, 424.
37. Brinker, C.J.; Ward, T.L.; Sehgal, R.; Raman, N.K.; Hietala, S.L.; Smith, D.M.; Hua, D.W.; Headley, T.J. J. Membr. Sci. **1993**, *77*, 165.
38. de Lange, R.S.A.; Hekkink, J.H.A.; Keizer, K.; Burggraaf, A.J. Microporous Mater. **1995**, *4*, 169.
39. de Lange, A.R.S.A.; Hekkink, J.H.A.; Keizer, K.; Burggraaf, A.J. J. Membr. Sci. **1995**, *99*, 57.
40. de Lange, A.R.S.A.; Keizer, K.; Burggraaf, A.J. J. Membr. Sci. **1995**, *104*, 81.
41. Fotou, G.P.; Lin, Y.S.; Pratsinis, S.E. J. Mater. Sci. **1995**, *30*, 2803.
42. Nair, B.N.; Elferink, J.W.; Keizer, K.; Verweij, H. J. Colloid Interface Sci. **1996**, *178*, 565.

43. Elferink, J.W.; Nair, B.N.; Keizer, K.; Verweij, H. J. Colloid Interface Sci. **1996**, *180*, 127.
44. de Lange, A.R.S.A. Microporous Sol–Gel Derived Ceramic Membranes for Gas Separation. Ph.D. Thesis, University Of Twente: The Netherlands, 1993.
45. Nair, B.N.; Keizer, K.; Maene, N.; Okubo, T.; Nakao, S.-I. *Surface Chemistry and Electrochemistry of Membranes*; Sorenson, T.S., Ed.; Marcel Dekker: New York, 1999; 125.
46. Uhlhorn, R.J.R. Ceramic Membranes for Gas Separation, Synthesis and Transport Properties. Ph.D. Thesis, University of Twente: The Netherlands, 1990.
47. Maier, W.F.; Schramm, H.O. Mater. Res. Soc. Symp. Proc. **1992**, *271*, 493.
48. de Vos, R.M.; Verweij, H. J. Membr. Sci. **1998**, *143*, 37.
49. de Vos, R.M.; Verweij, H. Science **1998**, *279*, 1710.
50. de Vos, R.M. High Selectivity High Flux Silica Membranes for Gas Separation. Ph.D. Thesis, University Of Twente: The Netherlands, 1998.
51. Puhlfurß, P.; Voigt, A.; Weber, R.; Borbe, M. J. Membr. Sci. **2000**, *174*, 123.
52. Brinker, C.J.; Sehgal, R.; Hietala, S.L.; Deshpande, R.; Smith, D.M.; Loy, D.; Ashley, C.S. J. Membr. Sci. **1994**, *94*, 85.
53. Brinker, C.J.; Raman, N.K.; Logan, M.N.; Sehgal, R.; Assink, R.A.; Hua, D.W.; Ward, T.L. J. Sol-Gel Sci. Technol. **1995**, *4*, 117.
54. Schafer, R.; Noack, M.; Kolsch, P.; Thomas, S.; Seidel-Morgenstern, A.; Caro, J. Sep. Purif. Technol. **2001**, *25*, 3.
55. Diniz da Costa, J.C.; Lu, G.Q.; Rudolph, V.; Lin, Y.S. J. Membr. Sci. **2002**, *198*, 9.
56. Chu, L.; Anderson, M.A. Microporous Mater. **1997**, *8*, 207.
57. Munoz-Agudo, M.J.; Gregorkiewitz, M. J. Membr. Sci. **1996**, *11*, 7.
58. Tsuru, T.; Wada, S.; Izumi, S.; Asaeda, M. J. Membr. Sci. **1998**, *149*, 127.
59. Tsuru, T.; Izumi, S.; Yoshioka, T.; Asaeda, M. AIChE J. **2000**, *46*, 565.
60. Julbe, A.; Balzer, C.; Guizard, C.; Cot, L. J. Sol-Gel Sci. Technol. **1995**, *4*, 89.
61. Raman, N.K.; Anderson, M.T.; Brinker, C.J. Chem. Mater. **1996**, *8*, 1682.
62. Raman, N.K.; Brinker, C.J. J. Membr. Sci. **1995**, *105*, 273.
63. Cao, G.Z.; Lu, Y.; Delattre, L.; Brinker, C.J.; Lopez, G.P. Adv. Mater. **1996**, *8*, 588.
64. Schwertfeger, F.; Glaubitt, W.; Schubert, U. J. Non-Cryst. Solids **1992**, *145*, 85.
65. Liu, C.; Komarneni, S. Mater. Res. Soc. Symp. Proc. **1995**, *371*, 217.
66. de Vos, R.M.; Maier, W.F.; Verweij, H. J. Membr. Sci. **1999**, *158*, 277.

67. Tsai, C.Y.; Tam, S.Y.; Lu, Y.F.; Brinker, C.J. J. Membr. Sci. **2000**, *169*, 255.
68. Wallace, S.; Brinker, C.J.; Smith, D.R. Mater. Res. Soc. Symp. Proc. **1995**, *371*, 241.
69. Otani, M.; Tsuru, T.; Asaeda, M. *Proc. 30th Society of Japan Chemical Engineering Congress, Japan*; 1997; 157.
70. Nair, B.N.; Keizer, K.; Okubo, T.; Nakao, S.-I. J. Membr. Sci. **1997**, *135* (2), 237.
71. Karger, J.; Ruthven, D.M. *Diffusion in Zeolite and Other Microporous Solids*; Wiley and Sons: New York, 1992.
72. Matsuda, A.; Matsuno, Y.; Katayama, S.; Tsuno, T. J. Mater. Sci. Lett. **1989**, *8*, 902.
73. Giessler, S.; da Costa, J.C.D.; Lu, G.Q. J. Nanosci. Nanotechnol. **2001**, *1*, 331.
74. de Lange, A.R.S.A.; Keizer, K.; Burggraaf, A.J. Ind. Eng. Chem. Res. **1995**, *34*, 3838.
75. Yoshida, K.; Hirano, Y.; Fujii, H.; Tsuru, T.; Asaeda, M. J. Chem. Eng. Jpn. **2001**, *34*, 523.
76. Breck, D.W. *Zeolite Molecular Sieves: Structure, Chemistry, and Use*; Wiley: New York, 1973.
77. Barrer, R.M. *Zeolites and Clay Minerals as Sorbents and Molecular Sieves*; Academic Press: New York, 1978.
78. Ruthven, D.M. *Principles of Adsorption and Adsorption Processes*; Wiley: New York, 1984.
79. Paul, D.R.; Keml, D. Polym. Sym. Eds. **1973**, *41*, 79.
80. Kemp, A.; Paul, D.R. J. Polym. Sci. **1974**, *12*, 485.
81. Kolsh, P.; Venzke, D.; Noack, M.; Toussaint, P.; Caro, J. J. Chem. Soc., Chem. Commun. **1994**, 2491.
82. Wernick, D.L. J. Membr. Sci. **1985**, *22*, 137.
83. Sano, T.; Mizukami, F.; Takaya, H.; Mouri, T.; Watanabe, N. Bull. Chem. Soc. Jpn. **1992**, *65*, 146.
84. Suzuki, H. U.S. Patent 4,699, 892, 1987.
85. Yamazaki, S.; Tsutsumi, K. Microporous Mater. **1995**, *4*, 205.
86. Bernal, M.P.; Piera, E.; Coronas, J.; Menedez, M.; Santamaria, J. Catal. Today **2000**, *56*, 221.
87. Poshusta, J.C.; Tuan, V.A.; Falconer, J.L.; Noble, R.D. Ind. Eng. Chem. Res. **1998**, *37*, 3924.
88. Dong, J.; Lin, Y.S. Ind. Eng. Chem. Res. **1998**, *37*, 2404.
89. Braunbarth, C.M.; Boudreau, L.C.; Tsapatsis, M. J. Membr. Sci. **2000**, *174*, 31.
90. Kita, H.; Horii, K.; Ohtochi, Y.; Tanaka, K.; Okamoto, K. J. Mater. Sci. Lett. **1995**, *14*, 206.

91. Masuda, T.; Hara, H.; Kouno, M.; Kinoshita, H.; Hashimoto, K. Microporous Mater. **1995**, *3*, 567.
92. Dong, J.; Wegner, K.; Lin, Y.S. J. Membr. Sci. **1998**, *148*, 233.
93. Geus, E.R.; van Bekkum, H.; Bakker, W.J.W.; Moulijn, J.A. Microporous Mater. **1993**, *1*, 131.
94. Sano, T.; Ejiri, S.; Yamada, K.; Kawakami, Y.; Yanagishita, H. J. Membr. Sci. **1997**, *123*, 225.
95. Pan, M.; Lin, Y.S. Microporous Mesoporous Mater. **2001**, *43*, 319–327.
96. Sano, T.; Yanagisawa, H.; Kiyozumi, Y.; Kitamoto, D.; Mizukami, F. Chem. Lett. **1992**, 2413.
97. Vroon, Z.A.E.P. Synthesis and Transport Studies of Thin Ceramic Supported Zeolites (MFI) Membranes. Ph.D. Thesis, University of Twente, Netherlands, 1995.
98. Jansen, J.C.; van Rosmalen, G.M. J. Cryst. Growth **1993**, *128*, 1150.
99. Yan, Y.; Davis, M.E.; Gavalas, G.R. Ind. Eng. Chem. Res. **1995**, *34*, 1652.
100. Bakker, W.J.W.; Kapejin, F.; Poppe, J.; Moulijn, J.A. J. Membr. Sci. **1996**, *117*, 57.
101. Jia, M.D.; Peinemann, K.V.; Behling, R.D. J. Membr. Sci. **1993**, *82*, 15.
102. Coronas, J.; Falconer, J.L.; Noble, R.D. AIChE J. **1997**, *43*, 1797.
103. Coronas, J.; Noble, R.D.; Falconer, J.L. Ind. Eng. Chem. Res. **1998**, *37*, 166.
104. Piera, E.; Fendler, A.G.; Dalmon, J.A.; Moueddeb, H.; Coronas, J.; Menendez, M.; Santamaria, J. J. Membr. Sci. **1998**, *142*, 97.
105. Davis, M.E. J. Am. Chem. Soc. **1987**, *109*, 25856.
106. Slangen, M.; Jabseb, J.C.; van Bekkum, H. Microporous Mater. **1997**, *9*, 259.
107. Kita, H.; Horita, T.; Asamura, H.; Tanaka, K.; Okamoto, K. *Proc. 5th International Conference on Inorganic Membranes, Nagoya, Japan*; 1998; 536.
108. Xu, X.C.; Yang, W.S.; Liu, J.; Lin, L.W. Adv. Mater. **2000**, *12*, 195.
109. Xu, X.C.; Yang, W.S.; Liu, J.; Lin, L.W. Microporous Mesoporous Mater. **2001**, *43*, 299.
110. Xu, X.C.; Yang, W.S.; Liu, J.; Lin, L.W. Sep. Purif. Technol. **2001**, *25*, 241.
111. Kumakiri, I.; Ymaguchi, T.; Nakao, S. Ind. Eng. Chem. Res. **1999**, *38* (12), 4682.
112. Kumakiri, I.; Yamaguchi, T.; Nakao, S. J. Chem. Eng. Jpn. **2000**, *33* (2), 333.
113. Lovallo, M.C.; Tsapatsis, M. AIChE J. **1996**, *42* (11), 3020.
114. Lovallo, M.C.; Boudreau, L.; Tsapatsis, M. Mater. Res. Soc. Symp. Proc. **1996**, *431*, 225.

115. Boudreau, L.C.; Tsapatsis, M. J. Membr. Sci. **1999**, *152*, 41.
116. Yamazaki, S.; Tsutsumi, K. Microporous Mater. **1995**, *5*, 245.
117. Kumakiri, I.; Yamaguchi, T.; Nakao, S. *Proceedings of the 5th International Conference on Inorganic Membranes, Nagoya, Japan*; 1998; B-306.
118. Kumakiri, I.; Yamaguchi, T.; Nakao, S. *Proceedings of the 6th International Conference on Inorganic Membranes, Montpellier, France*; 2000.
119. Xomeritakis, G.; Nair, S.; Tsapatsis, M. Microporous Mesoporous Mater. **2000**, *38*, 61.
120. Dong, J.; Lin, Y.S.; Hu, M.Z.; Peascoe, R.A.; Payzant, E.A. Microporous Mesoporous Mater. **2000**, *34*, 241.
121. Xu, W.; Dong, J.; Li, J.; Wu, F. Chem. Soc. Chem. Commun. **1990**, 755.
122. Matsukata, M.; Nishiyama, N.; Ueyama, K. Microporous Mater. **1993**, *1*, 219.
123. Dong, J.; Dou, T.; Zhao, X.; Gao, L. J. Chem. Soc., Chem. Commun. **1992**, 1056.
124. Crea, A.; Aiello, R.; Nastro, A.; Nagy, J. Zeolites **1991**, *11*, 521.
125. Nishiyama, J.; Ueyama, K.; Matsukata, M. Microporous Mater. **1996**, *7*, 299.
126. Nishiyama, J.; Matsuguji, T.; Ueyama, K.; Matsukata, M. Microporous Mater. **1997**, *12*, 293.
127. Yan, Y.; Davis, M.E.; Gavalas, G.R. J. Membr. Sci. **1997**, *123*, 95.
128. Nomura, M.; Yamaguchi, T.; Nakao, S. Ind. Eng. Chem. Res. **1997**, *36* (10), 4217.
129. den Exter, M.J.; van Bekkum, H.; Rijn, C.J.M.; Kapteijn, F.; Moulijn, J.A.; Schellevis, H.; Beenakker, C.I.N. Zeolites **1997**, *19*, 13.
130. Geus, E.R.; den Exter, M.J.; van Bekkum, H. J. Chem. Soc., Faraday Trans. **1992**, *88*, 3101.
131. Bai, A.; Jia, M.-D.; Falconer, L.; Noble, R.D. J. Membr. Sci. **1995**, *105*, 79.
132. Myatt, G.J.; Budd, P.M.; Price, C.; Carr, S.W. J. Mater. Chem. **1992**, *2*, 1103.
133. Koegler, J.H.; van Bekkum, H.; Jansen, J.C. Zeolites **1997**, *19*, 262.
134. Gouzinis, A.; Tsapatsis, M. Chem. Mater. **1998**, *10*, 2497.
135. Sasaki, Y.; Shimizu, W.; Ando, Y.; Saka, H. Microporous Mesoporous Mater. **2000**, *40*, 63.
136. Jia, M.D.; Chen, B.; Noble, R.D.; Falconer, J.L. J. Membr. Sci. **1994**, *90*, 1.
137. Wegner, K.; Dong, J.; Lin, Y.S. J. Membr. Sci. **1999**, *158*, 17.
138. Lovallo, M.C.; Gouzinis, A.; Tsapatsis, M. AIChE J. **1998**, *44*, 1903.

139. Xomeritakis, G.; Lai, Z.P.; Tsapatsis, M. Ind. Eng. Chem. Res. **2001**, *40*, 544.
140. Lin, Y.S.; Yamamoto, N.; Choi, Y.; Yamaguchi, T.; Okubo, T.; Nakao, S.-I. Microporous Mesoporous Mater. **2000**, *38*, 207–220.
141. Sano, T.; Hasegawa, M.; Kawakami, Y.; Kiyozumi, Y.; Yanagisita, H.; Kiamoto, D.; Mizukami, F. Stud. Surf. Sci. Catal. **1994**, *84*, 1175.
142. Gump, C.J.; Noble, R.D.; Falconer, J.L. Ind. Eng. Chem. Res. **1999**, *38*, 2775.
143. Kumakiri, I.; Sasaki, Y.; Shimizu, W.; Yamaguchi, T.; Nakao, S. *Proceedings of 13th International Zeolite Conference, Montpellier, France*; 2001.
144. Hedlund, J.; Noack, M.; Kolsch, P.; Creaser, D.; Caro, J.; Sterte, J. J. Membr. Sci. **1999**, *159*, 263.
145. Lai, R.; Gavalas, G.R. Microporous Mesoporous Mater. **2000**, *38*, 239.
146. Dong, J.; Lin, Y.S.; Liu, W. AIChE J. **2000**, *46*, 1957.
147. Baertsch, C.D.; Funke, H.H.; Falconer, J.L.; Noble, R.D. J. Phys. Chem. **1996**, *100*, 7676.
148. Kusakabe, K.; Kuroda, T.; Murata, A.; Morooka, S. Ind. Eng. Chem. Res. **1997**, *36*, 649.
149. Kusakabe, K.; Kuroda, T.; Morooka, S. J. Membr. Sci. **1998**, *148*, 13.
150. Van De Graaf, J.M.; Kapteijn, F.; Moulijn, J. *Zeolite Membranes in Structured Catalysis and Reactors*; Marcel Dekker: New York, 1997.
151. Kita, H.; Asanuma, H.; Tanaka, K.; Okamoto, K.; Kondo, M. Abstr. Pap.—Am. Chem. Soc. **Sep. 7, 1997**, *214*, 269-PMSE, Part 2.
152. Jafar, L.J.; Budd, P.M. Microporous Mater. **1997**, *12*, 305.
153. Sano, T.; Hasegawa, M.; Ejiri, S.; Kawakami, Y.; Yanagisawa, H. Microporous Mater. **1995**, *5*, 179.
154. Kondo, M.; Komori, M.; Kita, H.; Okamoto, K. J. Membr. Sci. **1997**, *133*, 133.
155. Morigami, Y.; Kondo, M.; Abe, J.; Kita, H.; Okamoto, K. Sep. Purif. Technol. **2001**, *25*, 251.
156. Koresh, J.E.; Sofer, A. J. Chem. Soc., Faraday Trans. **1980**, *76* (2), 2457.
157. Koresh, J.E.; Sofer, A. J. Chem. Soc., Faraday Trans. I **1986**, *82*, 2057.
158. Koresh, J.E.; Sofer, A. Sep. Sci. Technol. **1983**, *18*, 723.
159. Acharya, M.; Raich, B.A.; Foley, H.C.; Harold, M.P.; Lerou, J.J. Ind. Eng. Chem. Res. **1997**, *36*, 2924.
160. Linkov, V.M.; Sanderson, R.D.; Jacobs, E.P. J. Membr. Sci. **1994**, *95*, 93.
161. Jones, C.W.; Koros, W.J. Ind. Eng. Chem. Res. **1995**, *34*, 158.
162. Chen, Y.D.; Yang, R.T. Chem. Eng. Sci. **1992**, *47*, 3895.
163. Rao, M.B.; Sircar, S. J. Membr. Sci. **1993**, *85*, 253–264.

164. Fuertes, A.B.; Centeno, T.A. Microporous Mesoporous Mater. **1998**, *26*, 23–26.
165. Fuertes, A.B.; Centeno, T.A. J. Membr. Sci. **1998**, *144*, 105–111.
166. Kusakabe, K.; Gohgi, S.; Motooka, S. Ind. Eng. Chem. Res. **1998**, *37*, 4262.
167. Centeno, T.A.; Fuertes, A.B. Sep. Purif. Technol. **2001**, *25*, 379.
168. Shiflett, M.B.; Foley, H.C. J. Membr. Sci. **2000**, *179*, 275–282.
169. Strano, M.S.; Foley, H.C. AIChE J. **2001**, *47*, 66–78.
170. Mulder, M. *Basic Principles of Membrane Technology*; Kluwer: Norwell, MA, 1991.
171. Acharya, M.; Foley, H.C. J. Membr. Sci. **1999**, *161*, 1.
172. Geiszler, V.C.; Koros, W.J. Ind. Eng. Chem. Res. **1996**, *35*, 2999.
173. Hammel, J.J. US Patent, 4,853,001, 1989.
174. Vogel, W. *Structure and Crystallization of Glasses*; Pergamon Press: New York, 1971, Section 3.2.3, Edition Leipzig.
175. McMillan, P.W.; Matthews, C.E. J. Mater. Sci. **1976**, *11*, 1187.
176. McMillan, P.W. *Glass Ceramics*; Academic Press: New York, 1979.
177. Way, D.; Roberts, D.L. Sep. Sci. Technol. **1992**, *27*, 29.
178. Shelekhin, A.B.; Dixon, A.G.; Ma, Y.H. J. Membr. Sci. **1992**, *75*, 233.
179. Shelekhin, A.B.; Dixon, A.G.; Ma, Y.H. J. Membr. Sci. **1993**, *83*, 181.
180. Grosgogeat, E.J.; Fried, J.R.; Jenkins, R.G.; Hwang, S.-T. J. Membr. Sci. **1991**, *57*, 237.
181. Poshusta, J.C.; Noble, R.D.; Falconer, J.L. J. Membr. Sci. **2001**, *186*, 25.
182. Shiflett, M.B.; Foley, H.C. Science **1999**, *285*, 1902.
183. Rao, R.B.; Sircar, S. J. Membr. Sci. **1996**, *110*, 109–118.
184. Sircar, S.; Rao, M.B.; Thaeron, C.M.A. Sep. Sci. Technol. **1999**, *34*, 2081.
185. Miller, J.R.; Koros, W.J. Sep. Sci. Technol. **1990**, *25*, 1257.
186. Ma, Y.H.; Becker, Y.L.; Moser, W.R.; Dixon, A.G. Key Eng. Mater. **1991**, *61 & 62*, 337.
187. Lin, Y.S.; Ji, W.; Wang, Y.; Higgins, R.J. Ind. Eng. Chem. Res. **1999**, *38*, 2292.
188. Gavalas, G.R.; Megiris, C.E.; Nam, S.W. Chem. Eng. Sci. **1989**, *44*, 1829.
189. Lin, Y.S.; Burggraaf, A.J. AIChE J. **1992**, *38*, 445.
190. Lin, Y.S.; Burggraaf, A.J. Chem. Eng. Sci. **1991**, *46*, 3067–3080.
191. Lin, Y.S.; de Haart, L.G.J.; de Vries, K.J.; Burggraaf, A.J. J. Electrochem. Soc. **1990**, *137*, 3960–3966.
192. Okubo, T.; Inoue, H. J. Membr. Sci. **1989**, *42*, 109.
193. Besmann, T.M.; Lowden, R.A.; Sheldon, B.W.; Stinton, D.P. Proc. 11th Int. Conf. CVD, ECS Symp. Ser. **1990**, *90*, 482.

194. Lin, Y.S.; de Vries, K.J.; Brinkman, H.W.; Burggraaf, A.J. J. Membr. Sci. **1992**, *66*, 211.
195. de Haart, L.G.J.; Lin, Y.S.; de Vries, K.J.; Burggraaf, A.J. J. Eur. Ceram. Soc. **1991**, *8*, 59.
196. Xomeritakis, G.; Han, J.; Lin, Y.S. J. Membr. Sci. **1997**, *124*, 27.
197. Xomeritakis, G.; Lin, Y.S. AIChE J. **1998**, *44*, 174–183.
198. Kitao, S.; Asaeda, M. Key Eng. Mater. **1991**, *61 & 62*, 267.
199. Megiris, C.E.; Glezer, J.H.E. Ind. Eng. Chem. Res. **1992**, *31*, 1293–1299.
200. Ha, H.Y.; Nam, S.W.; Hong, S.A.; Lee, W.K. J. Membr. Sci. **1993**, *85*, 279–290.
201. de Vries, K.J.; Burggraaf, A.J.; Lin, Y.S. J. Phys., Colloq. **1989**, *50*, 861.
202. Lin, Y.S.; Burggraaf, A.J. J. Membr. Sci. **1993**, *79*, 65.
203. Cao, G.Z.; Brinkman, H.W.; Meijerink, J.; De Vries, K.J.; Burggraaf, A.J. J. Am. Ceram. Soc. **1993**, *76*, 2201–2208.
204. Cao, G.Z.; Brinkman, H.W.; Meijerink, J.; De Vries, K.J.; Burggraaf, A.J. J. Membr. Sci. **1993**, *83*, 221.
205. Lin, C.F.; Flowers, D.L.; Liu, P.K.T. J. Membr. Sci. **1994**, *92*, 45–58.
206. Wu, J.C.S.; Sabol, H.; Smith, G.W.; Flowers, D.L.; Liu, P.K.T. J. Membr. Sci. **1994**, *96*, 275.
207. Sea, B.K.; Watanabe, M.; Kusakabe, K.; Morooka, S.; Kim, S.S. Gas Sep. Purif. **1996**, *10*, 187.
208. Sea, B.K.; Kusakabe, K.; Morooka, S. J. Membr. Sci. **1997**, *130*, 41–52.
209. Nam, S.W.; Gavalas, G.R. AIChE Symp. Ser. **1989**, *85* (268), 68.
210. Tsapatsis, M.; Kim, S.; Nam, S.W.; Gavalas, G. Ind. Eng. Chem. Res. **1991**, *30*, 2152.
211. Tsapatsis, M.; Gavalas, G.R. AIChE J. **1992**, *38*, 847.
212. Tsapatsis, M.; Gavalas, G.R. J. Membr. Sci. **1994**, *87*, 281–296.
213. Prabhu, A.K.; Oyama, S.T. J. Membr. Sci. **2000**, *176*, 233–248.
214. Cooper, C.A.; Lin, Y.S. J. Membr. Sci. **2002**, *195*, 35.
215. Tai, N.H.; Chou, T.W. J. Am. Ceram. Soc. **1989**, *72*, 414.
216. Carolan, M.F.; Michaels, J.N. Solid State Ion. **1987**, *25*, 207.
217. Brinkman, H.K.; Cao, G.Z.; Meijerink, J.; De Vries, K.J.; Burggraaf, A.J. Solid State Ion. **1993**, *63–65*, 37.
218. Xomeritakis, G.; Lin, Y.S. Chem. Eng. Sci. **1994**, *49*, 3909.
219. Xomeritakis, G.; Lin, Y.S. Ind. Eng. Chem. Res. **1994**, *33*, 2607–2617.
220. Lin, Y.S. J. Membr. Sci. **1993**, *79*, 55.
221. Xomeritakis, G.; Pratsinis, S.E.; Lin, Y.S. J. Chem. Vapor Depos. **1996**, *4*, 173.
222. Hong, L.S.; Lai, H.T. Ind. Eng. Chem. Res. **1999**, *38*, 950–957.
223. Kim, S.; Gavalas, G.R. Ind. Eng. Chem. Res. **1995**, *34*, 168–176.
224. George, S.M.; Ott, A.W.; Klaus, J.W. J. Phys. Chem. **1996**, *100*, 13121.
225. Klaus, J.W.; Sneh, O.; George, S.M. Science **1997**, *278* (5345), 1934.

226. Berland, B.S.; gartland, I.P.; Ott, A.W.; George, S.M. Chem. Mater. **1998**, *10*, 2941.
227. Cameron, M.A.; Gartland, I.P.; Smith, J.A.; Diaz, S.F.; George, S.M. Langmuir **2000**, *16*, 7435.
228. Ott, A.W.; McCarley, K.C.; Klaus, J.W.; Way, J.D.; George, S.M. Appl. Surf. Sci. **1996**, *107*, 128.
229. Pan, M.; Cooper, C.; Lin, Y.S.; Meng, G.Y. J. Membr. Sci. **1999**, *158*, 235.
230. Burggraaf, A.J.; Vroon, Z.A.E.P.; Keizer, K.; Verweij, H. J. Membr. Sci. **1998**, *144*, 77.
231. Burggraaf, A.J. J. Membr. Sci. **1999**, *155*, 45.
232. Jackson, R. *Transport in Porous Catalysts*; Elsevier: New York, 1977.
233. Mason, E.A.; Malinauskas, A.P. *Gas Trasnport in Porous Media: The Dusty–Gas Model*; Elsevier: Amsterdam, 1983.
234. Krishna, R.; Wesseling, J.A. *Mass Transfer*; Ellis Horwood: New York, 1990.
235. Krishna, R. Chem. Eng. Sci. **1993**, *48*, 845.
236. Krishna, R.; Vlugt, T.J.H.; Smit, B. Chem. Eng. Sci. **1999**, *54*, 1751.
237. Kapteijn, F.; Bakker, W.J.W.; Zheng, G.; Moulijn, J.A. Microporous Mater. **1994**, *3*, 227.
238. Kapteijn, F.; Bakker, W.J.W.; Zheng, G.; Poppe, J.; Moulijn, J.A. Chem. Eng. J. **1995**, *57*, 145.
239. Yang, R.T. *Gas Separation by Adsorption Processes*; Butterworths: Boston, 1987.
240. Do, D.D. *Adsorption Analysis: Equilibrium and Kinetics*; Imperial College Press: London, 1998.
241. Shelekhin, A.B.; Dixon, A.G.; Ma, Y.H. AIChE J. **1995**, *41*, 58.
242. Xiao, J.; Wei, J. Chem. Eng. Sci. **1992**, *47*, 1123.
243. Xiao, J.; Wei, J. Chem. Eng. Sci. **1992**, *47*, 1143.
244. Kapteijn, F.; Bakker, W.J.W.; Zheng, G.; Moulijn, J.A.; van Bekkum, H. *Proc. 1st International Workshop on Catalytic Membrane, Leyon, France*; 1994.
245. Takabe, H.; Koshita, R.; Mizukamai, K.; Oumi, Y.; Ito, N.; Ku, M.; Fahmi, A.; Miyamoto, A. J. Membr. Sci. **1997**, *134*, 122.
246. van De Graaf, J.M.; van der Biji, E.; Stol, A.; Kapteijn, F.; Moulijn, J.A. Ind. Eng. Chem. Res. **1998**, *37*, 4010.
247. Gump, C.J.; Noble, R.D.; Falconer, J.L. J. Membr. Sci. **2000**, *173*, 35.
248. Kapteijn, F.; Bakker, W.J.W.; Van de Graaf, J.; Zheng, G.; Boppe, J.; Moulijn, J.A. Catal. Today **1995**, *25*, 213.
249. Van De Graaf, J.M.; Kapteijn, F.; Moulijn, J. AIChE J. **1999**, *45*, 497.
250. Van De Graaf, J.M.; Kapteijn, F.; Moulijn, J. Chem. Eng. Sci. **1999**, *54*, 1081.

251. Poshusta, J.C.; Noble, R.D.; Falconer, J.L. J. Membr. Sci. **1999**, *160*, 115.
252. Poshusta, J.C.; Tuan, V.A.; Pape, E.A.; Noble, R.D.; Falconer, J.L. AIChE J. **2000**, *46*, 779.
253. Vroon, Z.A.E.P.; Keizer, K.; Gilde, M.J.; Verwij, H.; Burggraaf, A.J. J. Membr. Sci. **1996**, *113*, 293.
254. Bakker, W.J.W.; van De Broeke, L.J.P.; Kapejin, F.; Moulijn, J.A. AIChE J. **1997**, *43*, 2025.
255. Sikavitsas, V.I.; Yang, R.T. Chem. Eng. Sci. **1995**, *50*, 2057.
256. Kusakabe, K.; Kuroda, T.; Uchino, K.; Hasegawa, Y.; Morooka, S. AIChE J. **1999**, *45*, 1220.
257. van den Broeke, L.J.P.; Bakker, W.J.W.; Kapteijn, F.; Moulijn, J. AIChE **1999**, *45*, 976.
258. Yang, M.; Crittenden, B.D.; Percera, S.P.; Moueddeb, H.; Dalmon, J.-A. J. Membr. Sci. **1999**, *156*, 1.
259. Flanders, C.L.; Tuan; Noble, R.D.; Falconer, J.L. J. Membr. Sci. **2000**, *176*, 43.
260. Funke, H.H.; Kovalchick, M.G.; Falconer, J.L.; Noble, R.D. Ind. Eng. Chem. Res. **1996**, *35*, 1575.
261. Xomeritakis, G.; Tsapatsis, M. Chem. Mater. **1999**, *11*, 875.
262. Keizer, K.; Burggraaf, A.J.; Vroon, Z.A.E.P.; Verweij, H. J. Membr. Sci. **1998**, *147*, 159.
263. Ciavarella, P.; Moueddeb, H.; Miachon, S.; Fiaty, K.; Dalmon, J.A. Catal. Today **2000**, *56*, 253.
264. Matsufuji, T.; Nishiyama, N.; Ueyama, K.; Matsukata, M. Catal. Today **2000**, *56*, 265.
265. Sakai, H.; Tomita, T.; Takahashi, T. Sep. Purif. Technol. **2001**, *25*, 297.
266. Li, S.; Tuan, V.A.; Falconer, J.L.; Noble, R.D. Chem. Mater. **2001**, *13*, 1865.
267. Li, S.; Tuan, V.A.; Falconer, J.L.; Noble, R.D. J. Membr. Sci. **2001**, *191*, 53.
268. Arruebo, M.; Coronas, J.; Menendez, M.; Santamaria, J. Sep. Purif. Technol. **2001**, *25*, 275.
269. Au, L.T.Y.; Yeung, K.L. J. Membr. Sci. **2001**, *194*, 33.
270. Lin, Y.S. Sep. Purif. Technol. **2001**, *25*, 39.
271. Guo, C.J.; Talu, O.; Hayhusrt, D.T. AIChE J. **1989**, *25*, 573.
272. Mentzen, B.F.; Gelin, P. Mater. Res. Bull. **1995**, *30*, 373.
273. Mentzen, B.F.; Lefebvre, F. Mater. Res. Bull. **1997**, *32*, 813.
274. Barrer, R.M. *Hydrothermal Chemistry of Zeolites*; Academic Press: London, 1982.
275. Matsukata, M.; Nishiyama, N.; Ueyama, K. Microporous Mater. **1996**, *7*, 109.
276. Kitao, S.; Kameda, H.; Asaeda, M. Membrane **1990**, *15*, 222.

277. Maier, W.F.; Tilgner, I.-C.; Wiedorn, M.; Ko, H.-C.; Ziehfreund, A.; Sell, R. Adv. Mater. **1993**, *5*, 730.
278. Peterson, R.A.; Anderson, M.A.; Hill, C.G., Jr. J. Membr. Sci. **1994**, *94*, 103.
279. van Gemert, R.W.; Cuperus, F.P. J. Membr. Sci. **1995**, *105*, 287.
280. Kim, M.H.; Li, H.X.; Davis, M.E. Microporous Mater. **1992**, *1*, 191.
281. Lai, R.; Gavalas, G.R. Ind. Eng. Chem. Res. **1998**, *37*, 4275.
282. Kusakabe, K.; Yoneshige, S.; Murakata, A.; Morooka, S. J. Membr. Sci. **1996**, *116*, 39.
283. Van De Graaf, J.M.; Kapteijn, F.; Moulijn, J. J. Membr. Sci. **1998**, *144*, 87.
284. Kumakiri, I. Preparation and Permeation—Mechanisms of Zeolite Membranes. PhD Thesis, University of Tokyo: Japan, 2000.
285. Liu, Q.; Noble, R.D.; Falconer, J.L.; Funke, H.H. J. Membr. Sci. **1996**, *117*, 163.
286. Kita, H.; Fuchida, K.; Horita, T.; Asamura, H.; Okamoto, K. Sep. Purif. Technol. **2001**, *25*, 261.
287. Bhandarkar, M.; Shelekhin, A.B.; Dixon, A.G.; Ma, Y.H. J. Membr. Sci. **1992**, *75*, 221.
288. Hayhusrt, D.T.; Paravar, A.R. Zeolites **1988**, *8*, 27.
289. Gump, C.J.; Tuan, V.A.; Noble, R.D.; Falconer, J.L. Ind. Eng. Chem. Res. **2001**, *40*, 65.
290. Kusakabe, K.; Ichiki, K.; Hayashi, J.; Maeda, H.; Morooka, S. J. Membr. Sci. **1996**, *115*, 65.
291. Vroon, Z.A.E.P.; Keizer, K.; Burggraaf, A.J.; Verweij, H. J. Membr. Sci. **1998**, *144*, 65.
292. Gora, L.; Nishiyama, N.; Jansen, J.C.; Kapteijn, F.; Teplyakov, V.; Maschmeyer, T. Sep. Purif. Technol. **2001**, *22–23*, 223.
293. Nishiyama, N.; Gora, L.; Teplyakov, V.; Kapteijn, F.; Moulijn, J.A. Sep. Purif. Technol. **2001**, *22–23*, 295.